BEHAVIOUR OF CONTINUOUSLY SUPPORTED SELF-COMPACTING CONCRETE DEEP BEAMS

Mahmoud A T KHATAB

Submitted for the Degree of
Doctor of Philosophy

Faculty of Engineering and Informatics

University of Bradford

2016

ABSTRACT

BEHAVIOUR OF CONTINUOUSLY SUPPORTED SELF-COMPACTING CONCRETE DEEP BEAMS

MAHMOUD KHATAB
University of Bradford, UK, 2016

Keywords: Self-compacting concrete, Continuous deep beams, Shear strength, Shear span-to-depth ratio, Shear reinforcement, Strut-and-tie model.

The present research is conducted to investigate the structural behaviour of continuously supported deep beams made with SCC. A series of tests on eight reinforced two-span continuous deep beams made with SCC was performed. The main parameters investigated were the shear span-to-depth ratio, the amount and configuration of web reinforcement and the main longitudinal reinforcement ratio. All beams failed due to a major diagonal crack formed between the applied mid-span load and the intermediate support separating the beam into two blocks: the first one rotated around the end support leaving the rest of the beam fixed on the other two supports. The amount and configuration of web reinforcement had a major effect in controlling the shear capacity of SCC continuous deep beams.

The shear provisions of the ACI 318M-11 reasonably predicted the load capacity of SCC continuous deep beams. The strut-and-tie model recommended by different design codes showed conservative results for all SCC continuous deep beams. The ACI Building Code (ACI 318M-11) predictions were more accurate than those of the EC2 and Canadian Code (CSA23.3-04). The proposed effectiveness factor equations for the strut-and-tie model showed accurate predictions compared to the experimental results. The different equations of the effectiveness factor used in upper-bound analysis can reasonably be applied to the prediction of the load capacity of continuously supported SCC deep beams although they were proposed for normal concrete (NC). The proposed three dimensional FE model accurately

predicted the failure modes, the load capacity and the load-deflection response of the beams tested.

ACKNOWLEDGMENTS

It is a pleasure to thank those who made this thesis possible. First and foremost, I would like to thank **Allah**; our Lord, the All-Knowing, the Almighty, the most Merciful and the most Compassionate.

I would like to express my sincere appreciation and special thanks to my supervisors **Prof. Ashraf Ashour, Prof. Dennis Lam and Dr. Therese Sheehan** for their excellent supervision, constant encouragement and approachability throughout the period of this work. I deeply appreciate **Prof. Ashour** for his great support and help, especially throughout the difficult time course of the fighting in my country, Libya.

Special thanks go to the **Laboratory staff** who were always ready to help in times of needs. I would like to particularly thank **Steve Robinson**, **Owen Baines** and **Michael Procter** for their expert advice and help during the experimental investigation.

I am forever deeply grateful to my dear family, **my parents, my wife and my son Ahmed, my brothers and my sisters** for their moral support, help and understanding during the whole period of this work.

I take the chance to thank and express my gratitude to all **my friends** for their encouragement, advice and understanding.

I do appreciate the grant and financial support provided by the Higher Education Institute in the **Libyan Government** needed to finish this research.

Finally, I would like to thank everybody who was involved in this work as well as expressing my apology to those I did not mention in this acknowledgment.

CONTENTS

LIST OF FIGURES

LIST OF TABLES

NOTATIONS

The following symbols are used in the present thesis:

A_s	Area of longitudinal bottom reinforcement
A'_s	Area of longitudinal top reinforcement
A_{sh}	Area of horizontal web reinforcement
A_{si}	the area of surface reinforcement crossing the strut
A_{sv}	Area of vertical web reinforcement
a	Shear span
a/d	Shear span-to-depth ratio
a/h	Shear span-to-overall depth ratio
b	Beam width
c	Concrete covers of bottom longitudinal reinforcement
c'	Concrete covers of top longitudinal reinforcement
d	Effective beam depth
d_a	Maximum size of aggregate
E_c	Modulus of elasticity of concrete
E_s	Modulus of elasticity of steel reinforcement
f_{ce}	Effective compressive strength of concrete
f_{cu}	Cube compressive strength of concrete

f_c'	Cylinder compressive strength of concrete
f_t	Tensile strength of concrete
f_y	Ultimate stress of steel reinforcement
f_y	Yield stress of steel reinforcement
G_f	Fracture energy of concrete
h	Overall depth of the concrete beam
K_c	The ratio of second stress invariant in tension to that in compression
L	Span length
l_{EP}	Width of the exterior bearing plate
l_{IP}	Width of the interior bearing plate
l_{LP}	Width of the load bearing plate
P_t	Total load capacity
r_c	Distance from instantaneous centre to middle point of yield line chord
r_s	Distance from instantaneous centre to the point where reinforcing bar crosses the yield line
s_h	Spacing between horizontal reinforcing bars
s_v	Spacing between vertical reinforcing bars
V_{ACI}	Shear capacity predicted by ACI shear provisions
V_{Exp}	Experimental shear force
V_u	Total shear capacity
v	Effectiveness factor of concrete
v_n	Normalised shear capacity
v_p	Viscosity parameter
W_c	Internal energy dissipated in concrete
w_c	Crack opening

W_E	external energy resulted from total applied load
W_I	Total internal energy dissipated in yield line
W_s	Internal energy in the steel reinforcing bar crossing a yield line
w_{ES}	Average effective width of the exterior concrete strut
w_{IS}	Average effective width of the interior concrete strut
w_t	Effective tie width which equals twice the concrete cover
w/c	Water-to-cement ratio
w/p	Water-to-powder
X_{ic}	Horizontal coordinate of the instantaneous centre
Y_{ic}	Vertical coordinate of the instantaneous centre
θ	Angle between the concrete strut and the longitudinal axis of the beam
β	Inclination of the yield line chord
β_s	A factor to account for the effect of cracking and confining reinforcement on the effective compressive strength of concrete in a strut
α	Angle between the relative displacement δ_c and the yield line chord
α_i	Angle between the axis of strut and the surface reinforcing bars crossing the strut
α_s	Angle between reinforcing bar crossing a yield line and relative displacement
α_{sh}	Angle between the relative displacement and horizontal reinforcing bar crossing a yield line
α_{sv}	Angle between the relative displacement and vertical reinforcing bar crossing a yield line
δ_c	Relative displacement vector of concrete across a yield line
δ_s	Relative displacement vector of reinforcement crossing a yield line
ξ	Size effect factor
ω	Rotational displacement of rigid block I in upper-bound analysis

ψ	Dilation angle
ϵ	Hyperbolic flow potential eccentricity
σ_{bo}/σ_{co}	Ratio of concrete strength in the biaxial state to that in the uniaxial state
σ_c	Compressive stress of concrete
σ_{cr}	Cracking stress of concrete
σ_t	Tensile stress of concrete
ε_{cu1}	Ultimate nominal strain of concrete
ε_{c1}	Strain at peak stress of concrete
ε_c	Compressive strain of concrete at any stress σ_c
ε_c^{in}	Inelastic strain of concrete
ε_t	Tensile strain of concrete at any stress σ_t
ε_{cr}	Cracking strain of concrete
ε_y	Yield strain of steel reinforcement
ε_u	Ultimate strain of steel reinforcement
$\emptyset_l$	Longitudinal reinforcement index
$\emptyset_h$	Horizontal reinforcement index
$\emptyset_v$	Vertical reinforcement index
λ	Normalised ultimate load capacity
ρ_{Bott}	Bottom longitudinal reinforcement ratio
ρ_h	Horizontal web reinforcement ratio
ρ_{Top}	Top longitudinal reinforcement ratio
ρ_v	Vertical web reinforcement ratio

ABBREVIATIONS

The following abbreviations are used in the present thesis:

COV	Coefficient of variation
FE	Finite element
GGBS	Ground granulated blast-furnace slag
HRWRA	High range water-reducing admixtures
NC	Normal concrete
RC	Reinforced concrete
SD	Standard deviation
SCC	Self-compacting concrete
STM	Strut-and-tie model
VMA	Viscosity modifying admixtures

CHAPTER ONE

INTRODUCTION

1.1 Introduction

Reinforced concrete deep beams have been very popular structural elements especially when construction requires space that is free of columns. They are used as a load distribution element that receives a high number of small loads and transfers them into a small number of reaction points. They can be found in different civil engineering applications such as stores, hotels, offshore structures, theatres, tanks, pile caps and others. They differ from shallow beams in terms of their small thickness when compared to their high depth and short span. The load transfer mechanism in deep beams is different from shallow beams. The main load transfer element in deep beams is a concrete strut formed between the loading point and support. The load carrying capacity of deep beams is dominated by their shear resistance. However, in shallow beams, especially after the formation of diagonal cracks, arch action becomes the dominant load transfer mechanism. Moreover, the capacity of shallow beams is more likely to be governed by strength in flexure while shear failure governs the capacity of deep beams.

In practice, continuously supported deep beams are mostly used in construction rather than simply supported ones. However, simply supported deep beams were intensively investigated more than the continuous ones. In the case of deep beams made with self-compacting concrete (SCC), all of

the existing research has been conducted on simply supported beams. The failure mode of continuous deep beams is significantly different from that of simply supported deep beams or that of shallow beams. The failure in continuous deep beams generally occurs in regions where high shear simultaneously occurs with high bending moment, whereas in simply supported deep beams the high shear and high moment do not occur in the same region.

In the current design codes, a deep beam is classified as a discontinuity region in which the strain distribution is nonlinear. In this case, deep beams should be analysed as a two dimensional plane stress problem or as a three dimensional element. The classical theory of elasticity is only valid to describe the behaviour of deep beams before cracking. After cracking, however, major redistribution of stresses takes place and the elasticity theory becomes invalid. Therefore, the current design codes suggest that deep beams should be designed either by nonlinear analysis in which the nonlinear strain distribution is taken into account or by the strut-and-tie model (STM). The behaviour of deep beams can also be predicted by numerical simulations such as nonlinear finite element methods.

1.2 Research significance

As mentioned above, there have been no research investigations on reinforced SCC continuous deep beams. This area of research is of special interest due to the high depth of deep beams, making it difficult for normal concrete (NC) to properly be placed and vibrated. SCC offers unique characteristics in quality and economy. It provides a significant quality,

improves productivity and achieves engineering properties similar to those of NC with more durable structures.

The use of SCC leads to the removal of vibration equipment which has a negative effect on the auditory sense of the workers and also people in the neighbourhood surrounding the construction site. Therefore, SCC is the most preferable building material especially when the construction site is close to residential areas. In addition, SCC has high flowability and passing ability which allow the use of complicated and tight formworks with congested reinforcement in the construction of different structural elements. Moreover, the ease of placement and the elimination of external vibration make SCC the most preferable concrete for deep beams which have tight dimensions and congested reinforcement, making it difficult for the compaction equipment to be used.

In addition, the lower amount and smaller size of coarse aggregate used in SCC lead to different behaviour from NC. Moreover, inadequate vibration causes high surface permeability, unfilled voids and micro-pores within NC which, in turn, results in negative effects on mechanical properties and durability of NC. SCC requires no vibration as it can easily flow and be placed under its self-weight with excellent surface finishes and homogenous distribution of concrete within the formwork, resulting low surface permeability and, consequently, improved durability.

1.3 Aims and objectives of the research

The main aim of this research is to investigate the behaviour of continuously supported deep beams made with SCC. The main objectives of the research are summarized below:

- To experimentally investigate the behaviour of continuously supported deep beams made with SCC.
- To examine the applicability of the design guide lines available for continuous deep beams against the experimental results of continuously supported SCC deep beams.
- To propose a new equation for the effectiveness factor of SCC that can be implemented in the lower-bound analysis of continuously supported SCC deep beams.
- To develop a three dimensional nonlinear finite element model to analyse the behaviour of SCC continuous deep beams and conduct a series of parametric studies. The proposed model will be evaluated against the present and previous experimental results.

1.4 Research methodology

To achieve the aims and objectives of this research, the following research strategy approaches have been employed:

- Eight full-scale continuously supported SCC deep beams were constructed and tested to study the influence of various parameters such as shear span-to-depth ratio, amount and configuration of web reinforcement and main longitudinal reinforcement ratios on the

behaviour of SCC continuous deep beams including cracking load, load carrying capacity, strains in reinforcement, deflection and shear strength.

- The design recommendations suggested by different codes of practice as well as the design methods proposed by researchers for the shear strength of continuous deep beams were assessed against the experimental results of continuous SCC deep beams.
- A three dimensional nonlinear finite element model using ABAQUS 6.12 has been developed to analyse the effect of different parameters considered in this research on the behaviour of SCC continuous deep beams and conduct a series of parametric studies to explore the structural behaviour of continuous SCC deep beams with extended parameter variations, both within and outside the range of experiments.

1.5 Report Structure

This chapter presents a general introduction about deep beams and self-compacting concrete. It also summarizes the importance as well as the main aims and objectives of the research. The next chapter explores and reviews the main findings of previous research on SCC including summary of fresh and hardened properties of SCC. It also includes a general overview of the current design codes of practice and guidelines for the analysis of continuous deep beams. Finally, it presents an analysis for the previous experimental and theoretical investigations on continuous deep beams and draw some conclusions on the effect of key parameters on the behaviour of continuous deep beams.

Chapter three presents the experimental investigation conducted on continuously supported SCC deep beams. The material properties and test methodology are described along with the test results and discussions.

In chapter four, the design recommendations suggested by current codes of practice as well as the design methods proposed by researchers are evaluated against the experimental results of SCC continuous deep beams and other results collected from previous studies on continuously supported NC deep beams. Moreover, new effectiveness factor equations are proposed to be implemented in the lower bound analysis of continuously supported SCC deep beams.

A three dimensional nonlinear finite element model using ABAQUS 6.12 software is proposed in chapter five to analyse the behaviour of reinforced SCC continuous deep beams. The finite element model is verified using the experimental results of the current study as well as different case studies from the literature

In chapter six, the three dimensional finite element model proposed in chapter five is used to carry out a series of parametric studies. The main aim of this chapter is to explore the structural behaviour of continuous SCC deep beams with extended parameter variations, both within and outside experimental range.

Finally, chapter seven summarizes the main conclusions from the current research and presents recommendations and suggestions for future work.

CHAPTER TWO
LITERATURE REVIEW

2.1 Introduction

In spite of the fact that SCC has been known as a construction material for less than 30 years which is considered as a very short history when compared to normal concrete (NC), it has been used in an extremely wide range of applications such as piles, retaining walls, columns, deep beams, marine structures and bridges. This has allowed a high amount of research and development to take place in the field of SCC. Therefore, an intensive range of journal papers and international conferences have been published during the last two decades and these publications were significantly increased in the last few years leading to a considerable richness of literature that describes different properties, features and applications of SCC.

This chapter presents an overview and summary of the most vital information on SCC and continuously supported deep beams. The literature of this research will be divided into two main parts. The first part will present the general behaviour of SCC including the fresh and hardened properties while the second part will review the different parameters that affect the behaviour of continuous deep beams and different theoretical and numerical methods that have been applied to predict the behaviour of deep beams.

2.2 Self-compacting concrete

SCC has been used in a wide range of applications and it is considered to be an important alternative for the conventional concrete. It offers another choice and expands the area of engineering properties for engineers and designers. The invention of SCC has significantly benefited the construction industry due to its unique features in quality and economy. In spite of the fact that SCC has been increasingly applied as a construction material since it was innovated in 1987, there are some disadvantages that counteract the use of SCC in wider applications. In this section, the most important advantages of SCC will be presented and evaluated against its disadvantages. Moreover, the fresh and hardened properties of SCC as well as some correlations between the hardened properties of SCC will be reviewed.

2.2.1 Advantages and disadvantages of SCC

One of the most important advantages of SCC is the elimination of vibration which reduces the number of in-situ workers, lowers the total cost of construction, decreases the construction time and minimizes the noise level. The elimination of vibration also helps to avoid any health problems that might be caused by the use of vibration equipment. It was reported that when SCC is used in large applications, the total time of construction and the number of workers can be reduced by about 20 to 30% with comparison to NC (Okamura and Ouchi, 2003). In addition, the production of SCC can overcome most of the disadvantages which may result from inadequate vibration and poor skills of labourers in the construction site. For example,

insufficient compaction leads to the existence of air voids within the fresh mixture which as a result reduces the strength properties of hardened concrete.

SCC can be used to fill some structural elements that cannot be properly vibrated such as piles, deep beams and columns. Moreover, SCC can flow through and fill the areas of congested reinforcement and complicated formwork without any segregation. It also provides a significant quality and better surface finish and results in engineering properties similar to those of NC. Finally, the use of SCC leads to structures with improved long-term durability compared to structures made with NC. The durability of concrete is in direct relation with the permeability of the surface layer which resists the attack of harmful actions such as sulphate, acids and alkali (BIBM et al., 2005). Low surface permeability requires special vibration and high degree of supervision during placement, surface finishing and curing. SCC requires no vibration as it can easily flow and be placed under its self-weight with excellent surface finishes and as a result a low surface permeability is achieved, leading to improved durability (BIBM et al., 2005).

On the other hand, there are some disadvantages that counteract the use of SCC in wider applications. Initially, in order to produce SCC with sufficient properties, it requires designers with high levels of experience to control the inconsistent properties of SCC. For example, SCC requires achieving high fluidity and passing ability with high segregation resistance at low water-to-powder (w/p) ratio to ensure reasonable hardened properties (Du and Folliard, 2005). Moreover, SCC has lower modulus of elasticity compared to NC due to the lesser amount and smaller particle size of coarse aggregate

(Parra et al., 2011; Turcry et al., 2002). Furthermore, the drying shrinkage of SCC is higher than that of NC due to the high cement content and low coarse aggregate content required for achieving the essential fresh and hardened properties (Hwang and Khayat, 2008; Kim et al., 1998; Heirman and Vandewalle, 2003). Furthermore, there is some concern among researchers and designers that SCC may not be strong enough in shear because of the lower amount and smaller size of coarse aggregate, higher fine materials content and higher paste volume making SCC more susceptible to cracks (Alrifai et al., 2013; Kim et al., 2007). Taylor (1974) illustrated that the aggregate interlock contributes about 50% of the total shear capacity of concrete. This means that the shear strength of SCC with low coarse aggregate content is significantly lower than that of NC (Hassan et al., 2008; Hassan et al., 2010a, 2010b; Lin and Chen, 2012). Finally, there are no standard methods or specifications for proportioning SCC materials and predicting its fresh and hardened properties. Although some publications applied different mix design approaches, none of these publications was published in full detail (Su et al., 2001; Chai, 1998; Su and Miao, 2003; Hwang and Hung, 2005).

However, these disadvantages can be reduced or eliminated. For example, the high drying shrinkage of SCC can be reduced or eliminated by the use of alternative cementitious materials such as fly ash and ground granulated blast-furnace slag (GGBS) (Maslehuddin et al., 1987; Sahmaran et al., 2007). The importance of high flowability, deformability and passing ability of SCC are significantly required in a wide range of applications and therefore the benefits obtained from the use of SCC overweight its drawbacks.

2.2.2 Fresh properties of SCC

The main difference between SCC and other concrete mixtures is the required targets for its fresh properties. To produce SCC with acceptable engineering properties, its fresh properties must be controlled and balanced. However, the main problem is that there are no standard methods for testing and measuring these properties. In this part of the literature review, the fundamental fresh properties of SCC such as flowability, passing ability, segregation resistance and filling ability are summarised with the most popular tests that are used to evaluate these properties.

2.2.2.1 Flowability

The flowability, sometimes called as deformability or fluidity, is the property of concrete that describes the ease of concrete to flow under its own weight without external energy. The flowability is affected by many factors such as the size, shape and volume of aggregate as well as the friction between the solid particles. However, the main factors that have the most effect on the flowability of concrete are the superplasticizer content, w/p ratio and powder content (Chai, 1998). The flowability of SCC is restricted by the shape and dimensions of the formwork as well as the volume and distribution of reinforcement. It can be assessed by the slump flow test or by L-box test. The recommended values for the average flow diameter of concrete ranges from 650 to 800 mm (Skarendahl and Petersson, 2000).

2.2.2.2 Passing ability

The passing ability or the resistance to blocking is defined as the ability of concrete to flow through narrow and complicated formwork and also through

congested reinforcement. The passing ability of concrete can be measured by the L-box test, U-box test and J-ring test (Skarendahl and Petersson, 2000). It can be assessed by performing the slump test with and without the J-ring and measuring the difference in the slump values in between them. The higher difference in the slump value with and without the J-ring indicates poor passing ability of concrete (Daczko, 2012). The passing ability depends mainly on the coarse aggregate content and the flowability of concrete. It is also restricted by the spacing of reinforcing bars (Noguchi et al., 1999; Chai, 1998).

2.2.2.3 Segregation resistance

The resistance to segregation is one of the most important among the fresh properties of SCC due to its high fluidity and the existence of free water in the mixture (Ozawa et al., 1990). Therefore, it must be carefully evaluated to guarantee a homogenous distribution for concrete within the formwork. The segregation resistance can be improved by increasing the paste volume and also by the addition of high range water-reducing admixtures (HRWRA) and viscosity modifying admixtures (VMA) to the concrete mixture (Skarendahl and Petersson, 2000; Daczko, 2012). The segregation resistance is not easy to evaluate and the known tests for measuring this property are not accurate enough (Chai, 1998; Skarendahl and Petersson, 2000). The most popular test to assess the resistance of concrete to segregation or separation is the sieve stability test. It can also be examined by either settlement (segregation) column test or penetration test (Skarendahl and Petersson, 2000).

2.2.2.4 Filling ability

The filling ability describes the ease of concrete to flow under its self-weight to totally fill all the spaces inside the formwork and between the reinforcement bars (Okamura et al., 2000). It can be measured by the slump flow test and the flow rate values which can be evaluated by either T_{500} or V-funnel tests (Skarendahl and Petersson, 2000). The greater the T_{500} value, the higher the plastic viscosity of concrete which results in higher filling ability (Daczko, 2012). The filling ability can be enhanced by adding superplasticizer and decreasing the amount of coarse aggregate (Sonebi and Bartos, 2002; Khayat et al., 1999)

2.2.3 Hardened properties of SCC

The main difference between SCC and NC is the lower coarse aggregate content and the higher powder content required to produce SCC. Therefore, this might result in dissimilarity between SCC and NC in terms of the hardened properties such as compressive and tensile strengths as well as the modulus of elasticity. The European guidelines for SCC reported that SCC and NC designed for similar strength should achieve comparable mechanical properties (BIBM et al., 2005). The mechanical properties are significantly affected by the type and content of the raw materials of SCC. For example, it was indicated that SCC made with a 10 mm maximum size of aggregate has higher strength and elastic modulus than that made with a higher maximum size of aggregate (Khaleel et al., 2011; Almeida-Filho et al., 2010).

On the other hand, ACI 237R (2007) pointed out that SCC and NC could have similar hardened properties if they are made with similar raw materials and designed to achieve similar strengths. It was also reported that the strength of SCC, in general, is similar to that of NC and the durability of SCC is better than NC (Jin, 2002; Mata, 2004). In this part of the literature, some mechanical properties of SCC, including compressive strength, tensile strength and modulus of elasticity, are briefly discussed.

2.2.3.1 Compressive strength

The compressive strength is the most important characteristic among the hardened properties of any concrete mixture. In general, SCC is used to produce high strength concrete because of the requirements of its fresh properties such as low w/p ratio and high powder content as well as the use of HRWRA. Domone (2007) reported that the compressive strength is affected more by the powder content rather than the w/p ratio. The powder content consists of cement and supplementary cementitious materials such as fly ash, GGBS and silica fume which are considered as the key factor that govern the compressive strength of any concrete mixture (Domone, 2006, Domone, 2007, Klug et al., 2003).

Klug et al. (2003) created a database to investigate the behaviour of SCC in the hardened state. They found that at similar w/p ratio, SCC and NC have similar compressive strength in the early and later stages. However, from the analysis of the database, they noticed that, in few cases, SCC achieved a 28-day compressive strength higher than that achieved by NC. The higher compressive strength of SCC can be attributed to the better interface between the aggregate and the cement mortar (BIBM et al., 2005). On the

other hand, Domone (2007) and Daczko (2012) reported that the development of the early-age strength is slower in SCC than in NC whereas the final strength is similar. The delay of the early-age strength of SCC can be attributed to the use of supplementary cementitious materials such as fly ash and GGBS. The early-age strength of SCC can significantly be improved by the use of HRWRA which also slightly improves the final strength of concrete (ACI 237R, 2007).

2.2.3.2 Splitting tensile strength

The tensile strength is important for estimating the load after which the cracks start to appear and propagate within reinforced concrete members subjected to flexure. It is directly related to the compressive strength. The higher the compressive strength of concrete, the higher tensile strength that can be achieved (Druta et al., 2014). Therefore, its value relies on the w/p ratio, the quantity and type of coarse aggregate and mainly the interlock between the aggregate particles and the cement paste (ACI 237R, 2007). In the literature, there are few studies that focus on the splitting tensile strength of SCC and there is no agreement between them about the behaviour of SCC under splitting tensile tests. Like compressive strength, the tensile strength of SCC can be similar to or higher than that of NC if they are made of similar mixture proportions (ACI 237R, 2007). Domone (2007) indicated that there is no clear difference in the value of splitting tensile strength between SCC and NC.

However, Klug et al. (2003) created a database to analyse the mechanical properties of SCC. They indicated that about one third of the data showed higher tensile strength achieved by SCC. They attributed that to the better

microstructure of SCC mixture due to the denser cement matrix and lower porosity within the interfacial transition zone. Klug et al. (2003) also indicated that the early-age splitting tensile strength depends on the use of supplementary cementitious materials similar to the case with compressive strength. These findings were also agreed by Fava et al. (2003) and Zhu et al. (2004) who illustrated that the tensile strength of SCC is normally higher than that of NC. Druta et al. (2014) also pointed out that, for SCC, the splitting tensile fracture occurs within the coarse aggregate particles compared to NC where the tensile fracture normally takes place through the interfacial transition zone.

2.2.3.3 Modulus of elasticity

Generally, similar to NC, the modulus of elasticity of SCC is decreased with decreasing the aggregate content and with increasing the paste volume (Daczko, 2012; ACI 237R, 2007; Klug et al., 2003). It is also affected by the compressive strength and the unit weight of concrete (ACI 237R, 2007). Parra et al. (2011) and Turcry et al. (2002) reported that the modulus of elasticity of SCC is normally 2% lower than that of NC because of the higher volume of cement paste required to produce SCC. In contrast, ACI 237R (2007) pointed out that for SCC and NC of similar compressive strength, the modulus of elasticity is about 10 to 15% less in SCC. However, contradictory results showed that for similar compressive strength, there is no clear difference in the modulus of elasticity between SCC and NC (Persson, 1999; Skarendahl and Petersson, 2000; Schindler et al., 2007). Other observations indicated that for low and medium compressive strength, the elastic modulus

of SCC is lower than that of NC by about 20 to 40% whereas for high strength concrete it is 5% less in SCC (Klug et al., 2003; Domone, 2007).

ACI 237R (2007) revealed that the modulus of elasticity of SCC can be improved by making a few adjustments to the raw materials specifically the sand-to-total aggregate ratio and the powder content. Moreover, Mörtsell and Rodum (2001) reported that SCC made with low powder content, less than 400 kg/m^3, developed a modulus of elasticity similar to NC made with same powder content.

2.2.4 Correlation between mechanical properties of SCC

In different design codes as well as in different international publications the compressive strength is used to estimate different mechanical properties of concrete such as tensile strength and modulus of elasticity.

With regard to the correlation between the compressive strength and the splitting tensile strength, the literature shows a clear difference between SCC and NC. Different studies showed that the ratio of tensile strength to compressive strength is 10 to 30% higher in SCC than in NC (Pentti, 1999; Gibbs and Zhu, 1999). In the literature different relationships were provided to estimate the value of tensile strength depending on the 28-day compressive strength. These relationships, however, are different from those provided by Hu et al. (2004) and Sinaei et al. (2012) for NC. Table 2.1 shows different equations collected from previous studies for predicting the tensile strength. It can be seen from these models that there is a clear disagreement among researchers about the relationship between compressive and tensile strength of SCC which is similar to the case of NC.

In terms of the relationship between the modulus of elasticity and the compressive strength for SCC, there are different equations in the literature that describe this relationship. These equations show a clear disagreement among researchers about the validity of using the same relationships developed for NC to calculate the modulus of elasticity of SCC. For example, ACI 237R (2007) showed that in order to estimate the modulus of elasticity of SCC, equations developed for NC can be used with reasonable accuracy. Kumar et al. (2011) also pointed out that the expression suggested by ACI Building Code for NC can be used to predict the modulus of elasticity of SCC with some conservatism. In contrast, the literature showed different expressions developed to calculate the modulus of elasticity of SCC. Table 2.1 illustrates the different models developed by previous studies for estimating the modulus of elasticity of SCC depending on the value of compressive strength. It is clearly shown that, the relationship between the compressive strength and modulus of elasticity of SCC has not been given a clear definition. This due to the disagreement among researchers about whether the elastic modulus of SCC is similar or lower than that of NC.

Table 2.1: Correlation between compressive strength, tensile strength and modulus of elasticity

References	Tensile strength (MPa)	Elastic modulus (MPa)
Parra et al. (2011)	$f_t = 0.28 * f_c'^{\frac{2}{3}}$	-
Hu et al. (2004)	$f_t = 0.33 * \sqrt{f_c'}$	-
Sinaei et al. (2012)	$f_t = 0.61 * \sqrt{f_c'}$	-
Felekoğlu et al. (2007)	$f_t = 0.43 * f_c'^{0.6}$	$E_c = 1570 * f_c'^{0.8}$
Dinakar et al. (2008)	$f_t = 0.82 * \sqrt{f_c'}$	$E_c = 4180 * \sqrt{f_c'}$
Topçu and Uygunoğlu (2010)	$f_t = 0.0602 * f_c' + 0.2009$	-
Sukumar et al. (2008)	$f_t = 0.0843 * f_c' + 0.818$	-

ACI 318R-14	-	$E_c = 4700 * \sqrt{f_c'}$
Kumar et al. (2011)	-	$E_c = 5300 * \sqrt{f_c'}$
Persson (2001)	-	$E_c = 3750 * \sqrt{f_c'}$
Leemann and Hoffmann (2005)	-	$E_c = 4740 * \sqrt{f_c'}$

where f_c' is the compressive strength in MPa, f_t is the tensile strength in MPa, E_c is the modulus of elasticity in MPa.

2.3 Structural elements made with SCC

Since it was invented in the late 1980s, SCC has been successfully used in wide range of structural elements. It has been widely used to fill steel tubular columns (Binh et al., 2016; Rui et al., 2013; Lu et al., 2010; Han et al., 2005; Schneider, 1998; etc) to overcome the difficulties arise from the use of NC in columns and improve the total capacity and fire resistance. It has also been used in shallow beams (Lachemi et al., 2005; Hassan et al., 2008; Salman et al., 2013; Shen et al., 2015; etc) and simply supported deep beams (Mohammadhassani et al., 2011; Mohammadhassani et al., 2012a, 2012b; Shah and Modhera, 2010, 2012; Rasheed and Alobaidi, 2012; etc). In the case of continuously supported deep beams, all the previous research investigations were conducted on continuous deep beams made with NC. Therefore, the main focus of the next sections will be on the behaviour of continuous NC deep beams. A database will be created consisting of continuously supported NC deep beams collected from different previous studies in order to investigate the effect of different parameters on the

behaviour of continuous NC deep beams and validate different design approaches that have been used to predict the capacity of continuous deep beams.

2.4 Definition of deep beams

Deep beams are structural elements that known by their high depth compared to the span length. Although the current design codes have recommended the clear span-to-depth ratio to define deep beams, there is disagreement on its limiting value. The shear provisions of the ACI Building Code (ACI 318M-11) define deep beams as a member whose clear span is equal to or less than four times its overall depth and, in another clause, as a member having a shear span-to-depth ratio less than 2. In contrast, the Euro Code 2 (EC2) considers any beam for which the span is not greater than three times its overall depth as a deep beam. On the other hand, the Canadian Standard (CSA23.3-04) classifies members having a clear span to overall depth ratio less than two as deep beams.

2.5 Continuous deep beams database

In order to deeply understand the behaviour of continuously supported deep beams and investigate the effect of different parameters on the behaviour of continuous deep beams, a database is created in this section. The database will also be used to assess the different design guidelines available for deep beams. Due to the fact that SCC has never been used in continuous deep beams, the collected database will consist of a number of continuous deep beams made with NC available in the literature. A total of 76 NC continuous deep beams were collected from six different previous investigations as

shown in Table 2.2. The full details of the beams in the database are shown in Appendix A.

Table 2.2: Database of NC continuous deep beams

Reference	No. of Beams	Range of parameters					Web reinforcement arrangement
		a/h	h mm	b mm	L mm	f_c' MPa	
Rogowsky et al. (1986)	16	1.0 1.67 2.0	500 600 1000	200	2100	15 - 47	Vertical Horizontal
Ashour (1997)	8	1.1 1.6	425 625	120	1340	23 - 39	Vertical Horizontal
Subedi (1998)	4	0.63 1.25 1.4	400 600	50 75	500 1000 1680	45 - 57	Vertical Horizontal
Asin (2000)	12	1.1 1.8	600 1000	150	2300	28 - 37	Vertical
Yang et al. (2007a)	24	0.5 0.6 1.0	600	160	600 720 1000	32 - 68	Vertical Horizontal
Yang et al. (2007b)	12	0.5 0.6 1.0	400 600 720	160	400 600 720 800 1000	32 - 77	None

where a/h is the shear span-to-overall depth ratio, h is the beam total depth, b is the beam width, L is the span length and f_c' is the concrete compressive strength.

In the database, as shown in Table 2.3, the shear span-to-overall depth ratio, a/h, ranged from 0.5 to 2.0, the overall depth of the beams, h, varied between 400 to 1000 mm and the span of the beams, L, ranged between 400 to 2300 mm. About half of the beams had $0.5 < a/h \leq 1.0$ while the

lowest number of beams had a/h ratio equal to or less than 0.5 as shown in Figure 2.1. Moreover, the tested beams were made with NC having a compressive strength, f_c', ranging between 15 and 77 MPa. More than 50 beams were made with a medium compressive strength ranging between 25 and 50 MPa whereas 20 beams had a compressive strength higher than 50 MPa and a very small number of beams were made with concrete of a compressive strength of less than 20 MPa as shown in Figure 2.2. Furthermore, the web reinforcement included four different arrangements: none, vertical only, horizontal only and orthogonal. As can be seen from Figure 2.3, the highest number of the beams had only vertical web reinforcement followed by beams without shear reinforcement. The horizontal reinforcement was used in 30 beams, half of them had no vertical reinforcement while the rest had both vertical and horizontal reinforcement.

Table 2.3: Range of parameters investigated in the database

Parameter	Range		Mean
	Min	Max	
f_c' (MPa)	15	77	46
a/h	0.5	2.0	1.25
h (mm)	400	1000	700
b (mm)	50	200	125
L (mm)	400	2300	1350

where a/h is the shear span-to-overall depth ratio, h is the beam total depth, b is the beam width, L is the span length and f_c' is the concrete compressive strength.

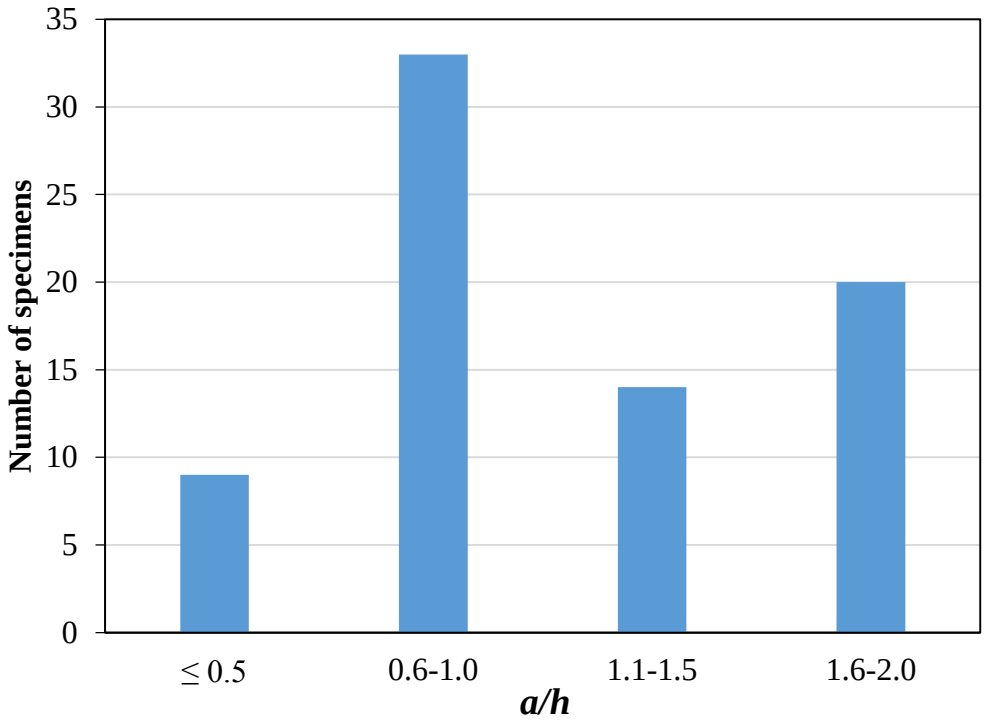

Figure 2.1: Distribution of *a/h* ratio of continuous deep beams in the database

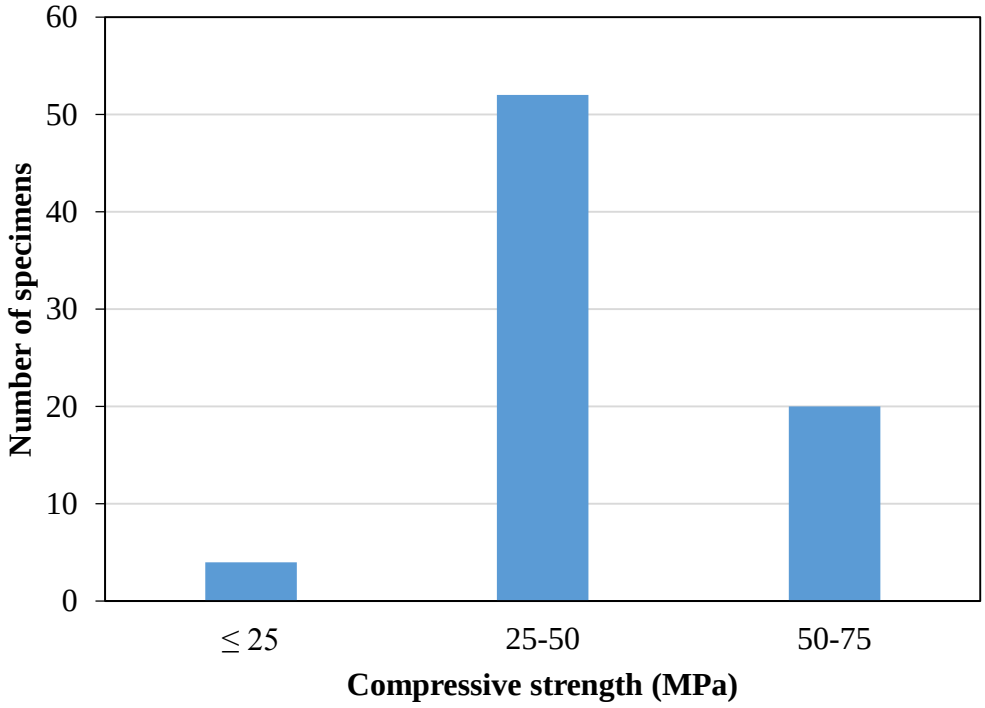

Figure 2.2: Distribution of compressive strength of continuous deep beams in the database

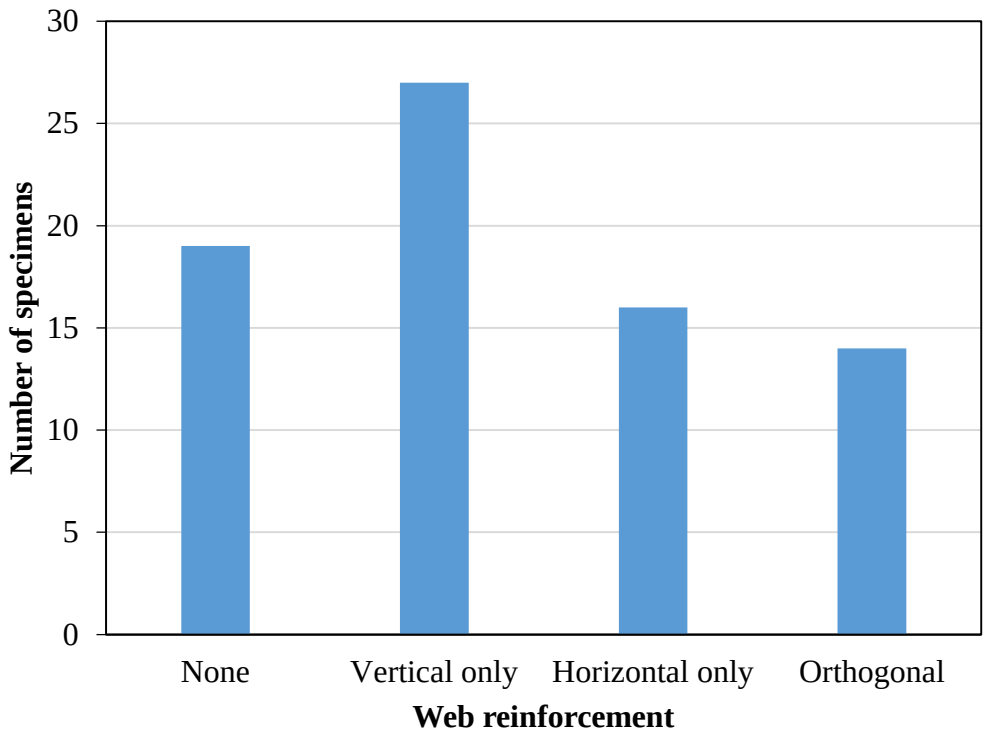

Figure 2.3: Distribution of web reinforcement arrangement of continuous deep beams in the database

All beams collected in the database failed in shear due to a major diagonal crack connecting the load and the intermediate support plates. This database will be used to validate the methods suggested by different design codes and different research investigations for predicting the load capacity of continuous deep beams (see section 2.7). The database will also be used to draw some relationships between the load capacity and some key parameters such as the effect of a/d ratio and compressive strength on shear capacity. Moreover, some of the continuous deep beams from the database will be used in chapter five as examples to validate the proposed finite element model.

2.6 Behaviour of deep beams

Due to the high depth and small a/d ratio, the structural behaviour of deep beams is significantly different from that of shallow beams. The main load transfer element in deep beams is a concrete strut formed between the loading points and supports (Ashour, 1997; Yang et al., 2007a, 2007b). The structural behaviour and strength of deep beams mainly depend on some key parameters. The most important among these parameters is the a/d ratio followed by the amount and configuration of web reinforcement which in turn is significantly affected by the a/d ratio as it will be discussed later in this section (Yang and Ashour, 2008). The compressive strength of concrete and the longitudinal top and bottom reinforcement are also important factors that influence the behaviour of deep beams. In this section, the structural behaviour of continuously supported deep beams is discussed including the mode of failure as well as the effect of the key parameters mentioned above on the behaviour of deep beams.

2.6.1 Failure modes

The failure modes of continuous deep beams is significantly different from that of simply supported deep beams or that of shallow beams. The failure in continuous deep beams generally occurs in regions where high shear simultaneously occurs with high bending moment, whereas in simply supported deep beams the high shear and high moment do not occur in the same region (Ashour, 1997; Asin, 2000). A number of experimental investigations on continuously supported deep beams showed that the main cause of failure in continuous deep beams is normally a major diagonal crack

that starts at the mid-depth of beams and extends along the distance between the edge of the load and intermediate support plates, separating the beam into two rigid blocks: one rotating about the end support leaving the rest of the beam fixed over the other supports, as shown in Figure 2.4 (Rogowsky et al., 1986; Ashour, 1997; Yang et al., 2007a, 2007b; Yang and Ashour, 2011).

In spite of the fact that the main cause of failure in deep beams is a major diagonal crack as mentioned above, the structural response of continuous deep beams can be described in different ways depending on the geometrical dimensions of the beam, the material properties and the amount and configuration of the reinforcement. For example, Rogowsky et al. (1986) observed that continuous deep beams having a/d ratio of 1.0 and large number of stirrups failed in a very ductile manner while those without or with low amount of vertical reinforcement exhibited brittle failure. The same study also showed that beams with a high a/d ratio failed due to a crushing of the compression strut along with opening of the diagonal cracks while those with a low a/d ratio failed due to opening of diagonal cracks. Similar modes of failure (compression strut crushing and concrete separation) were observed by Ashour (1997), Yang et al. (2007a, 2007b) and Asin (2000). On the other hand, deep beams might exhibit a premature failure or bearing failure due to the crushing of concrete under the loading plates. This mode of failure is not preferred as it leads the beam to fail before reaching its full capacity. This type of failure can be prevented by accurately considering the area of the load plates to properly distribute the load on the full body of the beam.

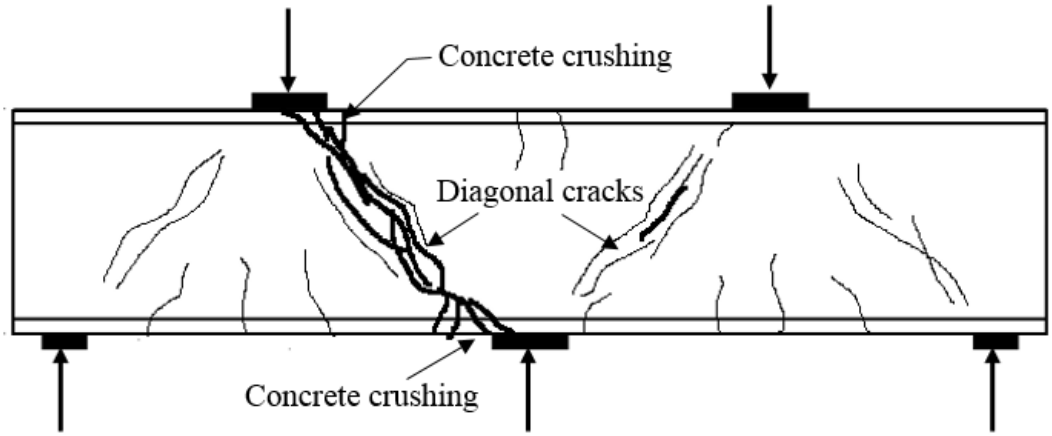

Figure 2.4: Mode of failure of continuously supported deep beams

2.6.2 Effect of shear span-to-depth ratio on the behaviour of continuous deep beams

As mentioned earlier, a/d ratio is one of the main parameters that control the shear strength of continuous deep beams. It is well known and has been approved by many research investigations that the shear strength remarkably increases with reducing the a/d ratio (Rogowsky et al., 1986; Ashour, 1997; Asin, 2000; Yang et al., 2007a, 2007b). Experimental results of continuous deep beams showed that the load capacity of beams having an a/d ratio of 0.5 was about twice that of beams having an a/d ratio of 1.0 (Yang et al., 2007a, 2007b). Figure 2.5 shows the relationship between the shear span-to- depth ratio, a/d, and the normalised load capacity, λ, ($\lambda = P_t/bhf_c'$) for the continuous deep beams without web reinforcement collected in the database (19 beams). The relationship clearly shows that irrespective of the value of the longitudinal reinforcement index ($\emptyset_l = A_s f_y/bhf_c'$), increasing the a/d ratio leads to a clear reduction in the normalised load capacity of continuous deep beams.

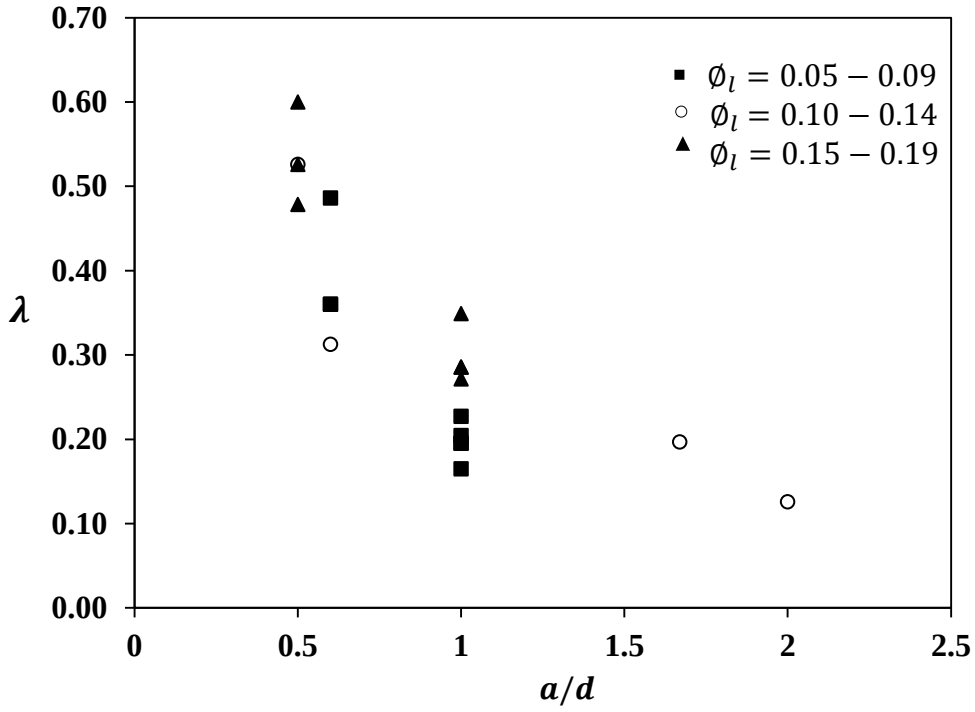

Figure 2.5: Effect of a/d ratio on the normalised load capacity of beams without web reinforcement

The a/d ratio also controls the effect of some other parameters such as web reinforcement and compressive strength on the strength of continuous deep beams. As it will be explained in the next section, as the a/d ratio increases, the horizontal web reinforcement becomes less effective while for low a/d ratio, the vertical web reinforcement becomes less effective in carrying loads (Yang and Ashour, 2008).

In addition, the a/d ratio has a significant effect on the crack propagation, crack width and failure modes. The higher the a/d ratio, the higher number of cracks occur and the higher depth of cracks were observed (Yang et al., 2007b). It was also shown that after the development of the diagonal crack, beams with a high a/d ratio failed quicker than those having a low a/d ratio

(Yang et al., 2007b). However, Ashour (1997) indicated that the higher the a/d ratio, the more ductility that can be obtained at failure.

2.6.3 Effect of shear reinforcement

The web reinforcement required for deep beams practically consists of either vertical bars perpendicular to the main longitudinal reinforcement of the beam, horizontal bars parallel to the main longitudinal reinforcement or both together. ACI 318M-11 stated that the area of web reinforcement required for deep beams in both directions shall not be less than $0.0025bs$, where s is the spacing between the vertical or horizontal web reinforcement bars and b is the beam web width. The effect of the type of shear reinforcement on the behaviour of deep beams significantly depends on the a/d ratio. As the a/d ratio decreases, the diagonal cracks become more vertical, indicating that the horizontal reinforcement has a greater effect on the strength of the beam and the vertical reinforcement becomes less effective. However, there is disagreement among researchers on the limits of the a/d ratio at which the vertical or horizontal web reinforcement becomes more prominent.

For continuously supported deep beams having an a/d ratio greater than 0.75, Rogowsky et al. (1986) illustrated that the horizontal web reinforcement has no effect on the load capacity of the tested beams. These results agreed with the results obtained by Ashour (1997) who showed that the vertical web reinforcement is more effective in carrying loads than the horizontal reinforcement for beams having a/d ratios of 0.8 and 1.18. However, experimental investigations conducted by Yang et al., (2007a, 2007b) revealed that the vertical web reinforcement is more prominent for an a/d

ratio equal to or greater than 1.0 while the horizontal web reinforcement has more influence on the shear capacity for an a/d ratio of 0.5.

It is difficult to decide whether the vertical or horizontal web reinforcement is more effective as it requires a large number of test specimens with different a/d ratios and different amounts and configurations of web reinforcement. However, Yang and Ashour (2008) concluded that the horizontal web reinforcement is more effective for an a/d ratio not greater than 0.6, otherwise the vertical reinforcement is more effective.

From the database presented earlier, Figures 2.6 and 2.7 show the effect of vertical shear reinforcement index, ϕ_v, ($\phi_v = A_{sv}f_y/s_v b f_c'$) and horizontal shear reinforcement index, ϕ_h, ($\phi_h = A_{sh}f_y/s_h b f_c'$) on the normalised load capacity of continuous deep beams for different a/d ratios, respectively. Figure 2.6 is for beams having vertical web reinforcement only while Figure 2.7 is for beams having horizontal web reinforcement only. In general, the normalised load capacity gradually increases with increasing the vertical or horizontal web reinforcement index. However, the increasing rate of the load capacity varies depending on the a/d ratio and the configuration of web reinforcement. For a higher a/d ratio ($1.0 \leq a/d \leq 2.0$), it can be clearly noticed that the vertical web reinforcement has more influence on the normalised load capacity. On the other hand, increasing the horizontal web reinforcement index led to a noticeable increase in the normalised load capacity with a higher rate of increase for beams having a low a/d ratio.

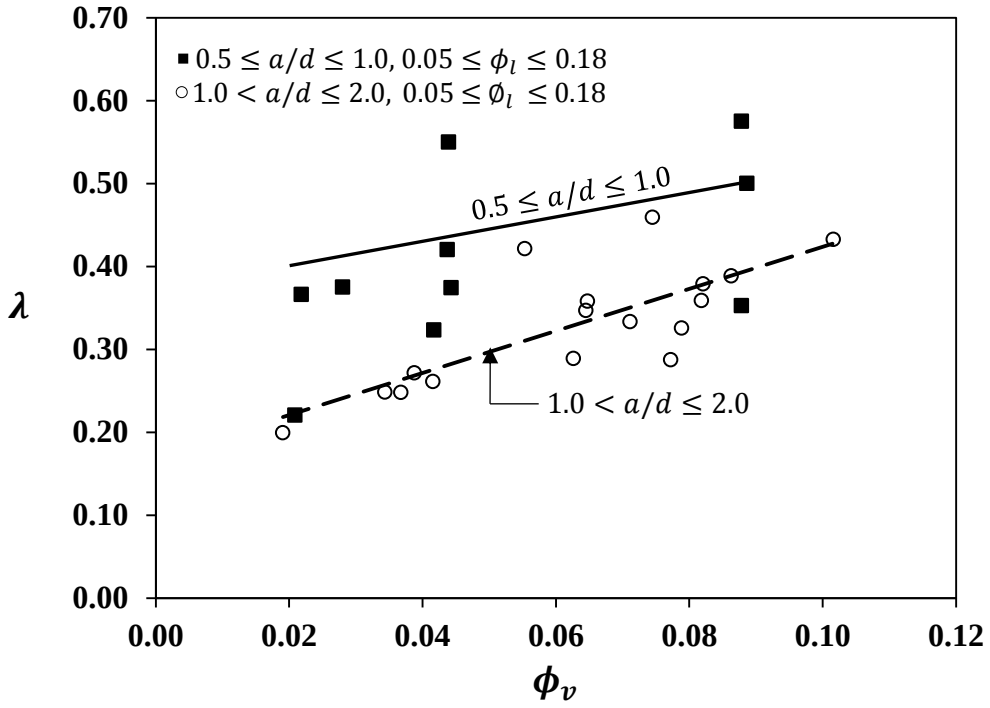

Figure 2.6: Effect of vertical reinforcement index on the normalised load capacity of beams having vertical reinforcement only

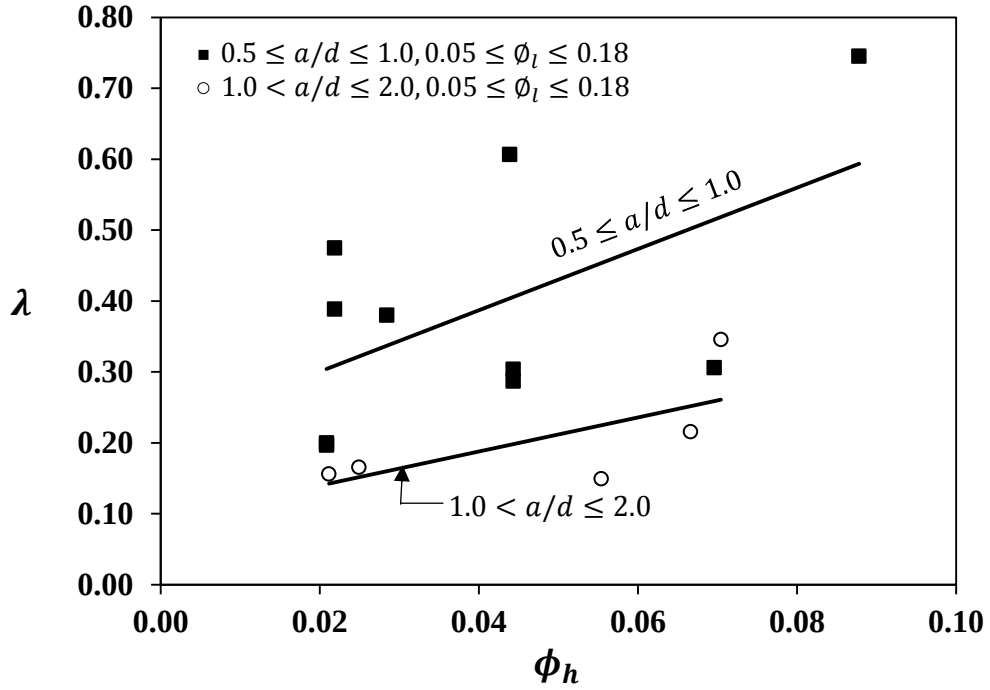

Figure 2.7: Effect of horizontal reinforcement index on the normalised load capacity of beams having horizontal reinforcement only

2.6.4 Effect of compressive strength

Compressive strength of concrete is considered as one of the most important factors that control the load carrying capacity of deep beams, especially those with a low a/d ratio. The load in deep beams is transferred through compression struts and the resistance of these struts mainly depends on the concrete compressive strength and the failure mainly occurs due to compression strut failure. However, there is a lack of research in the experimental investigations on continuously supported deep beams that has focused specifically on the relationship between the compressive strength and the load carrying capacity. Using the database of 76 continuous NC deep beams, there was no conclusion for the effect of compressive strength on the load capacity of continuous deep beams because of the effect of other parameters and therefore the relationship was not presented here. Generally, the load capacity of deep beams gradually increases with the increase in the compressive strength (Yang and Ashour, 2008). However, it was indicated that changing the value of the compressive strength does not have any effect on the structural behaviour of continuous deep beams such as the failure mode and the crack pattern (Yang et al., 2007a, 2007b).

2.6.5 Effect of longitudinal reinforcement

Similar to the compressive strength, there is a lack of information regarding the effect of the ratio of top and bottom longitudinal reinforcement on the behaviour of deep beams. Asin (2000) concluded that changing the amount of top or bottom longitudinal reinforcement does not have any clear effect on the shear strength of deep beams, but it had some effect on the distribution

of the support reactions. However, it was indicated that more variation in the strain along the longitudinal top and bottom reinforcement was observed for beams having a high a/d ratio which means that the effect of the longitudinal reinforcement ratio is more pronounced for beams with a high a/d ratio (Ashour, 1997).

2.7 Load capacity prediction methods for continuous deep beams

The theory of elasticity can be applied to deep beams before cracking. However, after cracking, deep beams exhibited a high redistribution of stresses and nonlinear strain which is difficult to describe accurately by elastic analysis. In the literature, different approaches have been developed to analyse shear in deep beams. The ACI Building Code provides special shear provisions to calculate the shear strength of deep beams. Moreover, the current design codes, namely: ACI Building Code (ACI 318M-11), Euro Code 2 (EC2) and Canadian Standard for the Design of Concrete Structures (CSA23.3-04) suggest that deep beams should be designed either by nonlinear analysis in which the nonlinear strain distribution is taken into account or by the strut-and-tie model (STM) which is considered as a lower-bound solution. On the other hand, a number of researchers (Wang et al., 1993; Ashour and Morley, 1996; Ashour and Rishi, 2000) developed a mechanism analysis based on the upper-bound theorem of the plasticity theory to predict the shear strength of deep beams. In this section, the shear provisions of the ACI 318M-11, the STM suggested by different design codes and the mechanism analysis are briefly reviewed. Moreover, the shear provisions of the ACI 318M-11 are verified against the experimental results

of the continuous deep beams in the database presented earlier. The full description of these approaches and the validation against the experimental results of SCC continuous deep beams tested in the current investigation as well as previous results of NC continuous deep beams are presented in chapter four.

Although the previously mentioned methods have been applied to analyse the shear of continuous deep beams, they can only predict the load capacity of deep beams. Therefore, it was important to find a numerical approach that can be used to predict the full behaviour of continuous deep beams. The finite element (FE) method can be used for achieving this aim. A review of the FE method and its applications in reinforced concrete members are presented in this section. Moreover, a three dimensional FE model is proposed in chapter five and verified against the current test results of continuously supported SCC deep beams.

2.7.1 Shear provisions of ACI 318M-11

Before 2002, the shear provisions of the ACI Building Code for the shear strength of deep beams were applicable for a member with a clear span-to-overall depth ratio not greater than 5 or a member with a shear span-to-depth ratio less than 2.5. However, since 2002, this condition has changed and the shear provisions can be applied to a member having a clear span-to-depth ratio not greater than 4 or a shear span-to-depth ratio less than 2. The shear provisions of ACI 318M-11 (Section11.7) state that the total shear capacity of deep beams, V_u, should be equal to or less than the value calculated from equation (2.1) below, provided that the web reinforcement is

distributed along the beam in both directions (vertical and horizontal) with an area of not less than $0.0025bs$ in each direction, where s is the spacing between the vertical or horizontal web reinforcement bars and b is the beam width.

$$V_u = 0.83\sqrt{f_c'}bd \quad (2.1)$$

where f_c' is the cylinder compressive strength of concrete in MPa, b is the beam width in mm and d is the beam effective depth in mm.

In this part of the literature, the predictions of the shear provisions suggested by the ACI 318M-11 are compared with the experimental results of 76 NC continuous deep beams collected from previous studies with the aim of validating the accuracy of the prediction of the ACI shear provisions for deep beams. Among the beams considered, only 15 beams had web reinforcement in both directions, satisfying the condition provided by the ACI 318M-11 as mentioned above. The rest of the beams had no web reinforcement, vertical only or horizontal only. Figure 2.8 shows comparisons between the results predicted by equation (2.1) of the shear provisions of ACI 318M-11 and experimental results of the continuous deep beams available in the database. The beams considered were divided into four groups depending on the configuration of the shear reinforcement in order to observe the accuracy of the prediction for different configurations of web reinforcement. The mean, the standard deviation and the coefficient of variation of the predictions of the four groups are shown in Table 2.4. It can be clearly seen that the ACI equation reasonably predicted the shear strength of continuous deep beams with orthogonal web reinforcement as

required by the ACI code. The most accurate prediction was obtained for beams having orthogonal web reinforcement with a mean, a standard deviation and a coefficient of variation of 1.02, 20% and 20%, respectively. For the other three groups, the accuracy of the predictions was much lower than those of beams having orthogonal web reinforcement. This can be attributed to the fact that all the groups of beams, apart from the one with orthogonal web reinforcement, do not satisfy the web reinforcement requirements for deep beams as mentioned above.

Table 2.4: The mean, SD and COV for predictions of ACI shear provisions for shear strength of NC continuous deep beams having different configurations of web reinforcement

Web reinforcement	Mean	Standard deviation (%)	Coefficient of variation (%)
None	0.84	35	41
Vertical reinforcement	0.87	20	23
Horizontal reinforcement	0.80	38	47
Orthogonal reinforcement	1.02	20	20

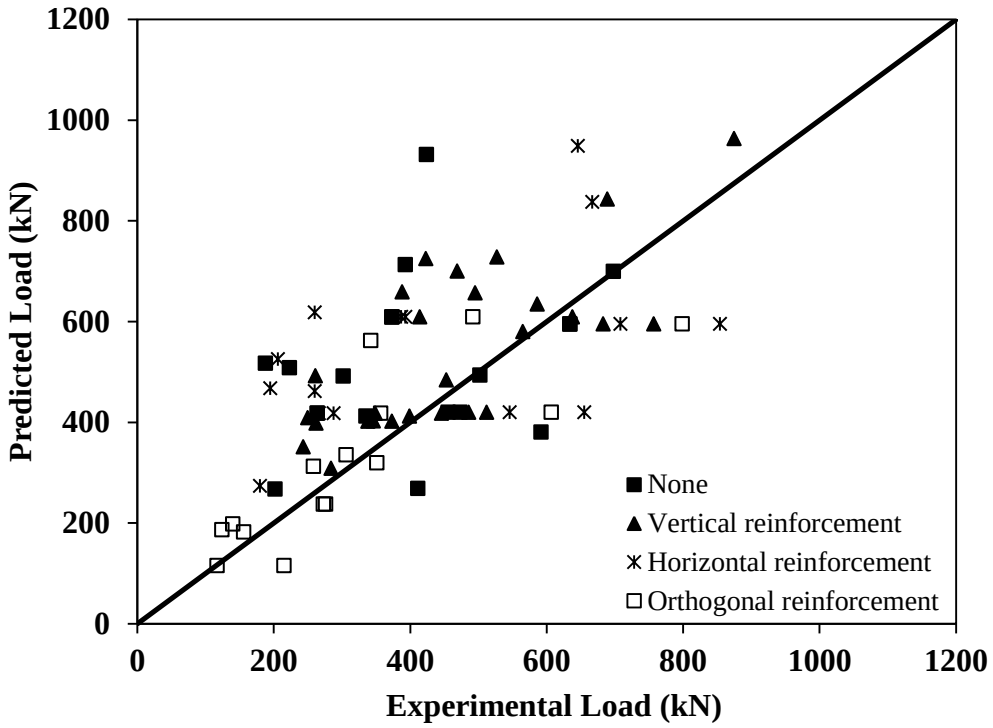

Figure 2.8: Comparisons between predictions of ACI 318M-11 shear provisions and previous experimental results of NC continuous deep beams

2.7.2 Strut-and-tie model in different design codes

The strut-and-tie model (STM) can be used for shear design and analysis of continuity or discontinuity regions and for the design of members in which a nonlinear distribution within the cross section is assumed (BS EN 1992-1-1:2004). In addition, different design codes such as ACI 318M-11, EC2 and CSA23.3-04 suggest the use of STM for the design of members with discontinuity regions such as deep beams and corbels. According to the definition of deep beams in ACI 318M-11, a discontinuity region (also defined as a D-region) is the region of the beam that extends up to twice the total beam depth between the support and the applied concentrated load as shown in Figure 2.9. The main difference between the different STMs suggested by the current design codes is the effectiveness factor which was

presented to overcome the disadvantages of using the plasticity theorem to analyse the behaviour of reinforced concrete and to account for the limited ductility of concrete (Ashour and Morley, 1996). More details about the analysis of continuous deep beams using STM will be given in chapter four.

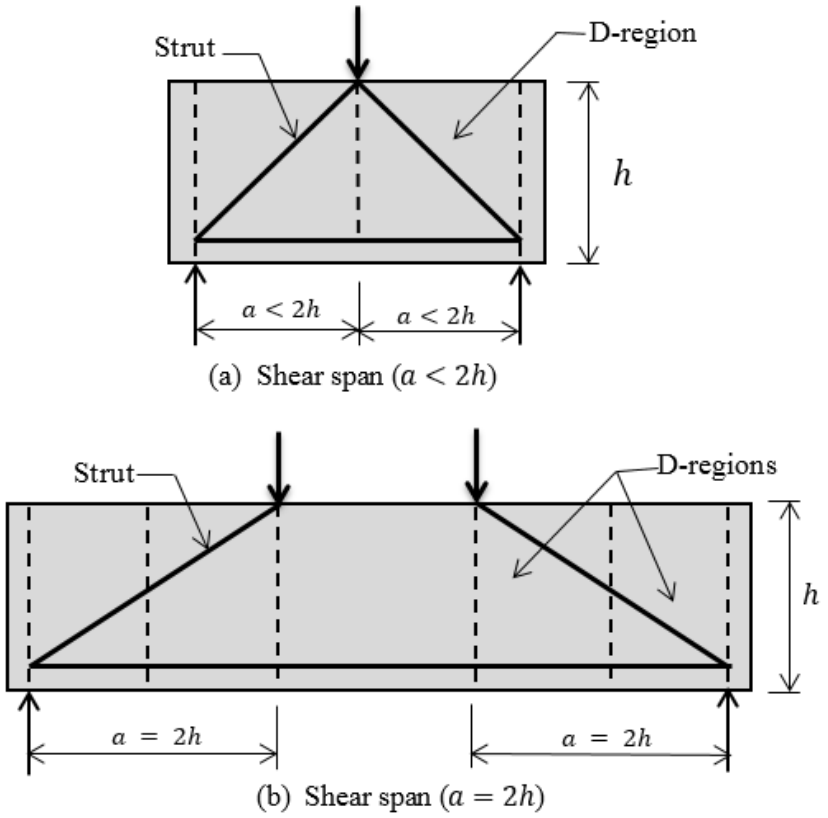

Figure 2.9: Description of discontinuity regions in deep beams (ACI 318M-11)

The STM model in different design codes is defined as a truss model consisting of struts and ties that intersect with concentrated loads at a joint defined as a node. The strut represents the compression member whereas the tie is the tension member. The ties in the STM can represent one or more of the longitudinal reinforcement layers. Moreover, a tension tie should be in the same position and direction as the member reinforcement as it consists of a reinforcement bar surrounded by a portion of concrete. The forces in

struts and ties can be determined by considering the equilibrium with the applied loads at the node.

Although the STM has been recommended by different design codes to analyse the shear strength of deep beams, there is a lack of information about using the STM for continuous deep beams. Yang et al. (2007a) and Yang and Ashour (2008) applied the STM based on the recommendations of ACI 318-05 to predict the load capacity of NC continuous deep beams. They showed that the prediction was unconservative for beams having an a/d ratio of 1.0 and for beams with a low amount of bottom longitudinal reinforcement and web reinforcement. The STM recommended by different design codes, namely ACI 318M-11, EC2 and CSA23.3-04 will be described in full details in chapter four and assessed against the experimental results of continuous NC deep beams collected from previous studies as well as the experimental results of continuously supported SCC deep beams tested in the present research.

2.7.3 Upper-bound analysis

The main difference between the upper-bound and lower-bound analysis is that the upper-bound analysis requires a geometrically admissible failure mechanism. After that, the energy principle can provide the load which is higher than the value of the collapse load. In the case of deep beams, the kinematic energy is provided by the rotation of a rigid part separated from the beam by a yield line. However, the lower-bound solution requires finding a load path to transfer the forces from the load point to the supports and then

the load capacity can be found by applying the equilibrium for the internal forces (Nielsen and Hoang, 2010).

The first application of the upper-bound approach for the analysis of shear strength of reinforced concrete beams was proposed by Nielsen (1975) assuming that the concrete beam at failure is separated by a straight yield line into two rigid blocks. In 1978, Nielsen and Braestrup applied the upper-bound analysis for the shear strength of prestressed reinforced concrete beams without shear reinforcement. In these studies, the solution of the shear strength of reinforced concrete beams was provided as a function of the shear span-to-depth ratio and longitudinal reinforcement and the prediction showed good agreement with the experimental results. After that, a number of research investigations tried to develop different techniques of the upper-bound analysis and apply these techniques for plain and reinforced concrete structures (Nielsen, 1984; Kemp and Al-Safi, 1981). The first upper-bound analysis applied specifically to deep beams was developed by Zainai (1987) and Zainai and Morley (1991). For continuously supported deep beams, Ashour and Morley (1996) developed a simplified upper-bound analysis based on the hyperbolic yield line separating two rigid concrete blocks as shown in Figure 2.10. The hyperbolic yield line provides less energy and is preferred to describe the concrete discontinuity region compared to the straight yield line (Jensen, 1979). Comparisons between experimental results and predictions of the simplified upper-bound analysis showed that the results were in reasonable agreement (Yang et al., 2007b; Yang and Ashour, 2008). The simplified upper-bound analysis proposed by Ashour and Morley (1996) will be described in full details in chapter four to

be used to predict the load capacity of continues SCC deep beams tested in the current study.

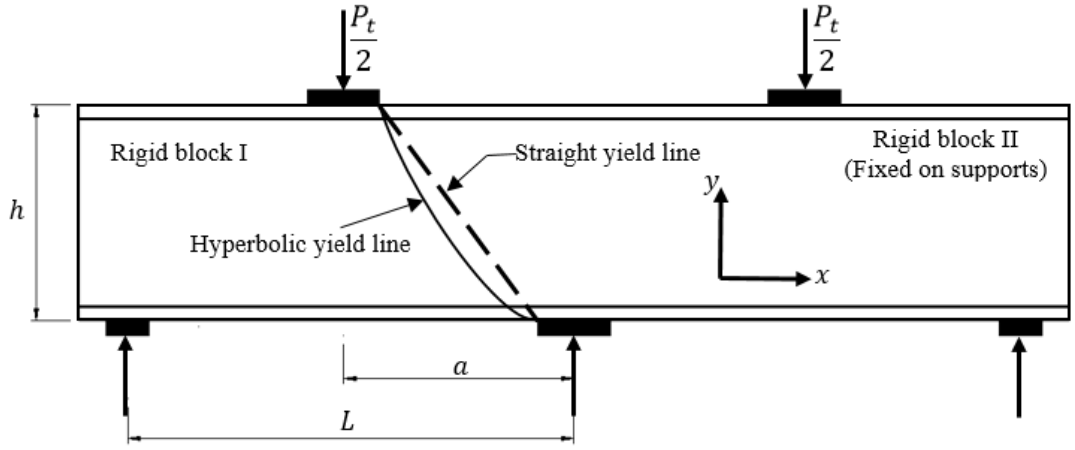

Figure 2.10: Shape of the yield line in the simplified upper-bound analysis (Ashour and Morley, 1996)

2.7.4 Finite element analysis

The concept of finite element (FE) method involves presenting the real structural system as a mesh of finite elements connected to each other at nodal points. The development of this method allows the modelling of the complicated non-linear behaviour of reinforced concrete (RC) structures. It has been a very important analytical model for predicting the load-deflection behaviour and analysing the stress distribution of RC members (Wolanski, 2004). It has also been successfully applied to predict the formation of cracks and analyse different failure characteristics of RC members (Wolanski, 2004; Wang et al., 1993).

The use of FE as an analytical model to predict the behaviour of RC structures is not a straightforward process. The behaviour of RC is very complicated because it consists of completely two different materials in terms

of physical and mechanical characteristics. The steel reinforcement is a homogenous material which can be easily defined whereas concrete is a heterogeneous material and is difficult to model. Moreover, the behaviour of RC is nonlinear even when subjected to small loads and it has a continuous variation under load increment because of the appearance of cracks. The nonlinear behaviour of RC results from concrete cracking under tension, the reinforcement yielding and concrete crushing under compression. Furthermore, the interaction between concrete and reinforcement is very complex due to the bond slip. In addition, there are many other factors which affect the behaviour of concrete such as creep and shrinkage. The accuracy of FE method relies on the selection of the finite elements to precisely represent the behaviour of concrete, reinforcement and the bond between concrete and reinforcement.

The earliest use of FE technique to analyse RC structures was published by Ngo and Scordelis (1967). They used a linear elastic model to analyse several simply supported RC beams by modelling concrete as two dimensional triangular finite elements taking into account the bond between the concrete and reinforcement. After the publication of Ngo and Scordelis (1967), the analysis of RC structures using FE models has exhibited significant development and considered as an important technique for studying the complex behaviour of RC structures and this has led to a high number of research investigations on the FE analysis of RC such as Nilson (1972), Scordelis et al. (1974), Bashur and Darwin (1978), Rots et al. (1985), Barzegar and Schnobrich (1986), Meyer and Okamura (1986), Keuser and Mehlhorn (1987), Vecchio (1989), Spacone et al. (1996)… etc.

In chapter five, a three dimensional nonlinear FE model using ABAQUS 6.12 is proposed in order to analyse and predict the behaviour of continuously supported SCC deep beams. The model will be verified against the experimental results of continuous SCC deep beams tested in the current research investigation as well as some case studies collected from previous investigations. In addition, the proposed FE model will be used in chapter six to conduct a parametric study with the aim of exploring the structural behaviour of continuous SCC deep beams with extended range of parameters.

2.8 Experimental investigations on simply supported SCC deep beams

Although SCC has been in existence for more than 30 years and has extensively been used in a wide range of structural applications, the number of research investigations in the use of SCC in deep beams is very limited. Only a few studies have focused on the structural behaviour of simply supported deep beams made with SCC (Mohammadhassani et al., 2011; Mohammadhassani et al., 2012a, 2012b; Shah and Modhera, 2010, 2012; Rasheed and Alobaidi, 2012; etc).

Experimental results showed that the main cause of failure in simply supported SCC deep beams is a diagonal crack extended from the load point to the support, similar to the failure mode of simply supported NC deep beams (Shah and Modhera 2010, 2012; Rasheed and Alobaidi, 2012; Mohammadhassani et al., 2011; Choi et al., 2012). The first flexural and diagonal cracks in SCC deep beams usually occur within the range of 25-42% and 45% of the failure load, respectively, (Mohammadhassani et al.,

2011, 2012a) compared to 10-30% and 30% in NC deep beams (Yang et al., 2003; Tan and Lu, 1999).

In terms of the shear strength of SCC deep beams, Shah and Modhera (2012) illustrated that there was a 35 to 45% reduction in shear strength of SCC deep beams in comparison with their NC counterparts. However, Choi et al. (2012) concluded that SCC deep beams having moderate amount of web reinforcement showed slightly higher shear strength when compared to their NC counterparts. The ultimate shear strength of SCC deep beams can be improved by 25 to 35% by partially replacing shear reinforcement with steel fibres (Shah and Modhera, 2010, 2012).

In general, the mid span deflection of deep beams is very small due to the large section depth in comparison to shallow beams. Shah and Modhera (2012) concluded that the mid span deflection of SCC deep beams is higher than NC ones. Moreover, experimental results showed that deflection of SCC deep beams decreased by adding horizontal web reinforcement to the stirrups and anchorage to the longitudinal bars (Rasheed and Alobaidi, 2012). However, the mid-span deflection of SCC deep beams considerably increased when steel fibres was added to the reinforcement (Shah and Modhera, 2010, 2012).

2.9 Concluding remarks

SCC is a modern type of concrete that can flow under its own weight without any compaction. It was developed to overcome the common durability problems arising with the use of NC. It is also preferred to be used for structural elements that cannot be easily vibrated such as deep beams due

to their high depth and congested steel reinforcement, making it difficult for normal concrete (NC) to properly be placed and vibrated. SCC provides significant quality, improves productivity and achieves engineering properties similar to those of NC with more durable structures.

This chapter presented an overview for the previous studies conducted on SCC and deep beams. More focus was given for continuously supported deep beams. Depending on the literature review presented above, the following conclusions can be drawn:

- The production of SCC requires achieving high flowability, high passing ability and high segregation resistance. Achieving these requirements involves reducing the amount of course aggregate, adding VMA and HRWRA, lowering the water-to-powder ratio and using supplementary cementitious materials such as fly ash, GGBS and silica fume.
- The literature shows that a few studies focused on investigating the behaviour of simply supported deep beams made with SCC. None of these studies were conducted on continuously supported SCC deep beams.
- There are many parameters controlling the shear strength of continuous deep beams, the most important among them are the shear span-to-depth ratio and the amount and configuration of web reinforcement.
- There are three approaches to predict the load capacity of continuously supported deep beams: the first is a lower-bound solution presented by the strut-and-tie model suggested by different design codes. The second one is an upper-bound solution developed by a number of researchers and finally the nonlinear finite element analysis.

- A numerical technique is essential to predict the full behaviour of continuous deep beams. The linear analysis can predict the behaviour of deep beams before cracking. However, after cracking, a major redistribution of stresses occurs and therefore, a nonlinear finite element model is required.

CHAPTER THREE
EXPERIMENTAL INVESTIGATION

3.1 Introduction

In chapter two, a literature review was presented on the properties of SCC and the structural behaviour of SCC and NC deep beams. This review shows that no experimental investigations were conducted to study the behaviour of continuously supported deep beams made with SCC. As a result, the main aim of the experimental investigation described in this chapter is to study the structural behaviour of reinforced SCC continuous deep beams. In particular, the effect of the shear span-to-depth ratio, a/d, the amount and configuration of shear reinforcement as well as the longitudinal reinforcement ratio on the performance of continuous deep beams made with SCC. The results of the experimental work are presented in this chapter. In addition, the experimental data would be used in the next chapter to assess the validity of using the simplified methods suggested by different design codes and different researchers in the load capacity prediction of continuous SCC deep beams. The experimental results will also be used in chapter five to validate

the numerical model proposed to predict the behaviour of SCC continuous deep beams.

3.2 Test specimens

The test specimens consisted of eight large-scale continuous SCC deep beams. The overall geometrical dimensions along with the reinforcement details for all tested beams are presented in Table 3.1, Figure 3.1 and Figure 3.2. All beams had the same span, L, 1240 mm and the same width, b, 160 mm. The main parameters investigated were the shear span-to-depth ratio, a/d, the amount and configuration of the web reinforcement and main longitudinal reinforcement ratio. The overall depth, h, of the test specimens was changed to achieve two different a/d ratios, namely 0.8 (h=600 mm) and 1.7 (h=300 mm). Beams B1 to B6 had the same overall depth of 600 mm and a/d ratio of 0.8 whereas beams B7 and B8 had a depth of 300 mm and a/d ratio of 1.7.

Table 3.1: Geometrical dimensions and reinforcement details of test specimens

Beam no.	f_c' MPa	h mm	d mm	L mm	Longitudinal reinforcement		Web reinforcement	
					Bottom	Top	Vertical	Horizontal
B1	31.1	600	560	1240	3Ø16 mm	3Ø16 mm	-	4Ø8 mm
B2	42.5				3Ø16 mm	3Ø16 mm	14Ø8 mm	-
B3	36.0				3Ø16 mm	3Ø16 mm	14Ø8 mm	4Ø8 mm
B4	46.0				3Ø16 mm	3Ø16 mm	14Ø8 mm	8Ø8 mm
B5	47.8				3Ø16 mm	3Ø16 mm	28Ø8 mm	4Ø8 mm
B6	50.4				5Ø16 mm	5Ø16 mm	14Ø8 mm	4Ø8 mm
B7	32.0	300	260		3Ø16 mm	3Ø16 mm	14Ø8 mm	-
B8	38.6				5Ø16 mm	5Ø16 mm	14Ø8 mm	-

where f_c' is the concrete compressive strength, h is the beam total depth, L is the span length, a is the shear span and d is the beam effective depth.

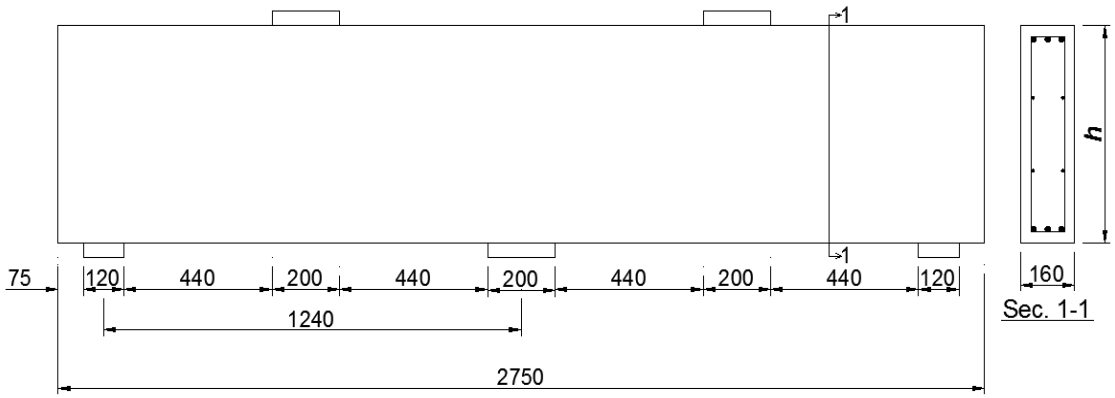

Figure 3.1: Geometrical dimensions of test specimens (dimensions in mm)

With regard to the web reinforcement, all the test specimens had either vertical reinforcement, horizontal reinforcement or orthogonal reinforcement. The vertical reinforcement consisting of 8 mm closed stirrups distributed uniformly along the beam length was varied between the test specimens. Specimen B1 had no vertical reinforcement, Specimen B5 had a high amount of vertical reinforcement (28 vertical stirrups spaced at 100 mm) and all other specimens had an intermediate amount of vertical reinforcement (14 vertical stirrups spaced at 200 mm). The horizontal web reinforcement was provided on both sides of the beam web at three different levels: none, 2 horizontal bars and 4 horizontal bars on each side as shown in Table 3.1 and Figure 3.2. All test specimens had the same top and bottom longitudinal reinforcement of 3 bars of 16 mm diameter except for two beams (B6 and B8) in which the amounts of top and bottom reinforcement were increased to 5 bars of 16 mm diameter. All the bottom reinforcing bars were extended to the full length and depth of the beam to ensure sufficient anchorage. The concrete cover to the centre of the main longitudinal bars was 40 mm while the clear cover to the face of the stirrups was 25 mm.

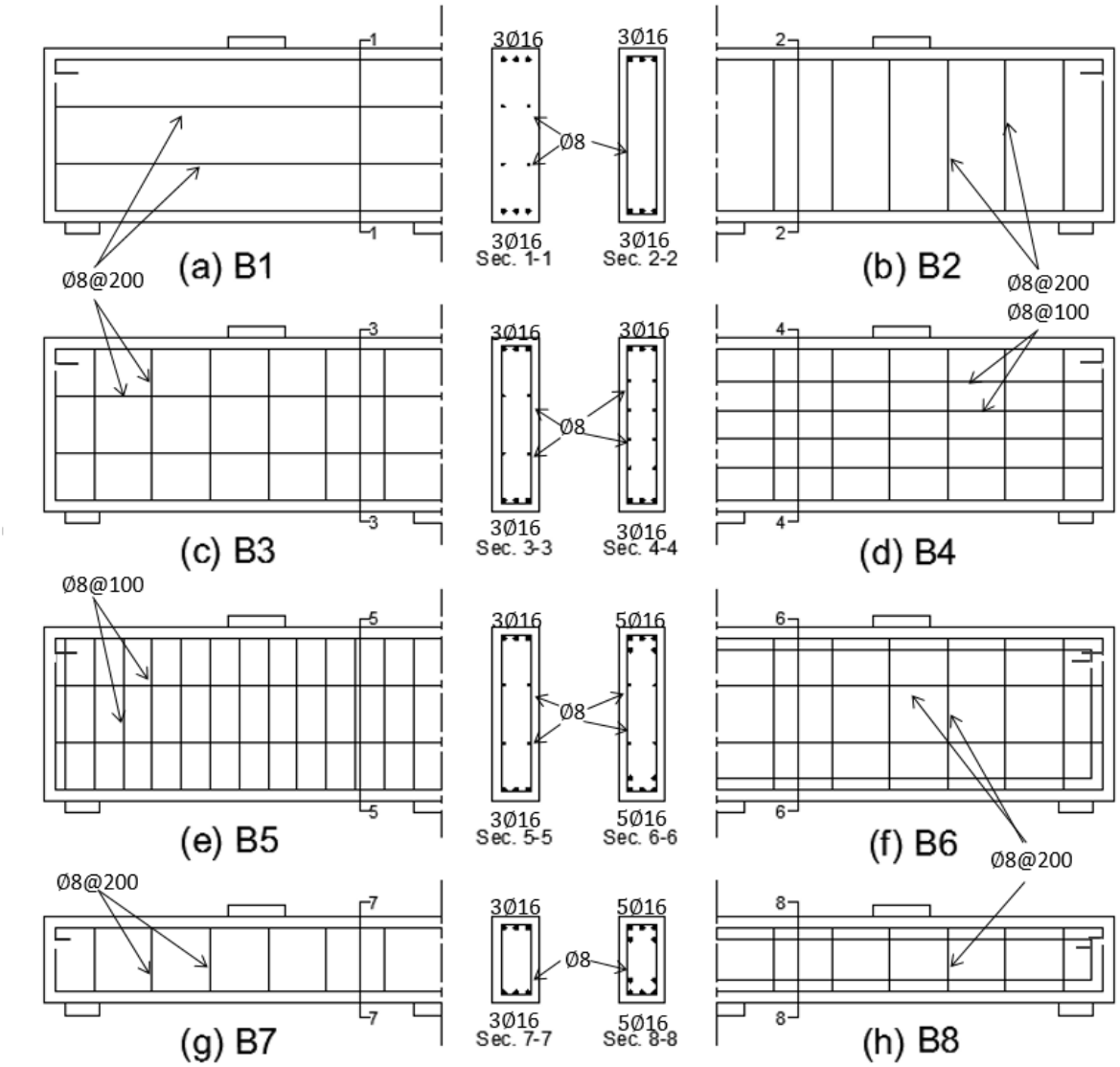

Figure 3.2: Details of test specimen reinforcement

3.3 Material properties

3.3.1 Self-compacting concrete

3.3.1.1 Ingredients and mix proportions

SCC was produced in the laboratory using readily available raw materials. The raw materials were proportioned using the method proposed by Su et al. (2001) and Su and Miao (2003). The full details of the mix design can be found in Appendix B. The concrete ingredients were ordinary Portland

cement (PC, class 52.5N), fly ash 450-S, 10 mm coarse aggregate, fine aggregate and superplasticizer (Glenium C315).

3.3.1.2 Fresh properties

The fresh properties, which included the flow ability, passing ability, segregation resistance and filling ability, were assessed by the slump flow, the T_{50} test, sieve stability test and the V-funnel test, respectively.

Initially, the slump flow test was performed by pouring the fresh concrete into the slump cone without compaction as the concrete was assumed to be compacted under its self-weight. Then, the cone was removed in the vertical direction. The slump flow value is the average diameter of the concrete flow as shown in Figure 3.3(a). In the same test, the T_{50} value was measured by calculating the time required for the concrete to flow for a distance of 50 cm from the centre of the slump cone.

After that, the resistance of concrete to segregation or separation was measured by conducting the sieve stability test. The test was performed by sieving about 2 litres of fresh concrete over a 5 mm sieve for 5 minutes as shown in Figure 3.3(b). The segregation resistance then was assessed by calculating the segregation index which is the value of mortar passing through the sieve divided by the original value of mortar in the volume of concrete prior to the test.

Finally, the V-funnel test was performed by filling SCC mixture into a funnel with a V shape having a trap door at its bottom face. Then, the trap door was opened allowing the concrete to flow as shown in Figure 3.3(c). The passing ability was assessed by calculating the time that the concrete takes to completely flow out of the funnel.

(a) Slump flow test

(b) Sieve stability test

(c) V-funnel Test

Figure 3.3: Tests of fresh properties of SCC

The results of the fresh properties compared to the requirements of the European Guidelines for SCC (BIBM et al., 2005) are shown in Table 3.2. It can be clearly seen that the concrete mix achieved all the requirements of SCC. The mixture had reasonable passing and filling ability values making it suitable to be used for the construction of deep beams having a small width and congested reinforcement. Moreover, the mixture had high segregation resistance of 7.0% which guarantee homogenous distribution for concrete within the formwork.

Table 3.2: Results of the fresh properties and the requirements of SCC

Test	Experimental results	Requirements
Slump flow average diameter	830 mm	Class SF3: 760-850 mm, suitable for application with highly congested reinforcement
V-funnel	8 sec	Class 1 : ≤ 8 sec: good filling ability through congested reinforcement and better surface finish
T_{50}	1.6 sec	Class 1 : ≤ 2 sec: good passing ability through congested reinforcement
Segregation	7.0%	≤ 15%

3.3.1.3 Concrete strength

The following control specimens were prepared during the casting of each beam: three 100 mm cubes and two 300 mm high by 150 mm diameter cylinders from each batch. The control specimens were tested on the same day as the deep beam test and the results of compressive strength for each test specimen are shown in Table 3.3. The cubes and cylinders were tested under direct compression in accordance with BS EN 12390-1:2012. The cube compressive strength, f_{cu}, and the cylinder compressive strength, f_c', shown in Table 3.3 were obtained from the average of compressive strengths of the tested control specimens: 12 cubes and 8 cylinders for beams having a depth of 600 mm and 6 cubes and 4 cylinders for beams having a depth of 300 mm. Table 3.3 also shows the relationship between the cube and cylinder compressive strengths which can be written in the form shown in equation (3.1) below:

$$f_c' \cong 0.843\, f_{cu} \tag{3.1}$$

where f_c' is the cylinder compressive strength of concrete and f_{cu} is the cube compressive strength of concrete.

Table 3.3: Reslts of cube and cylinders compressive strength

Beam no.	Curing time (days)	f_{cu} MPa	f_c' MPa	f_c'/f_{cu}
B1	134	36.1	31.1	0.86
B2	129	50.7	42.5	0.84
B3	111	42.6	36.0	0.85
B4	96	54.9	44.2	0.81
B5	119	57.4	47.8	0.83
B6	115	59.9	50.4	0.84
B7	172	37.2	32.0	0.86
B8	144	45.2	38.6	0.85

where f_c' is the cylinder compressive strength of concrete and f_{cu} is the cube compressive strength of concrete

3.3.2 Steel reinforcement properties

The mechanical properties of the longitudinal and web reinforcement were obtained from the tensile test of the steel reinforcing bars. The main longitudinal and web reinforcement have a yield strength, f_y, of 500 MPa and ultimate strength, f_u, of 625 MPa. The modulus of elasticity of the reinforcing bars, E_s, is 210 GPa.

3.4 Manufacturing and curing

The test specimens were cast in the laboratory using a concrete mixer having a capacity of 0.085 cubic metre. Beams B1 to B6 having a depth of 600 mm required four batches including the control specimens while beams B7 and B8 having a depth of 300 mm required two batches including the control specimens. All the test specimens were cast in a vertical position using two wooden moulds: one for beams B1 to B6 and the second one for the other two shallower beams (B7 and B8). After demoulding, all the beams and control specimens were stored in the same place in the lab and covered

by polyethylene sheets up to the testing date. The Curing times for all the beams up to the testing date are shown in Table 3.3.

3.5 Test set-up

All the specimens were tested under a symmetrical two-point loading system, using a loading frame of a capacity of 2500 kN as shown in Figure 3.4. After each load increment of 20 kN (6 kN/min), the load was kept constant to observe and capture any developed cracks. The middle support was designed to allow rotations only but no horizontal movement whereas the two end-supports were designed as a roller to allow rotation and horizontal movements. To avoid concrete bearing failure at the load application points, steel plates were used between the supports and the test specimens. The two end steel plates had a width of 120 mm while the middle and loading steel plates had a width of 200 mm. All the steel plates had a minimum length of 160 mm to cover the full width of the beam and a thickness of 20 mm except for the loading plates which were 40 mm thick. A top steel spreader beam was used to distribute the load from the loading actuator into two point loads.

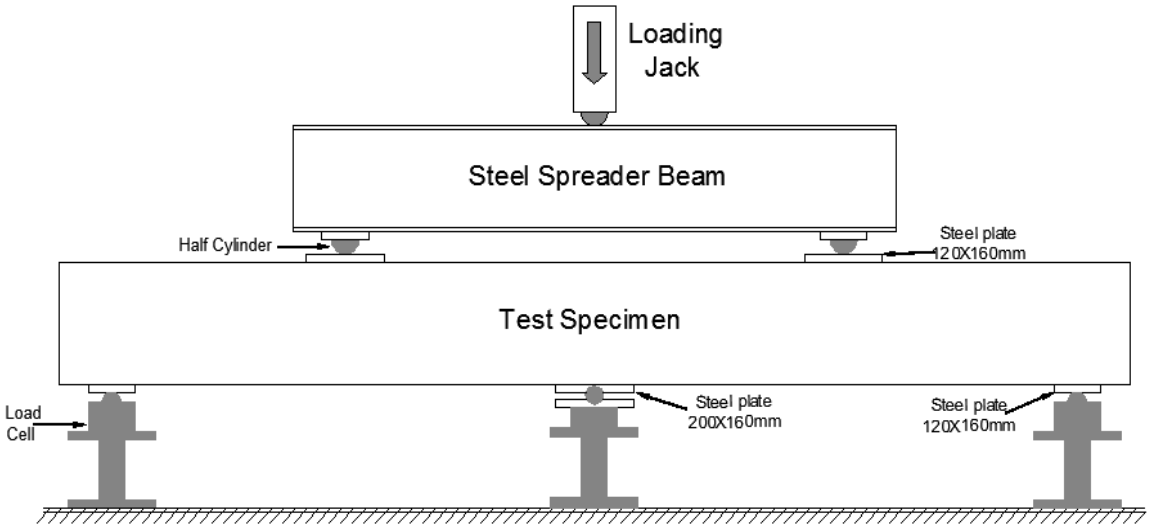

Figure 3.4: Test setup

3.6 Instrumentation

5 mm strain gauges were attached to the main longitudinal and web reinforcement at the most critical locations: six used for beams having either vertical or horizontal web reinforcement and ten for beams having vertical and horizontal reinforcement. The mid-span deflection of each span and the support settlements were measured using linear variable differential transducers (LVDT). One end support reaction was measured using a 1000 kN capacity load cell. The test results from strain gauges, LVDTs and load cell were captured automatically using a data logger. The surface of the test specimens was painted to mark the development of cracking during the test. Three high-professional cameras were setup to capture the flexural cracks in the mid span as well as the diagonal cracks formed between the intermediate support and load plates. The photos captured by these cameras were then used to estimate the crack widths by applying Image-Pro Plus software version 6.0. The positions of the strain gauges, the LVDTs and the cameras for all the test specimens are shown in Figure 3.5.

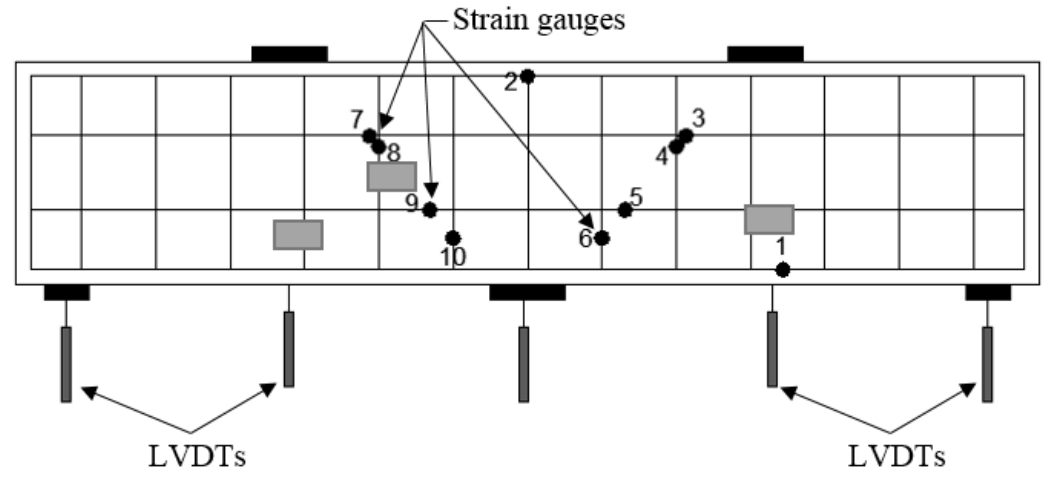

(a) Beams having h=600 mm

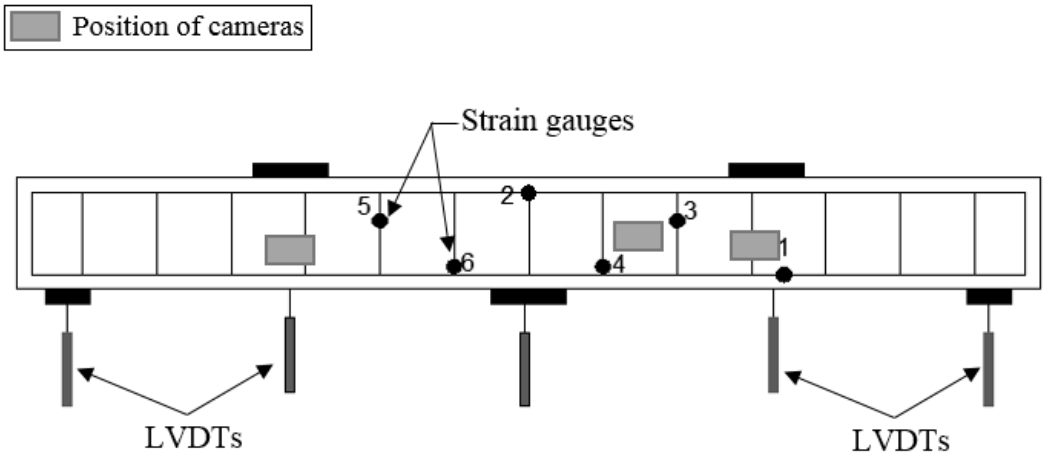

(b) Beams having h=300 mm

Figure 3.5: Position of strain gauges LVDTs and cameras for test specimens

3.7 Test results and discussions

3.7.1 Cracking propagation and failure modes

In general, all the beams tested exhibited similar cracking propagation and failure modes. The flexural cracks at mid-span and above the intermediate support occurred at approximately 12-17% and 60-70% of the failure load, respectively, while the first diagonal crack in most of the test specimens started at 30-40% of the failure load as presented in Table 3.4. The first flexural crack load at mid-span for all specimens was approximately half of

that of the first diagonal crack. The diagonal crack occurred suddenly at the mid-depth of the beam between the load point and the intermediate support. After increasing the load, the length and width of the first crack increased and more diagonal and flexural cracks developed. For all beams, the two faces in both spans of the test specimens had approximately the same crack propagation.

Table 3.4: First flexural and diagonal cracking loads, and failure load

Beam no.	1st flexural cracking load kN		1st diagonal cracking load kN (% of failure load)	Failure load kN
	Mid-span (% of failure load)	Over middle support (% of failure load)		
B1	220 (17%)	880 (68%)	470 (36%)	1295
B2	190 (12%)	1000 (60%)	480 (30%)	1674
B3	220 (16%)	900 (66%)	540 (39%)	1358
B4	260 (14%)	1100 (60%)	450 (25%)	1861
B5	240 (12%)	1190 (60%)	450 (23%)	1988
B6	230 (12%)	1160 (60%)	580 (30%)	1940
B7	80 (14%)	80 (14%)	200 (35%)	579
B8	90 (13%)	90 (13%)	270 (40%)	676

All the beams tested showed the same failure mode. The main cause of failure was a major diagonal crack started at the mid-depth of beams and extended along the distance between the edge of the load and intermediate support plates as shown in Figure 3.6: Fig. 3.6(a) and Fig. 3.6(b) for beams B4 and B5, respectively, with $h = 600\,mm$ whereas Fig. 3.6(c) and Fig. 3.6(d) for beams B7 and B8, respectively, with $h = 300\,mm$. At failure, concrete crushing occurred at the top of the beams at the contact point between the diagonal crack and the load plate. The significant diagonal crack separated the beam into two concrete blocks: one rotated about the exterior support while the other was fixed over the other two supports similar to the

failure mode observed in other investigations for continuous NC deep beams (Ashour, 1997; Yang et al., 2007a, 2007b).

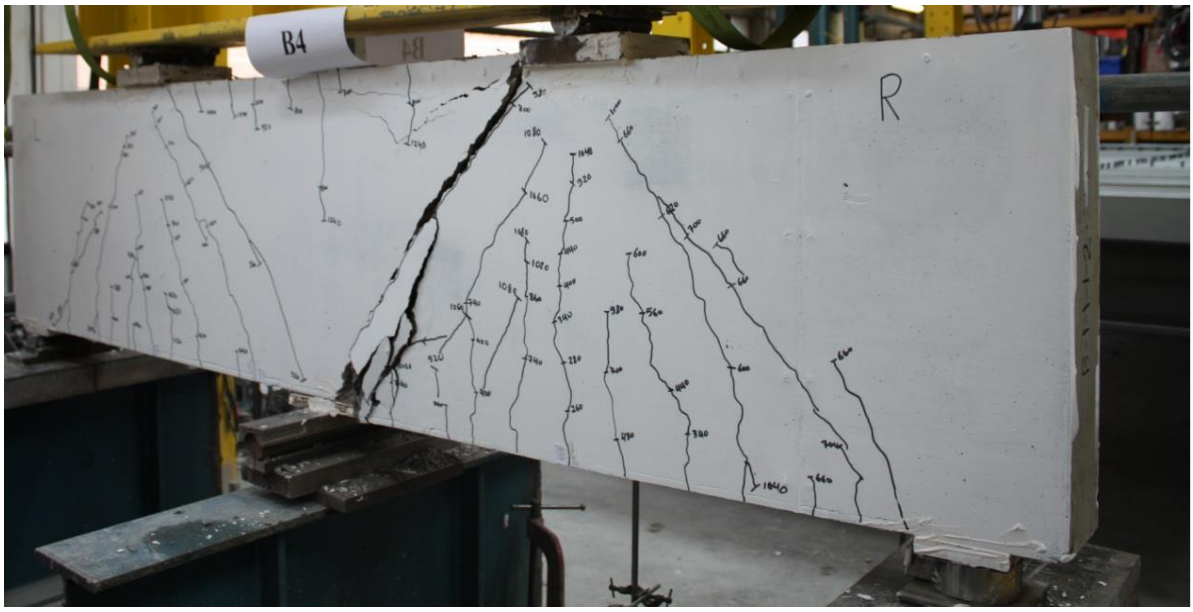

(a) B4

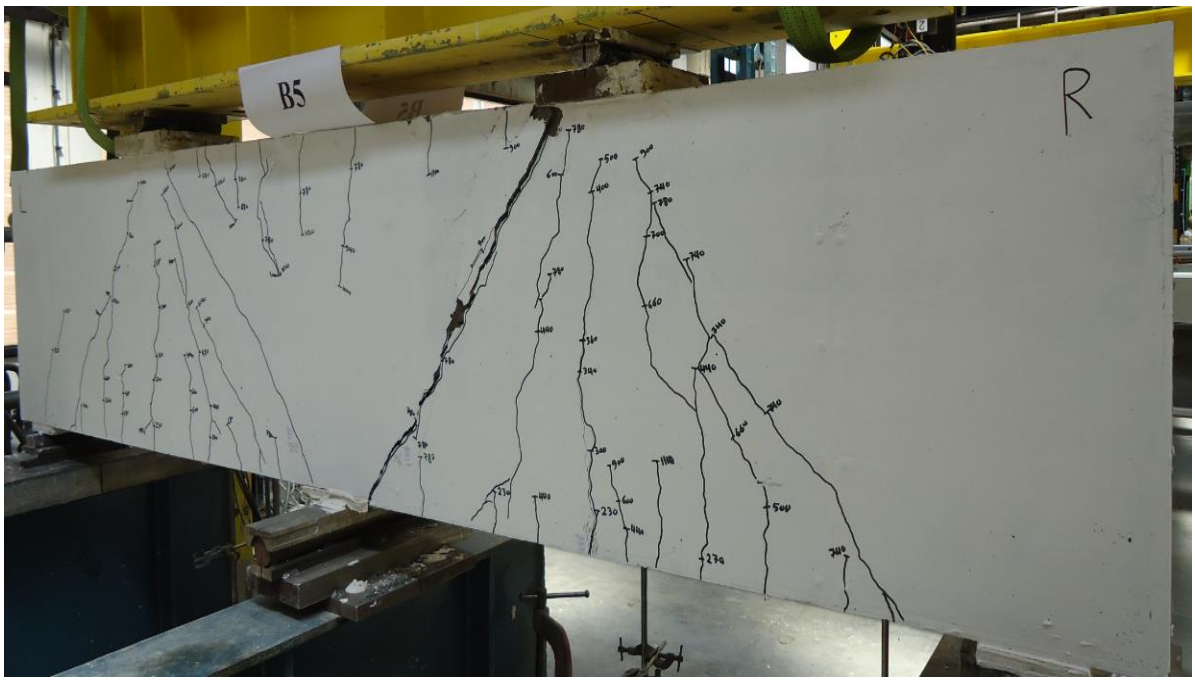

(b) B5

(c) B7

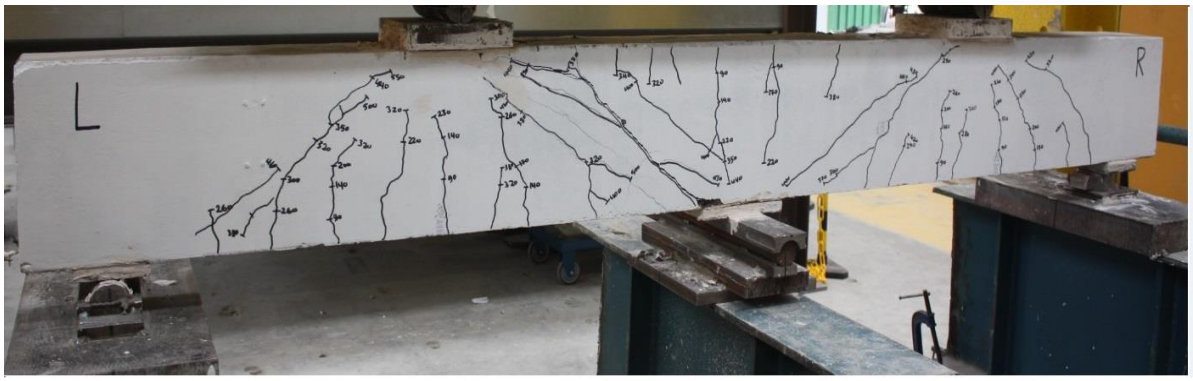

(d) B8

Figure 3.6: Crack propagation and failure modes of tested beams

3.7.2 Width of diagonal and flexural cracks

The relations between the total applied load and the width of cracks are shown in Figure 3.7: Fig. 3.7(a) for the mid-span flexural crack and Fig. 3.7(b) for the diagonal crack. The limitation for the flexural crack width of 0.4 mm according to EC2 is also plotted in Fig. 3.7(a). Three high quality digital cameras were used to capture three cracks: 2 used for the flexural cracks at mid-span, while the third used for the diagonal crack between the mid-span point load and intermediate support. The images of the cameras were then processed by Image-Pro Plus software version 6.0 to estimate the crack widths. Only one flexural crack is presented in Fig. 3.7(a) due to the similarity

in crack widths between the two spans. It can be observed that the horizontal web reinforcement played an important part in decreasing the width of flexural and diagonal cracks. Beams with horizontal or orthogonal web reinforcement (B1, B3, B4, B5 and B6) had less crack width than the beam with only vertical stirrups (B2). This is different from the results obtained by Yang et al. (2007a) who showed that a smaller diagonal crack width was observed in beams having vertical or orthogonal web reinforcement. This may be attributed to the fact that a/d ratio considered in the study conducted by Yang et al. was 1.0 compared with 0.8 in the current study. Beams with a smaller depth (B7 and B8) had a higher crack width at a lower applied load. Moreover, by comparing B3 and B6, it can be clearly noticed that increasing the amount of the main longitudinal reinforcement had a clear effect on both flexural and diagonal crack widths. EC2 limits the width of flexural cracks in reinforced concrete members to 0.4 mm. However, ACI 318M-11 does not give any limits for the crack width and relates the acceptable crack width to the type of structure. Older provisions of the ACI Building Code (before 1990) limits the crack width to 0.4 mm, similar to the EC2 limit. Comparing the results in Figure 3.7(a) and Figure 3.10(a) shows that for all the tested beams, the width of the main flexural crack at the mid-span exceeded the limit of 0.4 mm at the time when the bottom longitudinal reinforcement reached or were close to yielding. However, at the serviceability load of EC2 (0.67 of the failure load), the width of the main flexural crack exceeded the limit of 0.4 mm for four beams (B1, B2, B6 and B8) which had low amount of web reinforcement.

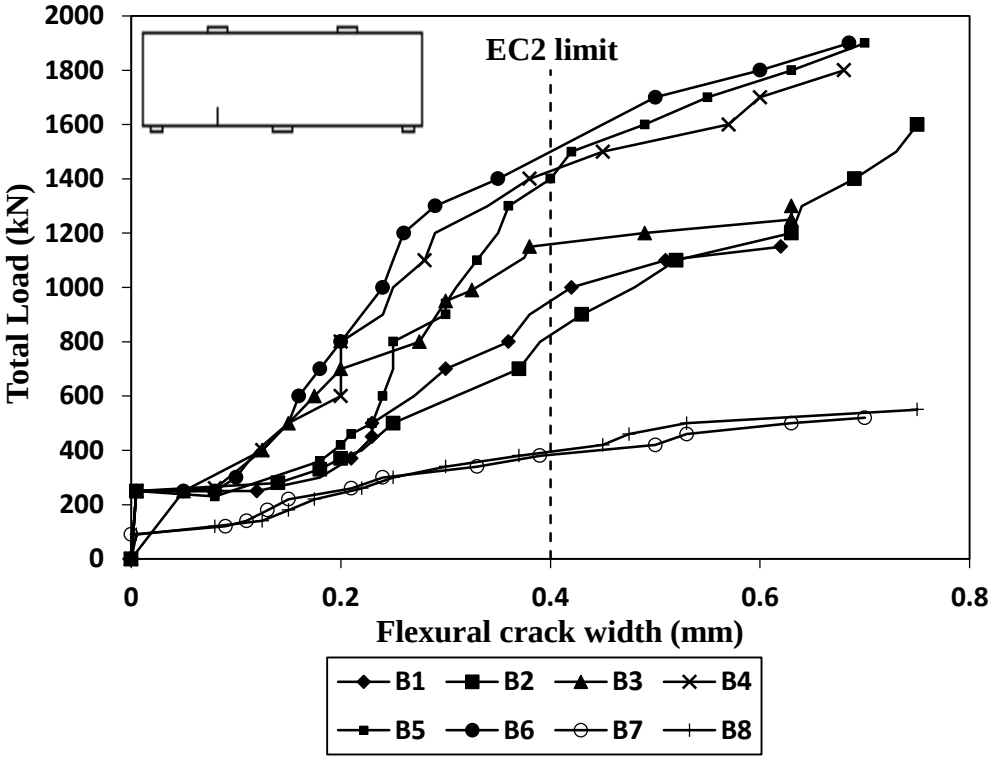

(a) Width of flexural crack

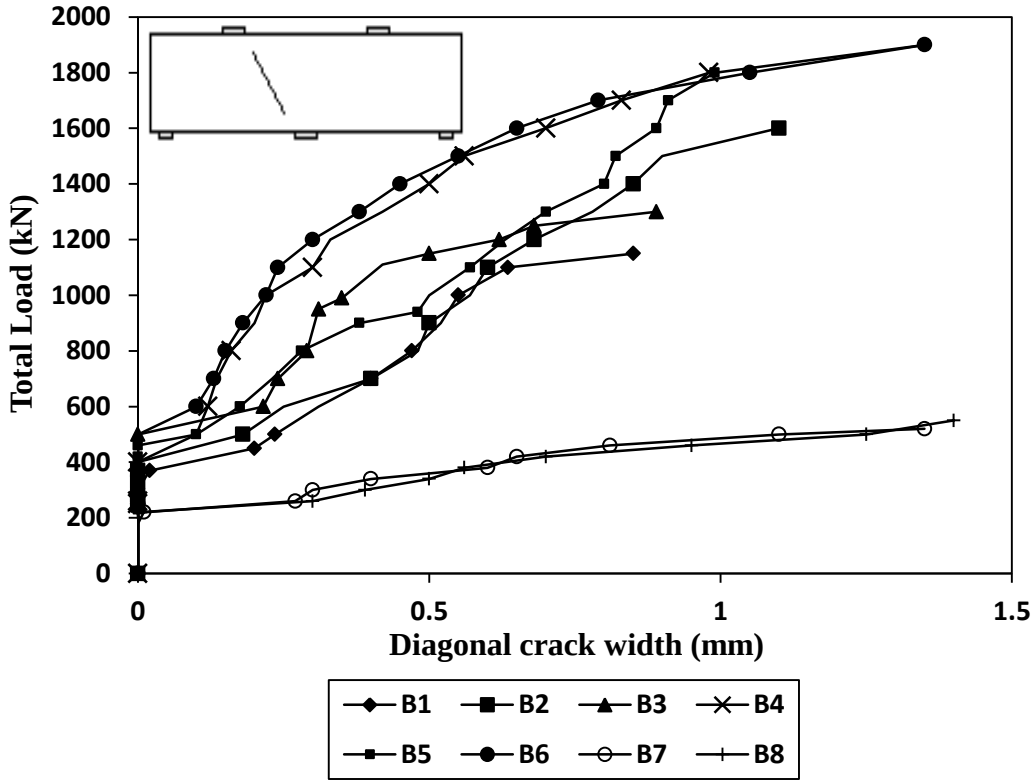

(b) Width of diagonal crack

Figure 3.7: Width of flexural and diagonal crack against total load

3.7.3 Support reactions and failure loads

Figure 3.8 plots the amount of the load transferred to the exterior support against the total applied load: Fig. 3.8(a) for beams having a depth of 600 mm and Fig. 3.8(b) for beams having a depth of 300 mm. The end-support reaction obtained from a linear elastic finite element (FE) analysis using ABAQUS software is also plotted in Figure 3.8. The concrete was modelled using 8-node linear brick, reduced integration element (C3D8R) whereas the reinforcing bars were modelled by a 2-node linear 3-D truss element (T3D2). The interaction between concrete and reinforcement was modelled by using the embedded region option available in ABAQUS 6.12 which represents perfect bond between concrete and reinforcement. The full details of the FE model can be found in chapter five. Up to the first crack, the relationship between the total applied load and the end-support reaction is approximately the same as predicted by the linear FE analysis. However, after the formation of the first diagonal crack, the prediction of the end-support reaction by the FE analysis was slightly lower than the experimental values for all the deeper beams as shown in Figure 3.8(a). This can be attributed to the fact that after concrete cracking, the applied load is transferred by the stress in the tensile reinforcement leading to a change in the slope of the load-deflection curve. This means that after cracking the redistribution of stresses increases the end support reaction more than that predicted by the linear elastic FE. For the two shallower beams (B7 and B8), the occurrence of the first diagonal crack did not have much effect on the agreement between the FE prediction and the experimental results.

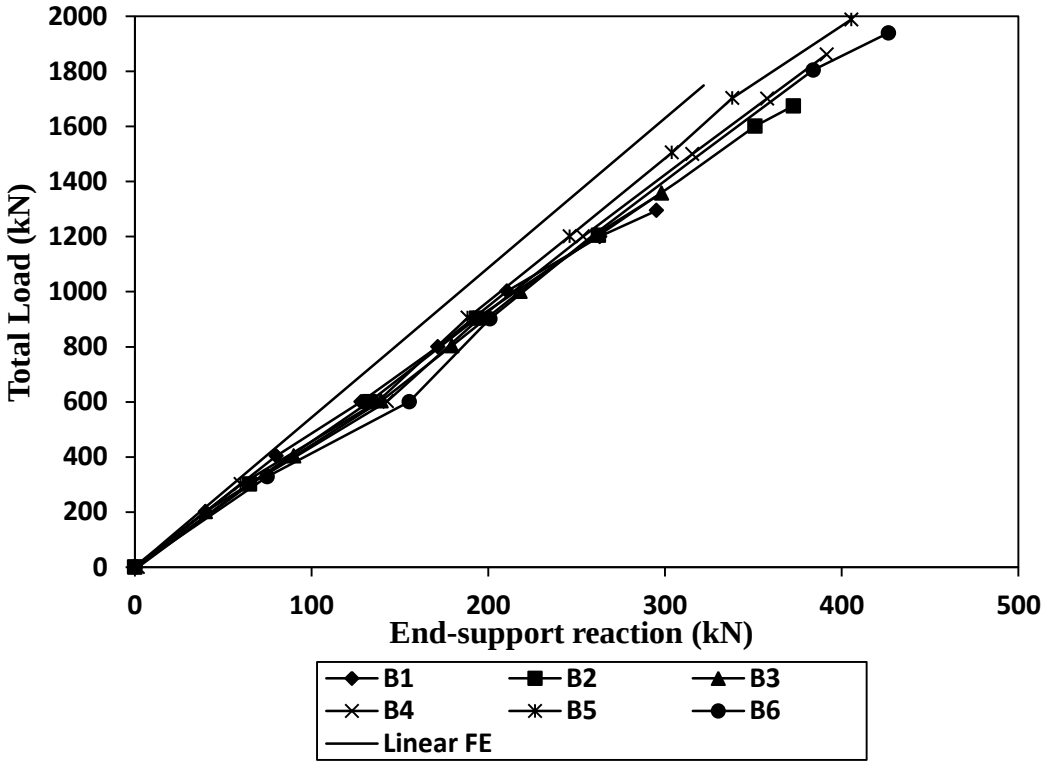

(a) Beams having *h*=600 mm

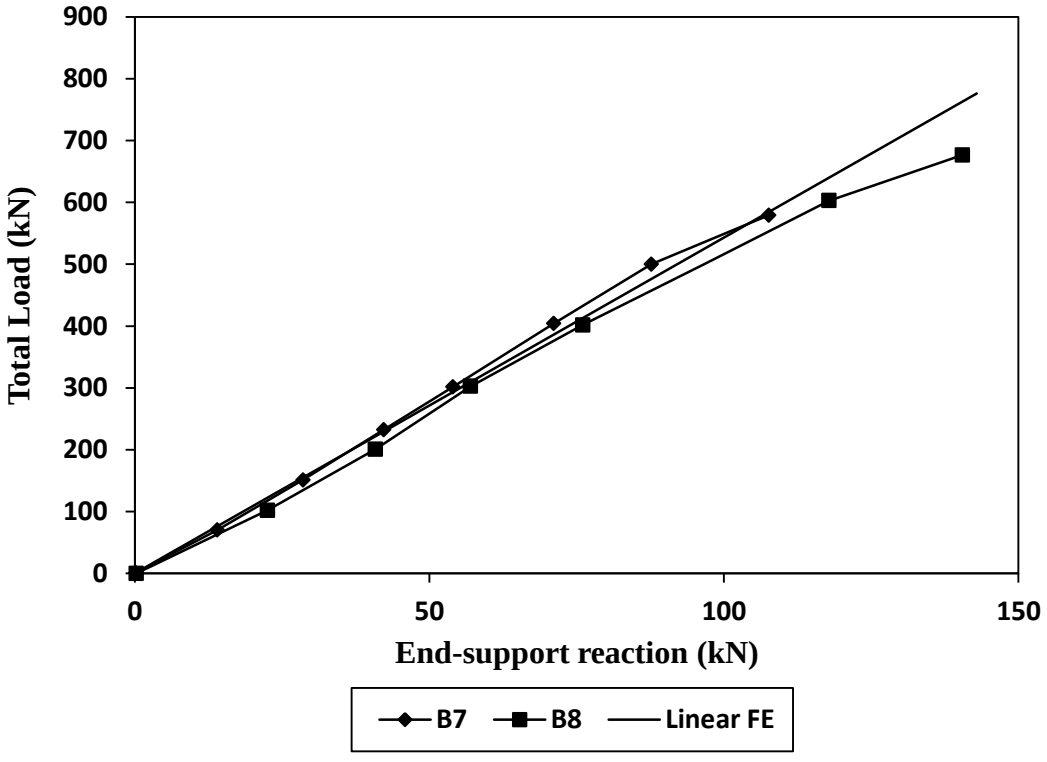

(b) Beams having *h*=300 mm

Figure 3.8: End support reaction versus total applied load

Table 3.5 presents the total failure load, P_t, the maximum shear force, V_{Exp}, and the normalised shear strength: $v_1 = V_{Exp}/bhf_c'$ and $v_2 = V_{Exp}/bh\sqrt{f_c'}$. It can be noticed that all the tested beams had approximately the same normalised shear strength v_1 of 0.12 when normalised by f_c'. However, the normalised shear strength v_2 by $\sqrt{f_c'}$ varies between 0.65 and 0.89. Depending on the normalised shear strength, it can be concluded that the maximum load of the tested beams is influenced by the concrete compressive strength.

Table 3.5: Failure loads, maximum shear forces and normalised shear strength

Beam no.	P_t kN	V_{Exp} kN	v_1	v_2
B1	1295	352.3	0.12	0.66
B2	1674	464.3	0.11	0.74
B3	1358	377.2	0.11	0.65
B4	1861	539	0.12	0.83
B5	1988	588.5	0.13	0.89
B6	1940	543.5	0.11	0.80
B7	579	181.8	0.12	0.67
B8	676	197.5	0.11	0.66

Note: P_t = total failure load, V_{Exp}= maximum shear force, v = normalised shear strength ($v_1 = V_{Exp}/bhf_c'$ and $v_2 = V_{Exp}/bh\sqrt{f_c'}$).

3.7.4 Mid-span deflections

The mid-span deflections for all specimens versus the total applied load are shown in Figure 3.9: Fig. 3.9(a) for beams having h =600 mm and Fig. 3.9(b) for beams having h =300 mm. The deflections in the two spans were similar and therefore only the mid-span deflections of the failed span are presented. The mid-span deflection measurements were adjusted to take into consideration the interior and exterior support settlements as recorded by the LVDTs at their locations. Up to the development of the first diagonal crack,

all the tested beams having the same depth had almost the same initial stiffness and consequently deflections, indicating that the initial stiffness is independent on the amount and configuration of the web reinforcement. For beams having a smaller depth (B7 and B8), the initial stiffness was lower than that of the deeper beams. After the development of the first diagonal crack, the beam stiffness significantly decreased leading to an increase in the mid-span deflection.

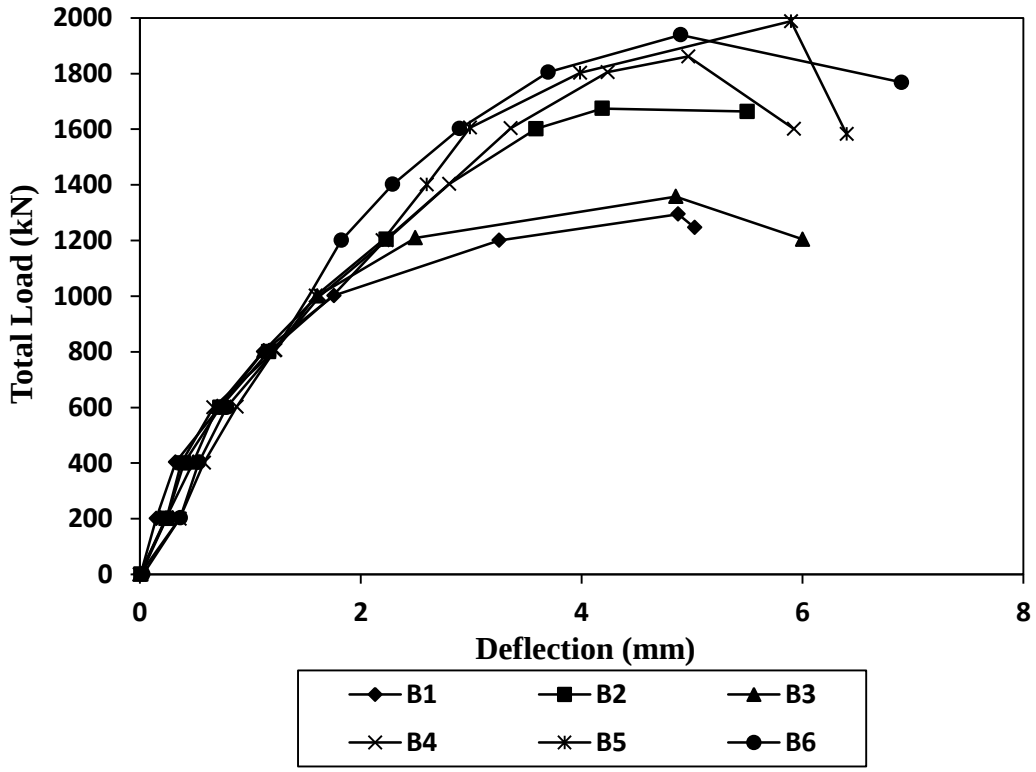

(a) Load-deflection curve for beams having h=600 mm

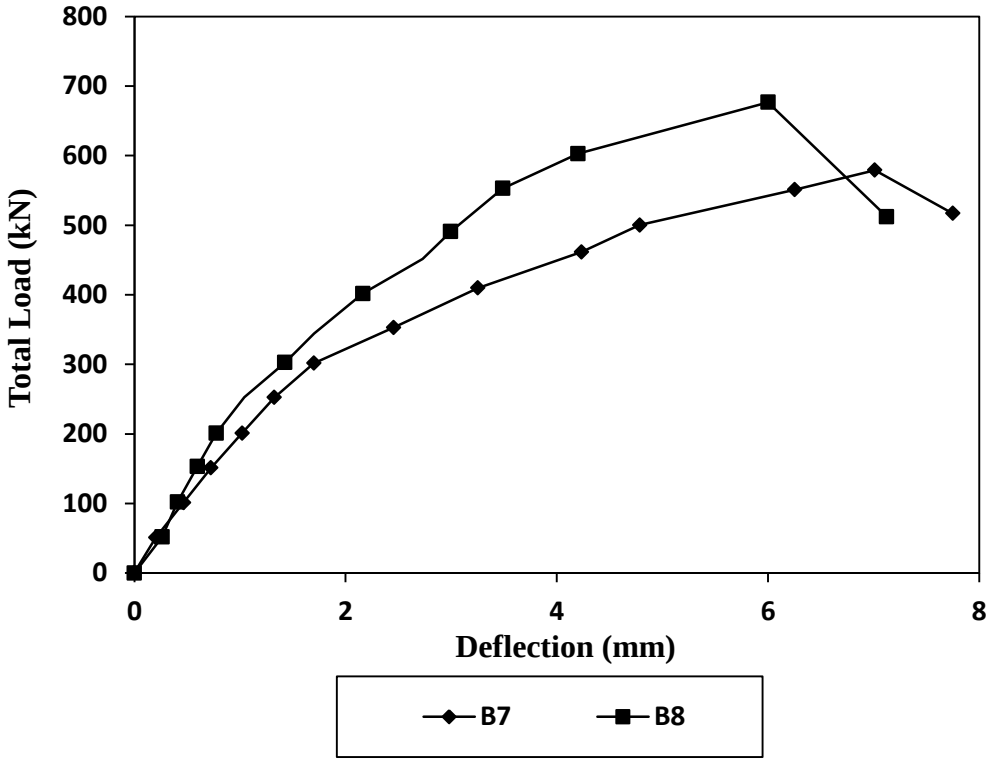

(b) Load-deflection curve for beams having h=300 mm

Figure 3.9: Mid-span deflection against total applied load

3.7.5 Strains in steel reinforcement

The relationship between the strains in steel reinforcement and the total applied load is shown in Figure 3.10: Fig. 3.10(a) for strains in bottom longitudinal steel bars, Fig. 3.10(b) for strains in top longitudinal steel bars, Fig. 3.10(c) for strains in horizontal web reinforcement and Fig. 3.10(d) for strains in vertical web reinforcement. The number of strain gauges used in each beam was selected depending on the amount of web reinforcement. For all beams, strain gauges were attached to the web reinforcing bars in the two spans. The strain readings in the two spans were almost the same and therefore only one span strains are presented in Figure 3.10. The significant redistribution of the strains in the web and longitudinal reinforcement started after the formation of the first diagonal crack.

For all beams, the highest strains were recorded for the web reinforcing bars crossing the main diagonal crack formed between the load plate and the intermediate support. Most of the web reinforcing bars reached the yield strain. Moreover, the strain in the bottom longitudinal reinforcement reached the yield strain for all beams except for two beams (B7 and B8). However, none of the top reinforcing bars yielded as indicated in Fig. 3.10(b).

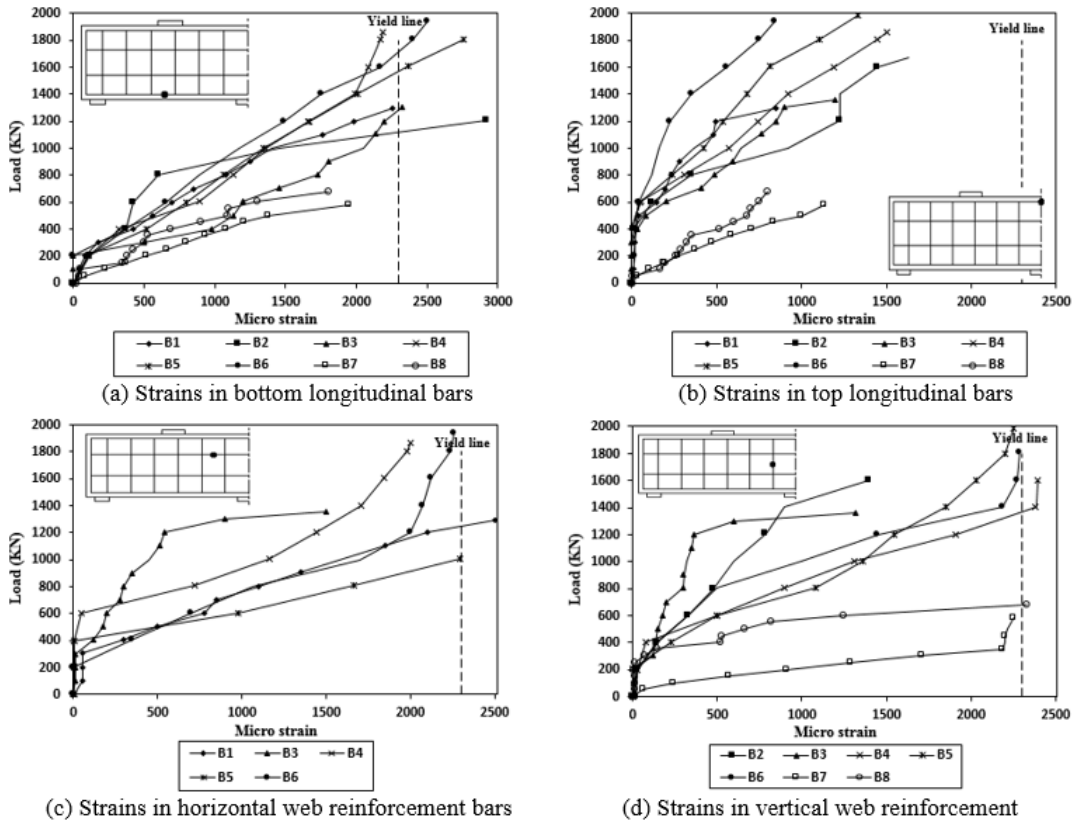

Figure 3.10: Total applied load against micro strain

In some cases, the strain gauges might not have been placed in the exact position of the major diagonal crack and therefore, yield could have occurred even though not shown by the strain readings. However, comparing the strain results of beams B4 (having horizontal and vertical web reinforcement), it can be seen that the vertical web reinforcement reached the yield strain before the horizontal one which almost reached the yield

strain at failure. Therefore, it can be concluded that the vertical web reinforcement is more effective in carrying loads than the horizontal web reinforcement for the shear span to depth ratio tested.

3.8 Concluding Remarks

Test results of eight continuously supported deep beams made with SCC were presented and discussed in this chapter. The parameters investigated were the shear span-to-depth ratio, the amount and configuration of web reinforcement and the longitudinal reinforcement ratio. Based on the experimental investigation presented in this chapter, the following conclusions are drawn:

- All the beams exhibited the same mode of failure irrespective of the shear span-to-depth ratio and amount and configuration of reinforcement. The main cause of failure is a major diagonal crack in the intermediate shear span started at the mid-depth of the beam and extended to connect the edges of the load and middle support plates.

- The shear strength of the tested beams is significantly controlled by the concrete compressive strength, and to a lesser degree by the amount and configuration of web reinforcement. For the shear span to depth ratio studied, the vertical web reinforcement had more effect on shear capacity than the horizontal web reinforcement.

- Beam having higher longitudinal reinforcement ratios had less crack width than those with low longitudinal reinforcement ratios.

- Up to cracking of concrete, the measured end support reactions of all the beams tested were very similar to the linear elastic finite element predictions. After cracking, however, the experimental reactions were slightly higher than the predictions.
- At initial stage of loading, all the beams tested had the same initial stiffness. However, when load was increased, the beam stiffness significantly decreased leading to a higher mid-span deflection.
- The major redistribution of the strains in the web and longitudinal reinforcement occurred after the formation of the first diagonal crack.
- The highest strains were recorded in the web reinforcing bars crossing the main diagonal crack formed between the load plate and the intermediate support.
- The strains in the web and bottom longitudinal reinforcement reached the yield strain for most of the beams tested while none of the top reinforcing bars yielded.

Although the experimental investigation is quite expensive and time consuming, it is required for the validation of any theoretical or numerical models. In the next chapter, the experimental results presented earlier are used to assess the validity of applying the simplified methods suggested by different design codes as well as those proposed by other researchers for the load capacity prediction of continuous SCC deep beams. The experimental results are also used in chapter five to validate the proposed FE model.

CHAPTER FOUR

SIMPLIFIED METHODS FOR LOAD CAPACITY PREDICTIONS

4.1 Introduction

In the current design codes, a deep beam is classified as a discontinuity region in which the strain distribution is nonlinear. In this case, the classical theory of elasticity is only valid to describe the behaviour of deep beams before cracking. After cracking, however, major redistribution of stresses takes place and the elasticity theory becomes invalid. Therefore, the current design codes suggest that deep beams should be designed either by nonlinear analysis in which the nonlinear strain distribution is taken into account or by the strut-and-tie model (STM). On the other hand, a number of researchers (Wang et al., 1993; Ashour and Morley, 1996; Ashour and Rishi, 2000) developed a mechanism analysis based on the upper-bound theorem of the plasticity theory to predict the shear strength of deep beams.

The main aim of this chapter is to cover the design recommendations suggested by different codes of practice as well as the design methods suggested by researchers for the shear strength of continuously supported deep beams. The recommendations of the current codes of practice investigated in this chapter include the shear provisions of the ACI Building Code (ACI 318M-11) and the strut-and-tie model suggested by ACI 318M-11, Euro Code 2 (EC2) and Canadian Standard for the Design of Concrete Structures (CSA23.3-04). The other design method considered is the Simplified Upper-bound technique developed by Ashour and Morley (1996).

Moreover, comparisons between the experimental results presented in chapter three and those predicted by the suggested design methods are presented to check the validity of applying these methods for SCC continuous deep beams and propose a new effectiveness factor for the strength of SCC. These simplified methods can only predict the load capacity of deep beams. Therefore, in order to predict the full behaviour of continuously supported SCC deep beams, a three dimensional non-linear finite element analysis will be presented in chapter five.

4.2 Shear Provisions of ACI 318M-11

In this section, comparisons between the experimental results and those predicted by the shear provisions of the ACI 318M-11 are presented. As mentioned in chapter two, the provisions of the ACI Building Code 318M-11 for shear strength of deep beams are applicable for a member with clear span to overall depth ratio not greater than 4. All the beams tested in chapter three satisfy the definition provided by the ACI Building Code for deep beams. The provisions of ACI 318M-11 (Section11.7) assume that the total shear capacity of deep beams, V_u, can be calculated from equation (4.1) below:

$$V_u = 0.83\sqrt{f_c'}bd \qquad (4.1)$$

where f_c' is the cylinder compressive strength of concrete in MPa, b is the beam width in mm and d is the beam effective depth in mm.

ACI 318M-11 also stated that to apply equation (4.1) for the prediction of shear strength of deep beams, the area of web reinforcement in both

directions (perpendicular and parallel to the longitudinal reinforcement) shall not be less than $0.0025bs$, where *s* is the spacing between the vertical or horizontal web reinforcement bars. In the current study, four of the beams tested satisfy this condition, namely B3, B4, B5 and B6. Table 4.1 presents the comparisons between the experimental results of the normalised shear capacity, v_{nEXP}, for the tested beams and that, v_{nACI}, predicted by the shear provisions of ACI 318M-11. The ratio between the shear strength obtained from the experimental results and that predicted by the ACI equation ranges from 0.845 to 1.145, with a mean value of 0.97, a standard deviation of 11% and a coefficient of variation of 11%. The predictions of the ACI 318M-11 are conservative only for three beams (B4, B5, and B6). For the rest of beams tested, except for beam B3, the unconservatism of the predictions can be attributed to the fact that these beams had web reinforcement in one direction only, not satisfying the condition mentioned above for the web reinforcement of deep beams. The discrepancy of the results between the tested beams can be attributed to the fact that the ACI equation determines the total shear strength of deep beams depending only on the concrete compressive strength. Overall, although equation (4.1) is very simple, its predictions are reasonably close to the experimental results.

Table 4.1: Comparisons between test results and shear provisions of ACI 318M-11

Beam no.	V_{EXP} kN	v_{nEXP}	V_{ACI} kN	v_{nACI}	v_{nEXP}/v_{nACI}
B1	352.3	0.118	415	0.139	0.849
B2	464.3	0.114	485	0.119	0.958
B3	377.2	0.109	446	0.129	0.845
B4	539	0.122	504	0.114	1.069
B5	588.5	0.128	514	0.112	1.145
B6	543.5	0.112	528	0.109	1.030
B7	181.8	0.118	195	0.127	0.931
B8	197.5	0.107	214	0.116	0.921
Mean					0.97
Standard deviation (%)					11
Coefficient of variation (%)					11

Note: V_{EXP} is the experimental shear strength, V_{ACI} is the predicted shear strength, $v_{nEXP} = V_{EXP}/bhf_c'$, $v_{nACI} = V_{ACI}/ bhf_c'$

4.3 Plasticity analysis

There are three fundamental theories on which the plasticity theorem is based, namely the lower-bound theorem, the upper-bound theorem and the uniqueness theorem. The lower-bound theorem can be developed by considering a safe and statically admissible stress distribution on or within the yield line. The load according to this theory can be obtained by considering the equilibrium of the internal and external forces and satisfying the static boundary conditions. The resultant load predicted by this theorem is lower than the failure load. On the other hand, the upper bound theorem can be derived by considering the kinematically admissible failure mechanism and the load calculated by this technique is higher than the

collapse load. The uniqueness theorem can be obtained by satisfying the two aforementioned theorems at the same time.

The lower-bound analysis can only be used for some simple cases. It requires finding a load path to transfer the forces from the load point to the supports and then the load capacity can be found by applying the equilibrium for the internal forces. However, for complicated loading conditions, it is easier to develop an upper-bound analysis as it just requires a geometrically admissible failure mechanism. After that, the energy principle can provide the load which is higher than the value of the collapse load. In the case of deep beams, the kinematic energy is provided by the rotation of a rigid part separated from the beam by a yield line. In this section, the test results presented in chapter three are compared with the prediction of STM which represents a lower-bound solution as well as the mechanism analysis of the upper-bound theorem in order to check the validity of using the plasticity analysis in predicting the load capacity of continuous SCC deep beams. It should be mentioned that these methods will be applied for the continuously supported SCC deep beams with varying the value of the effectiveness factor (v). Moreover, new equations for the effectiveness factor of SCC are proposed and validated against the experimental results. In the next section, some recommendations for the value of v collected from different design codes and also from previous research investigations are presented. The values of v presented are only those resulted in reasonable predictions for the load capacity of SCC continuous deep beams.

4.3.1 Effectiveness factor

The effectiveness factor, v, is presented to overcome the shortcomings of applying the plasticity theorem to analyse the behaviour of reinforced concrete and account for the limited ductility of concrete (Ashour and Morley, 1996). The value of the effectiveness factor mainly depends on the material properties, the geometrical dimensions and the reinforcement details (Nielsen and Hoang, 2010). There is disagreement among different codes of practice on the value of the effectiveness factor, as shown in Table 4.2. The ACI 318M-11 bases the value of the effectiveness factor on the amount of vertical and horizontal web reinforcement. This means that if the amount of web reinforcement satisfies the requirements shown in Table 4.2, the value of v is 0.64, otherwise v equals to 0.51. However, the value of the effectiveness factor suggested by the EC2 depends on the value of concrete compressive strength. On the other hand, the Canadian Standard recommends a value for the effectiveness factor based on the principal tensile strain of the steel reinforcement (ε_1) and the angle between the tie and strut (θ). The value of the principal tensile strain can be approximated as ($\varepsilon_1 = \varepsilon_s + (\varepsilon_s + 0.002)/(\tan\theta)^2$), where ε_s is the tensile strain in the ties. For the purpose of design, ε_s can be considered as the yield strain of the steel reinforcement which was obtained by conducting a tensile test on the steel bars. On the other hand, the angle between the strut and tie depends on the a/d ratio ($\tan\theta = d/a$). In the current study, all the beams tested had the same type of reinforcement which means that the value of the tensile strain is constant for all beams while the value of the a/d ratio is different. As a result, the value of the effectiveness factor according to the Canadian

Standard can be calculated based on the value of the a/d ratio as shown in Table 4.2.

Table 4.2: The value of the effectiveness factor v according to different design codes

Reference	Effectiveness factor	Notes
ACI 318M-11	$v = 0.85\beta_s$	$\beta_s = 0.75$ if: $\sum \frac{A_{si}}{bs_i} \sin \propto_i \geq 0.003$ $\beta_s = 0.6$ Otherwise
EC2	$v = 0.6\left(1 - \frac{f_c'}{250}\right)$	
CSA23.3-04	$v = \frac{1}{1.20 + 0.74(a/d)^2}$	≤ 0.85

Note: β_s is a factor to account for the effect of cracking and confining reinforcement on the effective compressive strength of concrete in a strut, A_{si} is the area of surface reinforcement crossing the strut, s_i is the spacing between the surface reinforcement bars crossing the strut, b is the beam web width, $\propto_i$ is the angle between the axis of strut and the surface reinforcing bars crossing the strut, a is the shear span and d is the effective depth of the beam.

On the other hand, a high number of research investigations suggested different formulas for v. As shown in Table 4.3, three equations for v were selected to be used in the analysis presented in this chapter. The selection of these formula was based on the accuracy of the predictions compared to the experimental results. As can be clearly seen from Table 4.3, the three selected formulas were based on different material and geometrical properties and varied from research to another. Neilsen (1984) proposed a formula for v based on the value of f_c'. The value of v resulting from this formula ranges from 0.3 to 0.8 for a concrete strength up 100 MPa. However, Vecchio and Collins (1993) considered v as a function of concrete strength and principal tensile and compressive strains in the steel reinforcement. This formula was modified by Yang and Ashour (2008) to reflect the size effect as shown in Table 4.3. It should be noted that this formula was proposed for the upper-bound analysis and it results in low effectiveness factor values.

Another formula was proposed by Warwick and Foster (1993) which considers the effect of a/d ratio in addition to the concrete strength and the value resulted from their formula must be less than 0.85.

Table 4.3: The value of the effectiveness factor v according to previous studies

Reference	Effectiveness factor	Notes
Nielsen (1984)	$v = 0.8 - \frac{f_c'}{200}$	
Yang and Ashour (2008)	$v = \frac{\xi}{1.0 + k_c k_f}$	$\xi = \frac{1}{\sqrt{1 + \frac{d}{25 d_a}}}$ $k_c = \frac{1 + sin\alpha}{1 - sin\alpha} \geq 1.0$ $k_f = 0.1825\sqrt{f_c'} \geq 1.0$
Warwick and Foster (1993)	$v = 1.25 - \frac{f_c'}{500} - 0.72\left(\frac{a}{d}\right) + 0.18\left(\frac{a}{d}\right)^2$	≤ 0.85

Note: f_c' is the cylinder compressive strength of concrete, f_y is the yield strength of steel reinforcement, ξ is the size effect factor, d is the beam effective depth, d_a is the maximum size of aggregate, a is the shear span, α is the angle between the relative displacement δ_c and the yield line chord as shown in Figure 4.3.

4.3.2 Strut-and-tie model in current design codes

The current design codes suggest that deep beams shall be designed using either nonlinear analysis or strut-and-tie model (STM). In this section, comparisons between the experimental results and the STM suggested by different design codes are carried out, namely the ACI Building Code (318M-11), the Euro Code 2 (EC2) and the Canadian Standard for the Design of Concrete Structures (CSA23.3-04). The main aim is to assess the validity of the STM, proposed for NC deep beams, for predicting the load capacity of SCC continuous deep beams. Initially, the STM will be used to predict the load capacity of continuous NC deep beams, shown in the database collected in chapter two, using the values of the effectiveness factor shown in Tables 4.2 and 4.3. After that, the STM will be applied to predict the load

capacity of continuously supported SCC deep beams tested in the current research investigation.

The total applied load is estimated by using a set of equations based on a simple STM shown in Figure 4.1. For two spans continuous deep beams, the total load, P_t, due to the failure of concrete struts can be determined from equations (4.2) to (4.5) below:

$$P_t = 2vf_c' b\,[w_{ES} + w_{IS}]\,Sin\,(\theta) \tag{4.2}$$

$$w_{ES} = w_t\,Cos\,(\theta) + \frac{[l_{EP} + 0.5l_{LP}]}{2}\,Sin\,(\theta) \tag{4.3}$$

$$w_{IS} = w_t\,Cos\,(\theta) + \frac{[\,l_{LP} + l_{IP}]}{4}Sin\,(\theta) \tag{4.4}$$

$$\theta = tan^{-1}\frac{(h - c - c')}{a} \tag{4.5}$$

where v is the effectiveness factor of concrete, f_c' is the cylinder compressive strength of concrete, b is the beam width, w_{ES} is the average effective width of the exterior concrete strut, w_{IS} is the average effective width of the interior concrete strut, θ is the angle between the concrete strut and the longitudinal axis of the beam, l_{EP} is the width of the exterior bearing plate, l_{IP} is the width of the interior bearing plate, l_{LP} is the width of the load bearing plate, h is the total height of the beam, c and c' are the concrete covers of the bottom and top longitudinal reinforcement, respectively, a is the shear span and w_t is the effective tie width which equals twice the concrete cover ($w_t = 2c$).

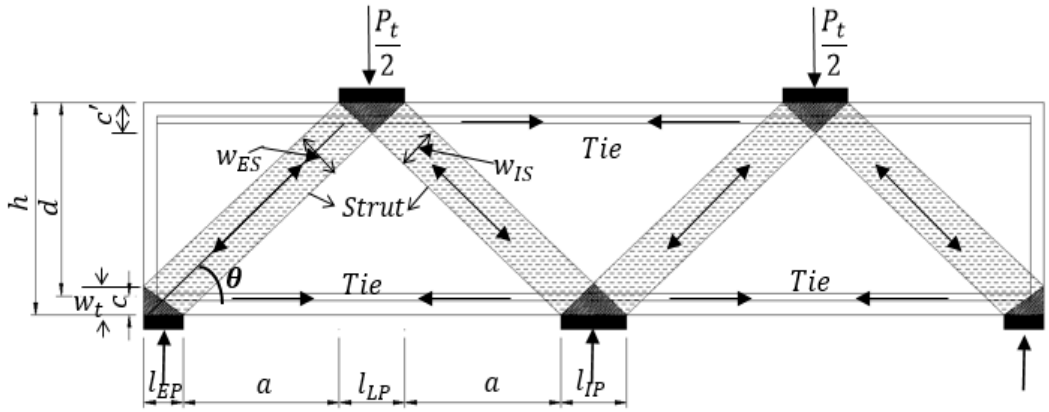

Figure 4.1: Schematic STM for continuous deep beams

In the above equations, the effectiveness factor of concrete is the only difference among the three design codes considered in the current comparison. Each design code suggests a different value for the effectiveness factor as presented in Table 4.2. Moreover, a number of researchers suggested different values for the effectiveness factor. Some of these values were selected to be used in this chapter as it was shown in Table 4.3.

Table 4.4 shows the mean, the standard deviation and the coefficient of variation for the predictions of the load capacity of continuously supported NC deep beams available in the literature. Moreover, Figure 4.5 shows comparisons between the experimental results of NC continuous deep beams collected from previous studies and those predicted by the STM for different effectiveness factor formulas provided by the current design codes considered. On the other hand, Figure 4.6 shows comparisons between the experimental results of continuous NC deep beams and those predicted by the STM for different effectiveness factor formulas proposed by different researchers. The effectiveness factor proposed by Yang and Ashour (2008)

was excluded from the comparisons as it was proposed for the mechanism analysis of the upper-bound theorem and it results in very low predictions compared to the experimental results. By comparing the values shown in Table 4.4, it can be seen that the effectiveness factor suggested by the ACI 318M-11 resulted in the most reasonable predictions with a mean, a standard deviation and a coefficient of variation of 1.15, 34% and 30%, respectively. The effectiveness factor proposed by Warwick and Foster (1993) also showed reasonable predictions compared to the other suggested values. It can be noticed from Figure 4.2 and 4.3 that irrespective of the value of the effectiveness factor, the predictions of STM are conservative for most of the beams.

Table 4.4: The mean, SD and COV for STM predictions of load capacity of NC continuous deep beams using different values for the effectiveness factor

Reference	Mean	Standard deviation (%)	Coefficient of variation (%)
ACI 318M-11	1.15	34	30
EC2	1.28	37	29
CSA23.3-04	1.47	76	37
Nielsen (1984)	1.28	35	28
Warwick and Foster (1993)	1.10	40	36

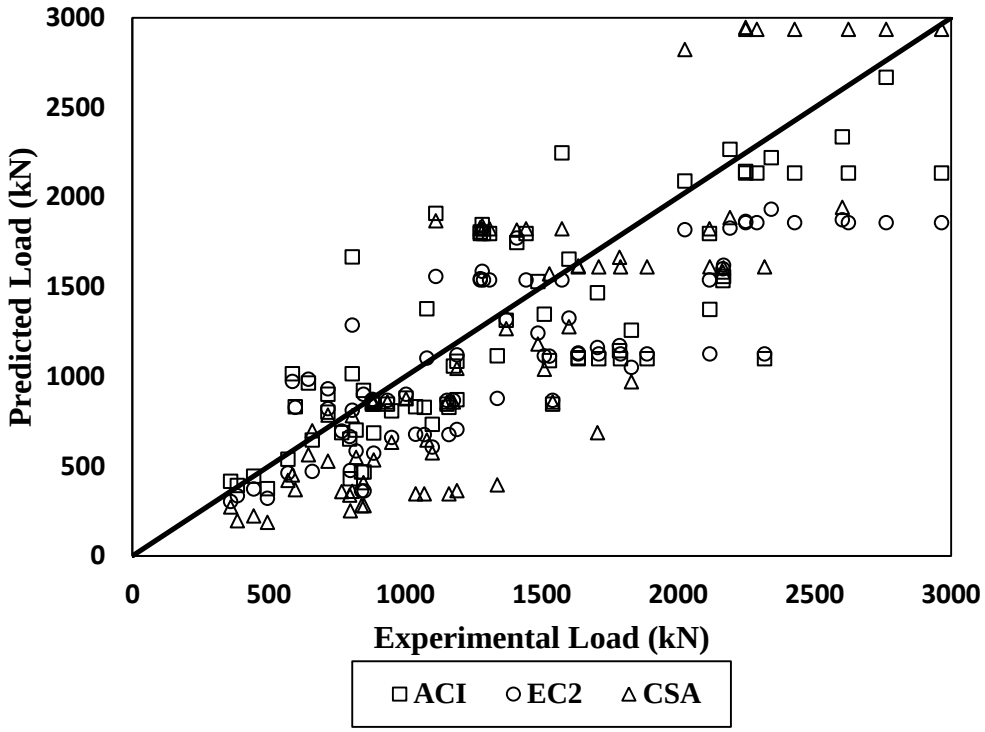

Figure 4.2: Comparisons between experimental results of NC continuous deep beams and predictions of STM using effectiveness factors suggested by different design codes

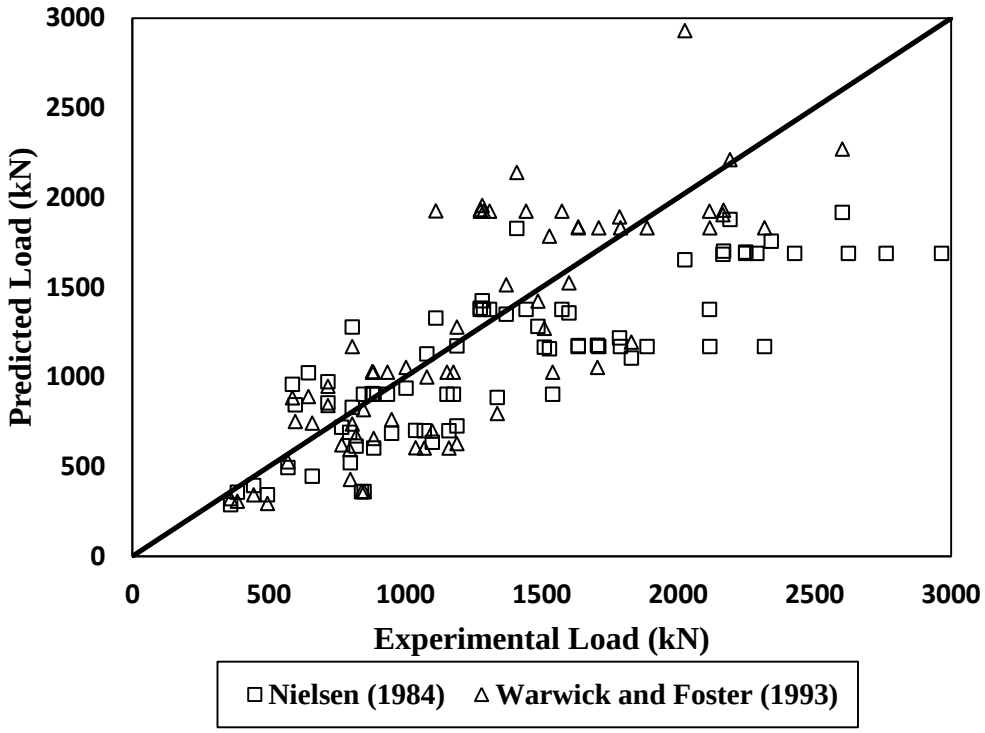

Figure 4.3: Comparisons between experimental results of NC continuous deep beams and predictions of STM using effectiveness factors suggested by different researchers

Similarly, the STM is used to predict the load capacity of continuously supported SCC deep beams tested in the current study. Table 4.5 and Figure 4.4 show the comparisons between the experimental results and those predicted by the STM using effectiveness factor formulas suggested by different design codes whereas Table 4.6 and Figure 4.5 show similar comparisons but for effectiveness factor formulas proposed by different researchers. The ACI prediction was the closest to the current test results with a mean of 1.15, a standard deviation of 4.1% and a coefficient of variation of 3.6%. The predictions of all the considered codes were conservative for all the SCC beams tested. Moreover, the predictions of the Canadian Code underestimate the results of SCC beams specifically those having high shear span-to-depth ratio. Furthermore, the effectiveness factor formulas proposed by Nielsen (1984) and Warwick and Foster (1993) also resulted in conservative predictions and the results were less accurate than those predicted by the ACI code.

It can be concluded that, the formulas of the effectiveness factor considered in this chapter for the lower-bound analyses resulted in conservative predictions for the load capacity of continuously supported SCC deep beams. Therefore, a proposed effectiveness factor for SCC will be presented in the next section with the aim of achieving more accurate predictions.

Table 4.5: Comparisons between test results and predictions of STM using effectiveness factors suggested by different design codes

Beam no.	P_{EXP}	P_{ACI}	P_{EC2}	P_{CSA}	P_{EXP}/P_{ACI}	P_{EXP}/P_{EC2}	P_{EXP}/P_{CSA}
B1	1295	1074	885	877	1.21	1.46	1.48
B2	1674	1466	1145	1197	1.14	1.46	1.40
B3	1358	1243	1001	1015	1.09	1.36	1.34
B4	1861	1587	1219	1296	1.17	1.53	1.44
B5	1988	1650	1256	1348	1.20	1.58	1.47
B6	1940	1739	1307	1420	1.12	1.48	1.37
B7	579	500	410	165	1.16	1.41	3.51
B8	676	602	480	198	1.12	1.41	3.41
Mean					1.15	1.46	1.93
Standard deviation (%)					4.1	7.2	95
Coefficient of variation (%)					3.6	4.9	49.2

Table 4.6: Comparisons between test results and predictions of STM using effectiveness factors suggested by different researchers

Beam no.	P_{EXP}	P_1	P_2	P_{EXP}/P_1	P_{EXP}/P_2
B1	1295	923	1049	1.40	1.23
B2	1674	1149	1380	1.46	1.21
B3	1358	1028	1196	1.32	1.14
B4	1861	1207	1477	1.54	1.26
B5	1988	1234	1526	1.61	1.30
B6	1940	1271	1594	1.53	1.22
B7	579	427	379	1.36	1.53
B8	676	488	444	1.39	1.52
Mean				1.45	1.30
Standard deviation (%)				10	15
Coefficient of variation (%)				7.0	11

Note: P_1 and P_2 are the total loads predicted by the STM using the effectiveness factor formula proposed by Nielsen (1984) and Warwick and Foster (1993), respectively.

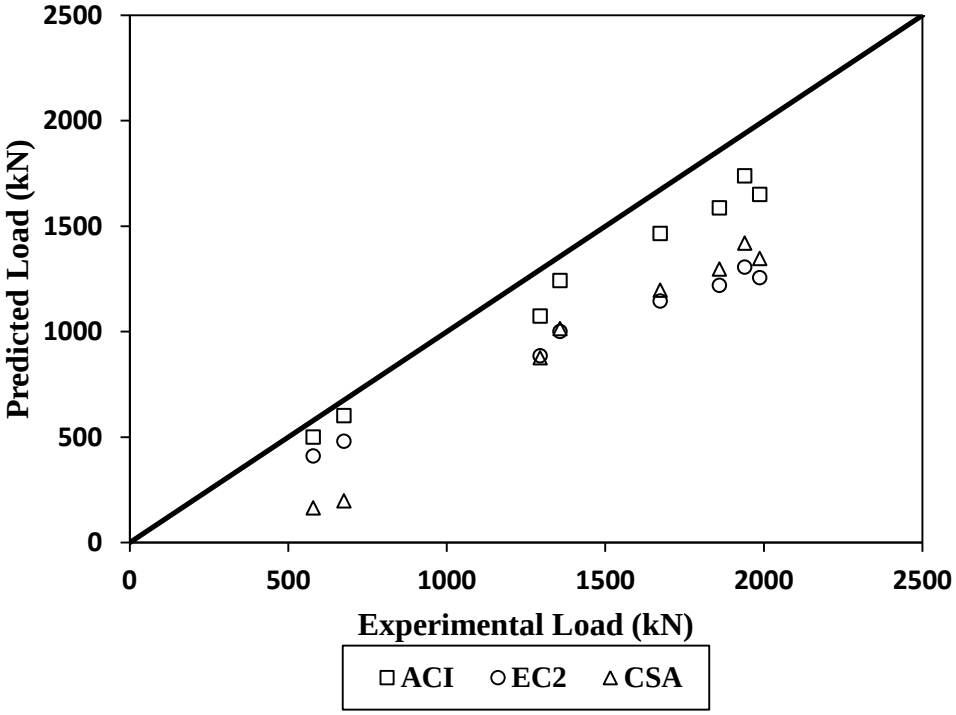

Figure 4.4: Comparisons between experimental results of SCC continuous deep beams and predictions of STM using effectiveness factors suggested by different design codes

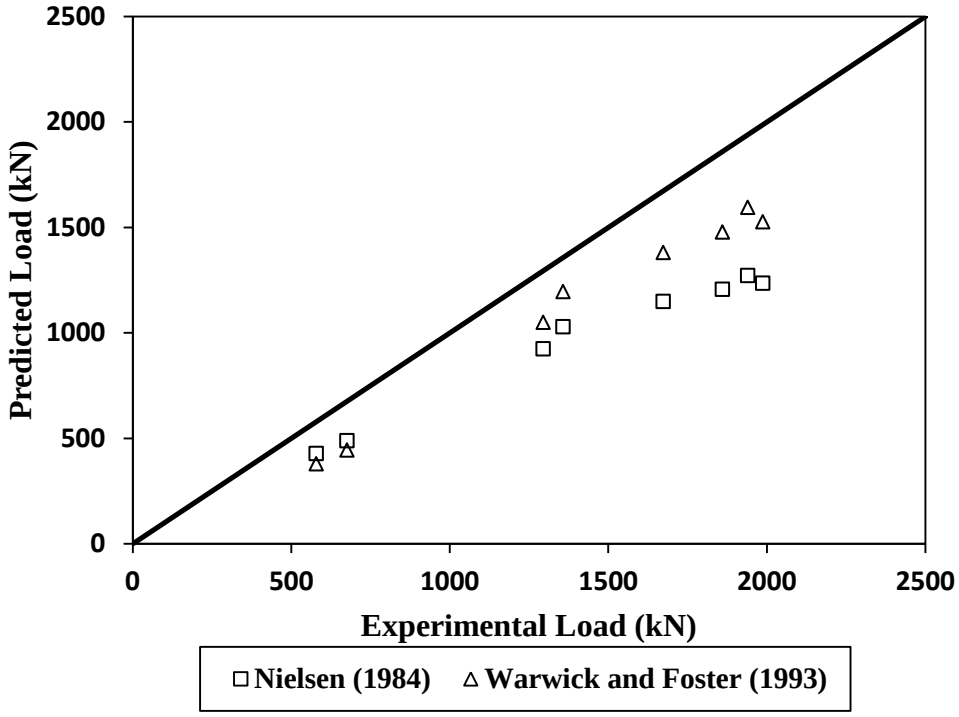

Figure 4.5: Comparisons between experimental results of SCC continuous deep beams and predictions of STM using effectiveness factors suggested by different researchers

4.3.3 Proposed effectiveness factor for SCC

As presented in the previous section, all of the effectiveness factor formulas considered for the lower-bound analysis of continuously supported SCC deep beams resulted in conservative results for all of the beams tested. Therefore, a modified value for the effectiveness factor for SCC is needed with the aim of achieving better predictions.

Based on a regression analysis of the experimental results of the beams tested in the current study, three new equations for the effectiveness factor of SCC are suggested in order to achieve more accurate predictions. As mentioned earlier in this chapter, the value of the effectiveness factor mainly depends on the material properties and geometrical dimensions. Therefore, the proposed equations have been expressed in terms of concrete strength,

effective depth and maximum size of coarse aggregate as shown in Table 4.7.

Table 4.7: Proposed effectiveness factor formulas for lower-bound analysis of continuous SCC deep beams

Formula no.	Effectiveness factor
Formula I	$v = 0.43 + 0.6\left(1 - \frac{f_c'}{250}\right)\frac{1}{\sqrt{1 + \frac{d}{25d_a}}}$
Formula II	$v = 0.6\left(1 - \frac{f_c'}{250}\right) + \frac{0.55}{\sqrt{1 + \frac{d}{10d_a}}}$
Formula III	$v = \left(1 - \frac{f_c'}{250}\right) \Big/ \sqrt{1 + \frac{d}{150d_a}}$

where f_c' is the concrete compressive strength, d_a is the maximum size of coarse aggregate and d is the beam effective depth.

As can be seen from Table 4.7 above, the proposed formulas were based on the effectiveness factor equation suggested by EC2. The ratio between the beam depth, d, and maximum size of aggregate, d_a, is included in the proposed equations to reflect the influence of the size effect. In the plasticity theory, the size effect could not be considered because of the fact that the nominal stress at failure must be independent of size (Bazant and Kim 1984). Therefore, in order to take the size effect into account, the only way is to consider it in the effectiveness factor. The maximum size of aggregate presents one of the main differences between SCC and NC where smaller size of coarse aggregate is required for SCC. In addition, it is well known that the shear strength decreases as the beam depth increases. It was proved that the nominal shear stress is inversely proportional to the term $\left[\sqrt{1 + \frac{d}{d_a}}\right]$

(Bazant and Kim 1984). In all the proposed equations, the higher the beam depth, d, the lower is the value of the effectiveness factor which as a result leads to lower shear strength.

The comparisons between the experimental load capacity of continuously supported SCC deep beams and the predictions of the lower-bound analysis using the proposed effectiveness factor equations are shown in Table 4.8 and Figure 4.6. It can be seen that all the proposed formulas achieved accurate predictions for the load capacity of the beams tested with a mean, a standard deviation and a coefficient of variation of approximately 1.0, 7.0% and 7.0%, respectively. All the proposed equations resulted in approximately similar results with very low variation between them as can be seen from Figure 4.6. It can be concluded that the proposed formulas are able to provide highly accurate predictions for the capacity of continuous SCC deep beams. However, more validation for the proposed formulas is needed due to the fact that the only data available on continuous SCC deep beams is the data collected in the current study.

Table 4.8: Comparisons between test results and predictions of STM using effectiveness factor formulas suggested in current study

Notation	P_{EXP}	Formula I		Formula II		Formula III	
		P_{PRE}	P_{EXP}/P_{PRE}	P_{PRE}	P_{EXP}/P_{PRE}	P_{PRE}	P_{EXP}/P_{PRE}
B1	1295	1216	1.06	1246	1.04	1259	1.03
B2	1674	1625	1.03	1638	1.02	1629	1.03
B3	1358	1395	0.97	1419	0.96	1424	0.95
B4	1861	1748	1.06	1752	1.06	1734	1.07
B5	1988	1811	1.10	1810	1.10	1787	1.11
B6	1940	1899	1.02	1891	1.03	1859	1.04
B7	579	625	0.93	638	0.91	631	0.92
B8	676	742	0.91	754	0.90	738	0.92
Mean			1.01		1.00		1.01

Standard deviation (%)	6.8		7.3		7.3
Coefficient of variation (%)	6.7		7.3		7.2

where P_{EXP} is the experimental load capacity of the beams tested in the current study and P_{PRE} is the load capacity predicted by the STM model using the proposed effectiveness factor formulas.

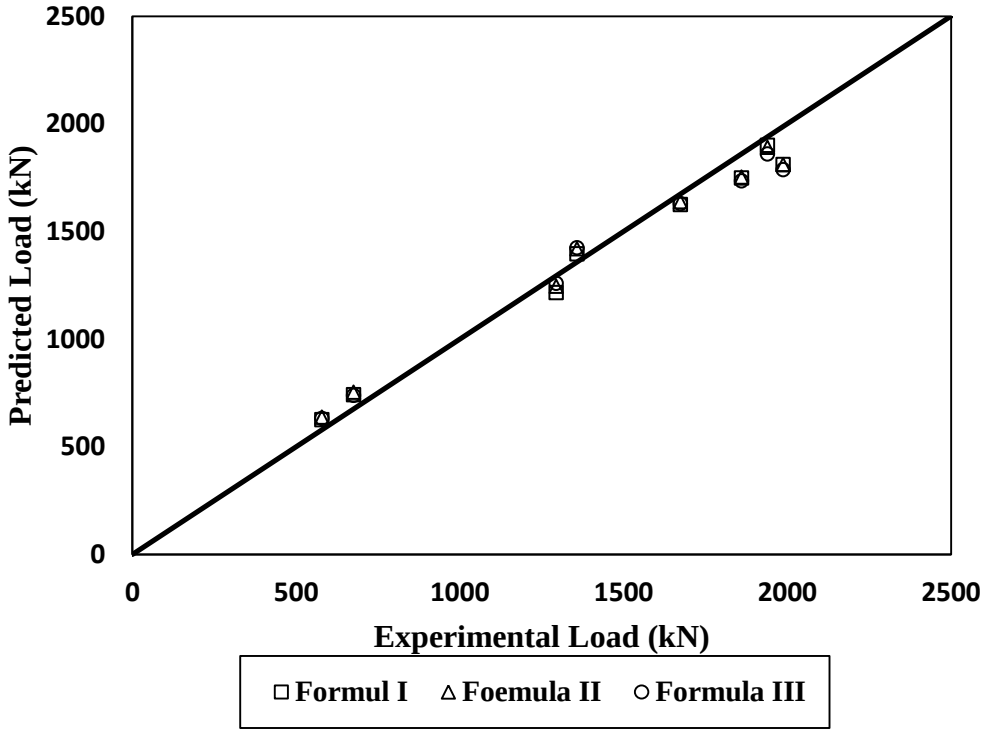

Figure 4.6: Comparisons between experimental results of SCC continuous deep beams and predictions of STM using effectiveness factors suggested in the current study

4.3.4 Upper-bound analysis

Previous experimental studies on NC continuous deep beams (Rogowsky et al., 1986; Ashour, 1996; Subedi, 1998; Yang et al., 2007a, 2007b) in addition to the current experimental investigation on SCC continuous deep beams showed that the main cause of failure in continuous deep beams is a major diagonal crack formed between the applied mid-span load and the intermediate support separating the beam into two rigid blocks: the first one

rotated around the end support, leaving the rest of the beam fixed on the other two supports.

In this section, the mechanism analysis of the upper-bound theory proposed by Ashour and Morley (1996) is used to predict the load capacity of continuously supported SCC deep beams described in chapter three. In their study, the yield line is used to represent the diagonal crack for the mechanism of failure described above as shown in Figure 4.7. The concrete is modelled as a rigid perfectly plastic material obeying the modified Coulomb failure criteria with zero tension cut-off while the steel reinforcement is assumed to be a rigid perfectly plastic material in tension and compression having a yield strength f_y and carrying only longitudinal tensile and compressive stresses. As the resistance of concrete is very weak in tension compared to compression and the ductility of concrete in tension is very limited, the tensile strength of concrete is not taken into account in this analysis (Ashour and Morley, 1996).

In the mechanism analysis of the upper-bound theorem, the total load carrying capacity, P_t, of a two-span continuous deep beam can be found by equating the total internal energy, W_I, to the external energy, W_E, resulted from the total applied load P_t. The total internal energy, W_I, can be calculated from equation (4.6) by adding the energy dissipated by concrete, W_c, along the yield line to the energy in the steel reinforcing bars, W_s, (longitudinal, vertical and horizontal) crossing the yield line as shown in Figures 4.7 and 4.8.

$$W_I = W_c + W_s \qquad (4.6)$$

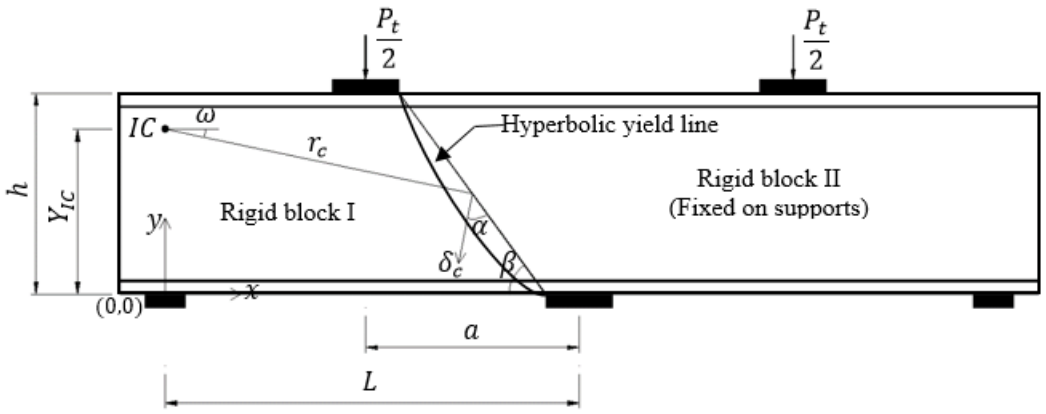

Figure 4.7: Failure mechanism of two-span continuous deep beams (Ashour and Morley, 1996)

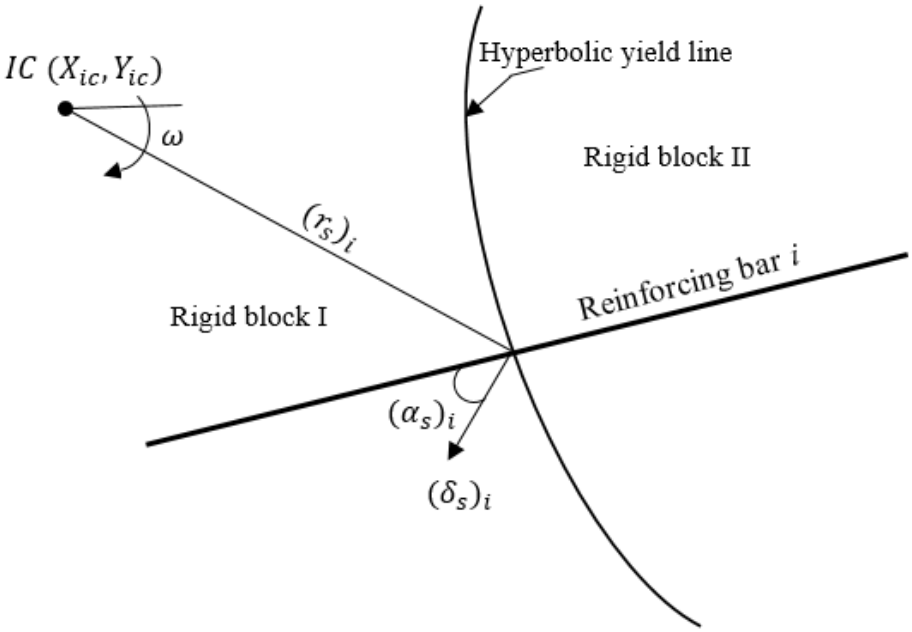

Figure 4.8: Reinforcement crossing the yield line (Ashour and Morley, 1996)

The total internal energy depends on the position of the instantaneous centre, IC, around which the concrete rigid block I is assumed to rotate. Therefore, the total applied load mainly depends on the position of the instantaneous centre $IC\ (X_{ic},\ Y_{ic})$. As shown in Figure 4.7, the horizontal coordinate (X_{ic}) of the instantaneous centre matches with that of the centre of end support plate because the concrete rigid block I is fixed on the end

support and rotation is allowed with no vertical movements. In this case, the value of the total load capacity depends on the vertical coordinate (Y_{ic}) of the instantaneous centre and therefore, the internal energy dissipated by concrete along the yield line can be calculated from equation (4.7). By changing the value of Y_{ic}, different load capacities can be obtained among which the lowest value is taken due to the fact that the failure occurs at the lowest strength. Excel software was used to find the position of the instantaneous centre along the vertical line passing through the centre of the end support plate. The value of Y_{ic} was changed along this vertical line to find the lowest load capacity.

Based on the above explanation and as the relative displacement of the concrete, δ_c, is equal to ωr_c and the relative displacement of the steel reinforcement, δ_s, is equal to ωr_s, the total internal energy dissipated in concrete, W_c, and that in steel reinforcement, W_s, can be calculated from equations (4.7) and (4.8), respectively, as follows:

$$W_c = \frac{b f_{ce} h}{2 sin\beta} \omega r_c \, (1 - sin\alpha) \tag{4.7}$$

$$W_s = \sum_{i=1}^{n} \omega (r_s)_i \, (A_s)_i (f_y)_i cos(\alpha_s)_i \tag{4.8}$$

where b is the beam width, f_{ce} is the effective compressive strength of concrete, h is the beam total depth, ω is the rotational displacement of rigid block I, r_c is the distance from the instantaneous centre to the middle point of the yield line chord, α is the angle between the relative displacement δ_c and the yield line chord, β is the inclination of the yield line chord, n is the number of reinforcing bars crossing the yield line, $(r_s)_i$ is the distance between the

instantaneous centre to the point where the reinforcing bar i crosses the yield line, $(A_s)_i$ and $(f_y)_i$ are the area and yield strength of the reinforcing bar i crossing the yield line and $(\alpha_s)_i$ is the angle between the reinforcing bar i crossing the yield line and the relative displacement δ_s.

The effective compressive strength of concrete f_{ce} used in the prediction of the load capacity is calculated from equation (4.9) below:

$$f_{ce} = v f_c' \tag{4.9}$$

where v is the effectiveness factor of concrete presented earlier in this chapter and f_c' is the cylinder compressive strength of concrete.

In fact, the total internal energy dissipated in the steel reinforcement includes the energy in the longitudinal top and bottom reinforcement as well as the vertical and horizontal web reinforcement. The total internal energy dissipated in the steel reinforcement requires calculating the value of α_s for each reinforcing bar crossing the yield line. For horizontal and vertical reinforcing bars, the value of $cos(\alpha_s)_i$ can be calculated from equations (4.10) and (4.11), respectively, as follows:

$$cos(\alpha_{sh})_i = \frac{|Y_{ic} - y_i|}{(r_s)_i} \tag{4.10}$$

$$cos(\alpha_{sv})_i = \frac{|X_{ic} - x_i|}{(r_s)_i} \tag{4.11}$$

where $(\alpha_{sh})_i$ is the angle between the relative displacement and the horizontal reinforcing bar i crossing the yield line, $(\alpha_{sv})_i$ is the angle between the relative displacement and the vertical reinforcing bar i crossing the yield

line, y_i and x_i are the distance between the global coordinates and the point where the horizontal and vertical reinforcing bars intersect with the yield line.

As mentioned earlier in this section, the total load carrying capacity P_t of a two-span continuous deep beam can be calculated by equating the total internal energy, W_I, to the external energy, W_E. By adding equation (4.7) to equation (4.8), the total internal energy, W_I, can be found from equation (4.12) below:

$$W_I = \frac{bf_{ce}h}{2sin\beta}\omega r_c\,(1 - sin\alpha) + \sum_{i=1}^{n} \omega (r_s)_i\,(A_s)_i (f_y)_i cos(\alpha_s)_i \qquad (4.12)$$

The total external energy, W_E, resulted from the load applied at the point of the mid-span, $P_t/2$, can be calculated from equation (4.13) below:

$$W_E = \omega a \frac{P_t}{2} \qquad (4.13)$$

where a is the shear span of the beam measured from the centre of the support to the point of the applied load.

By equating the total internal energy calculated from equation (4.12) to the external energy calculated from equation (4.13), the total load capacity, P_t, can be found from equation (4.14) below:

$$P_t = \frac{b}{a}\left[\frac{vf_c' hr_c\,(1 - sin\alpha)}{sin\beta} + 2\sum_{i=1}^{n} (r_s)_i\,(A_s)_i (f_y)_i cos(\alpha_s)_i\right] \qquad (4.14)$$

As mentioned earlier in this section, equation (4.14), proposed by Ashour and Morley (1996) for NC continuous deep beams, is applied in the present study to predict the total load capacity of SCC continuous deep beams using

different values for the effectiveness factor of concrete. The results obtained from this analysis are presented below.

Table 4.9 and Figure 4.9 show the comparisons between the experimental results of SCC continuous deep beams and those predicted by the upper-bound analysis for different effectiveness factor formulas provided by the current design codes considered. It can be clearly noticed that all the considered codes showed reasonable predictions compared to the experimental results. The most accurate results were obtained by using the effectiveness factor recommended by ACI 318M-11 with an average of 1.03, standard deviation of 20% and a coefficient of variation of 20%. The predictions clearly underestimate the load capacity of beams having web reinforcement in one direction only (B1 and B2). Moreover, the accuracy of the load capacity predicted by the upper-bound analysis considerably decreased for beams having high shear span-to-depth ratio (B7 and B8). However, the overall predictions showed reasonable accuracy and the results were in most cases close to the experimental results.

Table 4.9: Comparisons between test results and predictions of upper-bound analysis for different v values recommended by design codes

Beam no.	P_{EXP}	P_{ACI}	P_{EC2}	P_{CSA}	P_{EXP}/P_{ACI}	P_{EXP}/P_{EC2}	P_{EXP}/P_{CSA}
B1	1295	968	977	957	1.34	1.33	1.35
B2	1674	1347	1337	1333	1.24	1.25	1.26
B3	1358	1446	1354	1338	0.94	1.00	1.01
B4	1861	1646	1506	1509	1.13	1.24	1.23
B5	1988	1932	1782	1789	1.03	1.12	1.11
B6	1940	2016	1851	1865	0.96	1.05	1.04
B7	579	710	714	630	0.82	0.81	0.92
B8	676	903	902	806	0.75	0.75	0.84

Mean	1.03	1.07	1.10
Standard deviation (%)	20	21	18
Coefficient of variation (%)	20	19	16

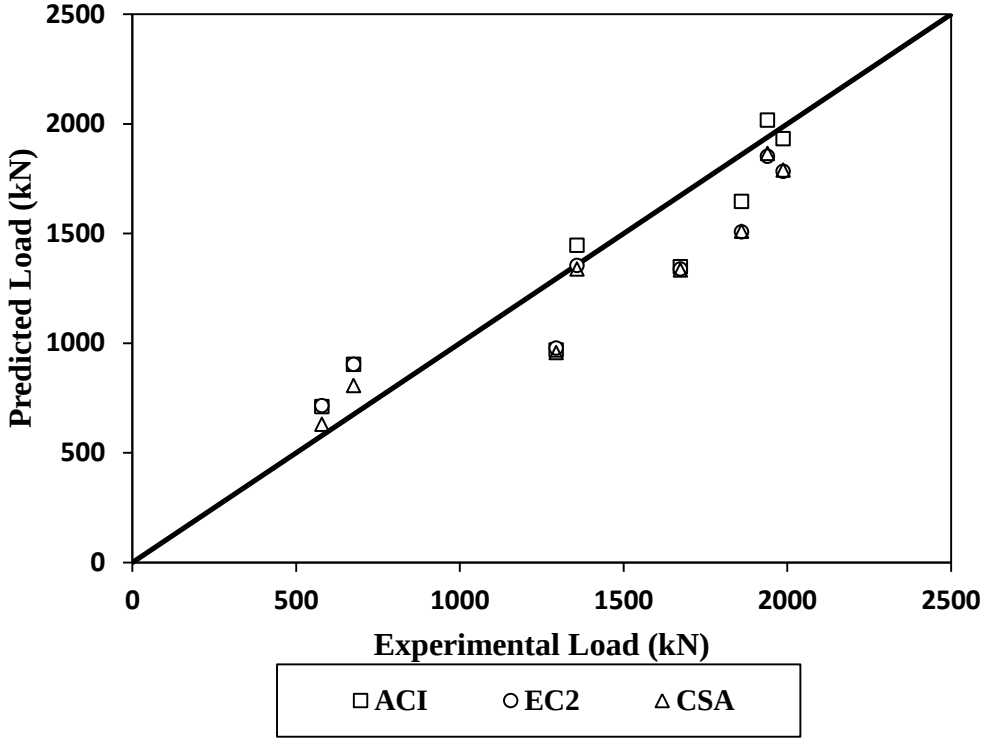

Figure 4.9: Comparisons between experimental results and predictions of upper-bound analysis for different v values recommended by design codes

On the other hand, comparisons between the experimental results and those predicted by the upper-bound analysis for different effectiveness factor formulas collected from different previous studies are presented in Table 4.10 and Figure 4.10. For all the effectiveness factor formulas considered, the load capacity predicted by the upper-bound analysis showed reasonable agreement with the experimental results of SCC continuous deep beams. The results obtained using the effectiveness factor proposed by Warwick and Foster (1993) were the most accurate with an average of 1.02, standard deviation of 18% and a coefficient of variation of 17%. The predictions were more accurate for beams having orthogonal web reinforcement (B3 to B6).

However, using the effectiveness factor proposed by Yang and Ashour (2008) led to more accurate predictions for beams having high shear span-to-depth ratio (B7 and B8).

Table 4.10: Comparisons between test results and predictions of upper-bound analysis for different v values recommended by previous studies

Beam no.	P_{EXP}	P_1	P_2	P_3	P_{EXP}/P_1	P_{EXP}/P_2	P_{EXP}/P_3
B1	1295	1053	772	1027	1.23	1.68	1.26
B2	1674	1415	1063	1408	1.18	1.57	1.19
B3	1358	1431	1117	1412	0.95	1.22	0.96
B4	1861	1581	1212	1584	1.18	1.54	1.17
B5	1988	1855	1479	1864	1.07	1.34	1.07
B6	1940	1922	1535	1939	1.01	1.26	1.00
B7	579	743	625	707	0.78	0.93	0.82
B8	676	932	797	895	0.73	0.85	0.76
Mean					1.02	1.3	1.02
Standard deviation (%)					19	30	18
Coefficient of variation (%)					19	23	17

Note: P_1, P_2 and P_3 are the total loads predicted by the upper-bound analysis using the effectiveness factor formula proposed by Nielsen (1984), Yang and Ashour (2008) and Warwick and Foster (1993), respectively.

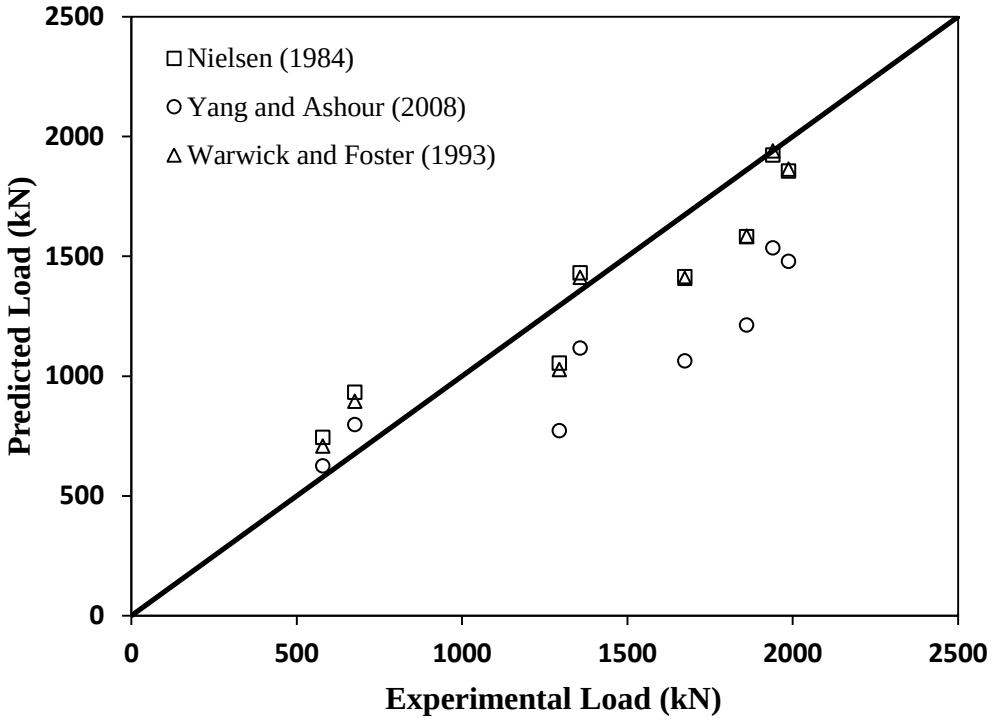

Figure 4.10: Comparisons between experimental results and predictions of upper-bound analysis for different v values collected from previous studies

4.4 Concluding remarks

Comparisons between the experimental results presented in chapter three and those predicted by a number of design methods suggested by different codes of practice as well as previous research investigations were presented in this chapter. The comparisons aimed to assess the validity of applying these methods, which were proposed for NC deep beams, in predicting the load capacity of SCC continuous deep beams. The design methods considered in this analysis included the shear provisions of the ACI 318M-11, the strut-and-tie method suggested by different codes of practice and the mechanism analysis of the upper-bound theory proposed by Ashour and Morley (1996). The investigation of the lower and upper-bound analyses mainly focused on using different effectiveness factor equations

recommended by the current design codes as well as those proposed by previous researchers. New formulas for the effectiveness factor were suggested to be used in the lower-bound analysis of continuous SCC deep beams. Based on the investigation carried out in this chapter, the following conclusions can be drawn:

- The simplified provisions of the ACI Building Code, which were proposed for the shear strength of NC deep beams, accurately predicted the shear strength of continuously supported SCC deep beams. However, the prediction was unconservative for beams having web reinforcement in one direction only.
- The strut-and-tie model recommended by different design codes showed conservative results for all beams tested. The ACI Building Code (318M-11) predictions were more accurate than those of the EC2 and Canadian Code (CSA23.3-04).
- The proposed equations of effectiveness factor used in the lower-bound analysis can be applied for the prediction of the load capacity of continuously supported SCC deep beams with high level of accuracy. However, more data on continuous SCC deep beams is required for more validation for the proposed equations.
- The mechanism analysis of the upper-bound theory reasonably predicted the load capacity of two-span continuous SCC deep beams. However, the prediction accuracy decreased for beams having shear reinforcement in one direction only and beams having high shear span-to-depth ratio.
- Among the three theoretical approaches considered in this chapter, the most accurate prediction for the load capacity of SCC continuous deep

beams were achieved by the strut-and-tie model using the effectiveness factor equations proposed in the current study with a mean of 1.00, a standard deviation of 7.00% and a coefficient of variation of 7.00%.

It can be concluded that, although the theoretical methods considered in this chapter were mainly proposed based on results of NC deep beams, they can be used to predict the load capacity of two-span continuous SCC deep beams with high level of accuracy. These simplified methods can only predict the load capacity of deep beams. Therefore, a three dimensional non-linear finite element analysis using ABAQUS software will be presented in the next chapter to predict the full behaviour of continuously supported SCC deep beams and carry out a parametric study in chapter six to investigate the effect of extended range of parameters on the load carrying capacity of continuously supported SCC deep beams.

CHAPTER FIVE

FINITE ELEMENT ANALYSIS

5.1 Introduction

Because of the high cost and time consuming of experimental investigations on full-scale test specimens, methods of modelling continuous deep beams are required to improve the understanding of the behaviour of continuous SCC deep beams, provide additional insight into the experimental works and investigate the effects of various parameters. One method of modelling RC structures is the Finite Element (FE) method.

This chapter presents computational procedures that were developed parallel to the experimental investigation. The computational analysis reported in this thesis was performed using a three dimensional FE package programme, namely ABAQUS, version 6.12. ABAQUS is an important FE tool that can be used to model the complicated behaviour of reinforced concrete members subjected to various loading conditions. It has been used to model the cracking behaviour and tension stiffening of reinforced concrete. The proposed ABAQUS model is validated against the experimental results of continuous SCC deep beams described in chapter three and some examples collected from previous studies. In addition, the proposed model is used to conduct a parametric study in chapter six in order to investigate the behaviour of continuous SCC deep beams with extended parameter variations, both within and outside the range of experiments.

5.2 The finite element model

As mentioned above, ABAQUS is employed to investigate the behaviour of continuously supported SCC deep beams. In the investigation of the behaviour of continuous SCC deep beams, the three dimensional ABAQUS model was developed by defining the concrete beams, the steel reinforcing bars including the longitudinal as well as the horizontal and vertical web reinforcement and the loads and supporting steel plates as individual sections. The dimensions of these elements used in the model are exactly the same as those used in the experimental investigation. Due to the symmetry in geometry, boundary conditions and loading arrangement, the symmetric feature available in ABAQUS was exploited by modelling only half of the beam, taking the centreline of the middle support as the axis of symmetry, as shown in Figure 5.1.

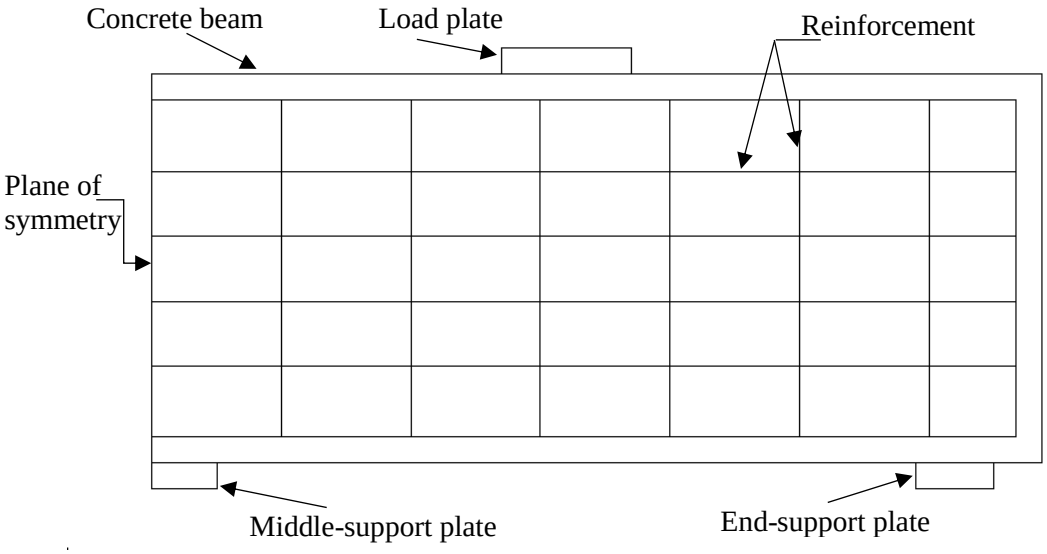

Figure 5.1: Typical ABAQUS model of continuous deep beam

5.2.1 Element Type

In the FE, generally, the selection of the element type for each part of the model is important due to its clear effect on the accuracy of the results and computational time. In ABAQUS, there are different types of elements available. The most commonly used for modelling RC structures are the continuum elements as they can be used to define almost any shape and to model linear or nonlinear behaviour. In the proposed model, the concrete was modelled using an 8-node linear brick, reduced integration element (C3D8R). The reduced integration element was selected to decrease the simulation time as it has only one Gauss point and fewer integration points are computed (ABAQUS Inc, 2012).

In terms of the steel reinforcement, the reinforcing bars, including the longitudinal and web reinforcement, were modelled by a 2-node linear 3-D truss element (T3D2). The truss element in ABAQUS can be used in two or three dimensions to present a slender structural element that resists and transfers only axial forces. It can also be used to model components where strain is calculated from the change in length (ABAQUS Inc, 2012). The advantage of using a truss element is that the perfect-bond can easily be defined by embedding the steel bars into a host region (concrete beam).

5.2.2 Mesh Size

In FE, the mesh size represents a very important factor that significantly affects the accuracy of the results and the simulation time. It is well known that, in the FE modelling, the finer the mesh size, the more accurate the results that can be achieved. However, a finer mesh size requires more

computational resources and time. In terms of the FE modelling of RC members, especially in the case of plain concrete or concrete with low amount of reinforcement where only a few cracks physically developed in the member, refining the mesh may lead to narrower crack bands and as a result more convergence problems (Alih and Khelil, 2012). However, the mesh sensitivity can be eliminated if the cracks are reasonably distributed (ABAQUS Inc, 2012). In the case of deep beams, heavy reinforcement is used and as a result the mesh sensitivity is reduced. In order to choose the appropriate mesh size, the model was run using different numbers of elements and the results were compared with the experimental results (See section 5.3.1).

5.2.3 Interaction between concrete and reinforcement

One of the most important factors that affects the accuracy of the results is modelling the interaction between concrete and steel reinforcement. In a numerical analysis, choosing suitable contact conditions between different parts of the model must be carefully considered to allow the transfer of the forces between these parts. The ABAQUS library provides a wide range of contact models required to define the interaction between different parts of any model. In the current research investigation, the reinforcing bars are assumed to have a perfect bond with the surrounding concrete. Therefore, the interaction between concrete and reinforcement was modelled by using the embedded region option available in ABAQUS 6.12 which represents perfect bond between concrete and reinforcement.

5.2.4 Concrete model

In terms of the behaviour of concrete, the concrete damaged plasticity model was used to define the concrete in the current study. This model is designed to model the concrete under arbitrary loading, including cycling loading and assumes an isotropic damaged elasticity in tension and compression to present the inelastic behaviour of concrete. The concepts of stiffness recovery effects under cyclic loading and the elastic stiffness resulting from the plastic strain in tension and compression are also considered in the concrete damaged plasticity model. The damaged plasticity model can be used for plain concrete as well as for RC structures subjected to monotonic, cycling and dynamic loading under low confining pressure (ABAQUS Inc, 2012).

In order to define concrete in the damaged plasticity model, initially, it is required defining the damaged plasticity parameters which include five parameters. Then the elastic behaviour of concrete is defined including the elastic modulus and the poisson's ratio. After that, the behaviour of concrete in compression is defined followed by the behaviour of concrete in tension.

5.2.4.1 Concrete damaged plasticity parameters

The damaged plasticity parameters include five variables that must be taken into account. Some of these parameters are given a specific value in ABAQUS whereas the others have a range between two values. Two parameters have a specific value in ABAQUS. Firstly, the hyperbolic flow potential eccentricity (ϵ) which is defined in ABAQUS as a small positive number that represents the rate at which the hyperbolic flow potential

approaches its asymptote. The default value given in ABAQUS for ϵ is 0.1 which is the value selected for the current model. The second parameter is the ratio of concrete strength in the biaxial state to that in the uniaxial state (σ_{bo}/σ_{co}). The value chosen for the proposed model is 1.16 which is the default value in ABAQUS.

On the other hand, there are three parameters that are not given a specific value in ABAQUS. Firstly, the dilation angle (ψ) which is defined as a material parameter that controls the plastic strain of concrete. It is also defined as the internal friction angle of concrete or the angle of inclination of the failure surface which evaluates the inclination of the plastic potential under high confining pressure. Higher dilation angle values result in more ductile behaviour of concrete whereas low values lead to brittle concrete behaviour (Malm, 2009). The minimum value accepted in ABAQUS is close to zero while the maximum value is 56.3°. In the current model, the value of the dilation angle that gave the closest results to the experimental results was 54°. This value was selected through a comparison between the load-deflection results of the current model and that obtained from the experimental investigation as shown in Section 5.3.2.

Secondly, the ratio of the second stress invariant in tension to that in compression (K_c), the value of which must be between 0.5 and 1.0. After comparing the results for different K_c values with the experimental results (See Section 5.3.3), the default value of 0.667 given in ABAQUS was selected for the proposed model. The final parameter is the viscosity parameter which represents the relaxation time of the viscous system and helps to overcome some convergence problems. It was mentioned that a

small value should be used for the viscosity parameter to influence the simulation time and improve the convergence of the model (Lapczyk and Hurtado, 2007). The default value given in ABAQUS for the viscosity parameter is zero. However, the value selected for the proposed model is 0.01 to reduce the simulation time (See section 5.3.4).

The values of the parameters required to define the concrete damaged plasticity model are shown in Table 5.1. These values were selected after carrying out a parametric study as shown in Section 5.3.

Table 5.1: Concrete damaged plasticity parameters used in the proposed ABAQUS model

Dilation angle	Eccentricity	σ_{bo}/σ_{co}	K_c	Viscosity parameter
54°	0.1	1.16	0.667	0.01
where σ_{bo}/σ_{co} is the ratio of initial equibiaxial compressive yield stress to initial uniaxial compressive yield stress, K_c is the ratio of the second stress invariant in tension to that in compression.				

5.2.4.2 Elastic behaviour

The linear elastic behaviour of concrete can be easily defined in ABAQUS. It requires inserting the values of Poisson's ratio and Young's modulus (E_c). In the proposed ABAQUS model, the value of Poisson's ratio was taken equal 0.2 and, the value of E_c can be calculated from equation (5.1) below, according to the EC2. The value of the E_c was then reduced by 25% depending on the findings of some research investigations which pointed out that the modulus of elasticity of SCC is lower than that of NC by about 15-40% (Klug et al., 2003; Domone, 2007; ACI 237R, 2007).

$$E_c = 22000 \left[\frac{f_c' + 8}{10}\right]^{0.3} \quad (5.1)$$

where E_c is the elstic modulus of concrete in MPa and f_c' is the cylinder compressive strength of concrete in MPa.

5.2.4.3 Compression behaviour

In addition to the previously defined parameters, the damaged plasticity model requires defining the behaviour of concrete in compression and tension. The behaviour of concrete under uniaxial compression is defined by using the stress-strain relationship outside of the elastic range. In other words, it requires providing the compressive stress of concrete as a function of the inelastic strain in a tabular form. For SCC, there are almost no definitive studies on the stress-strain relationship. Only one study was conducted by Kumar et al. (2011) trying to develop a new constitutive model to predict the stress-strain response of SCC. However, when comparing this constitutive model with that suggested by EC2, it can be clearly seen that no clear difference can be found except for the descending branch of the two curves in which a small difference can be noticed as shown in Figure 5.2. Therefore, the stress-strain relationship according to the EC2 was adopted in the proposed model.

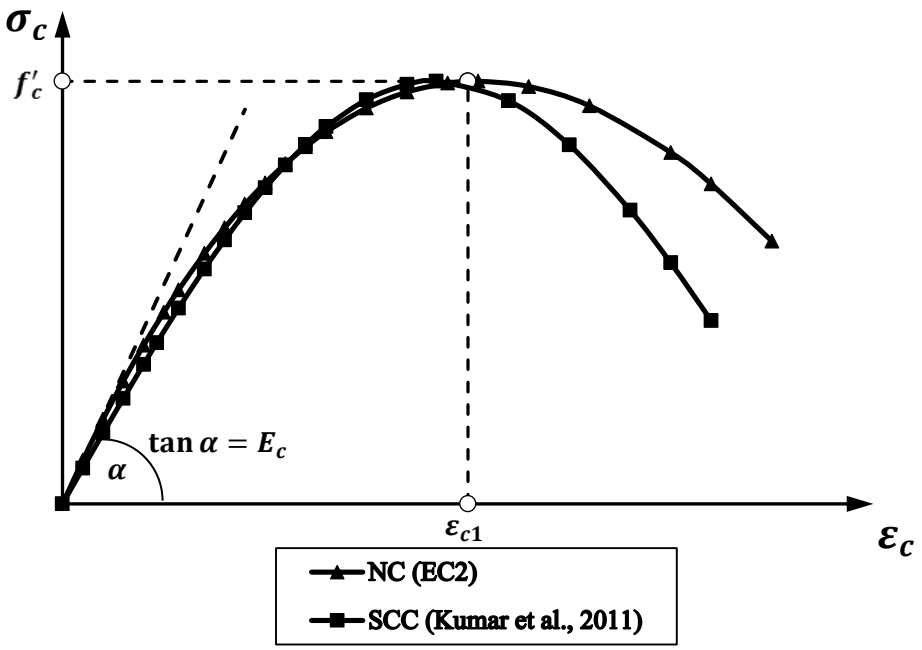

Figure 5.2: Comparison between the stress-strain relationship of NC (EC2) and SCC (Kumar et al., 2011)

The stress-strain relationship defined according to the EC2 is shown in Figure 5.3. The relation between the stress and strain of concrete is assumed to be approximately linear up to about 40% of the ultimate stress of concrete. After this point, the relationship exhibits a steady softening up to the ultimate stress of concrete. As the compressive strength of concrete is reached, the material stiffness falls down to zero and, after that, concrete exhibits a strain softening up to crushing of concrete. Equations (5.2) to (5.5), provided by the EC2, were used to build up the stress-strain relationship of concrete in the current study.

$$\sigma_c = f_c' \frac{K\eta - \eta^2}{1 + (K-2)\eta} \tag{5.2}$$

$$K = 1.05\, E_c \varepsilon_{c1} / f_c' \tag{5.3}$$

$$E_c = 22000 \left[\frac{f_c' + 8}{10}\right]^{0.3} \tag{5.4}$$

$$\eta = \varepsilon_c / \varepsilon_{c1} \tag{5.5}$$

where σ_c is the compressive stress of concrete in MPa, f_c' is the mean value of concrete cylinder compressive strength in MPa, E_c is the elastic modulus of concrete in MPa, ε_c is the compressive strain of concrete at any stress σ_c and ε_{c1} is the strain at peak stress.

It should be noted that the value of E_c calculated from equation (5.4) was reduced by 25% to account for the lower modulus of elasticity of SCC compared to NC as indicated in chapter two. It should also be noted that these equations can be used for strain from zero up to the ultimate nominal strain (ε_{cu1}). The values of ε_{c1} and ε_{cu1} can be obtained from Table 3.1 in the EC2.

After plotting the complete stress-strain relationship, the inelastic strain of concrete (ε_c^{in}) at any stress σ_c can be calculated from equation (5.6) below:

$$\varepsilon_c^{in} = \varepsilon_c - \frac{\sigma_c}{E_c} \qquad (5.6)$$

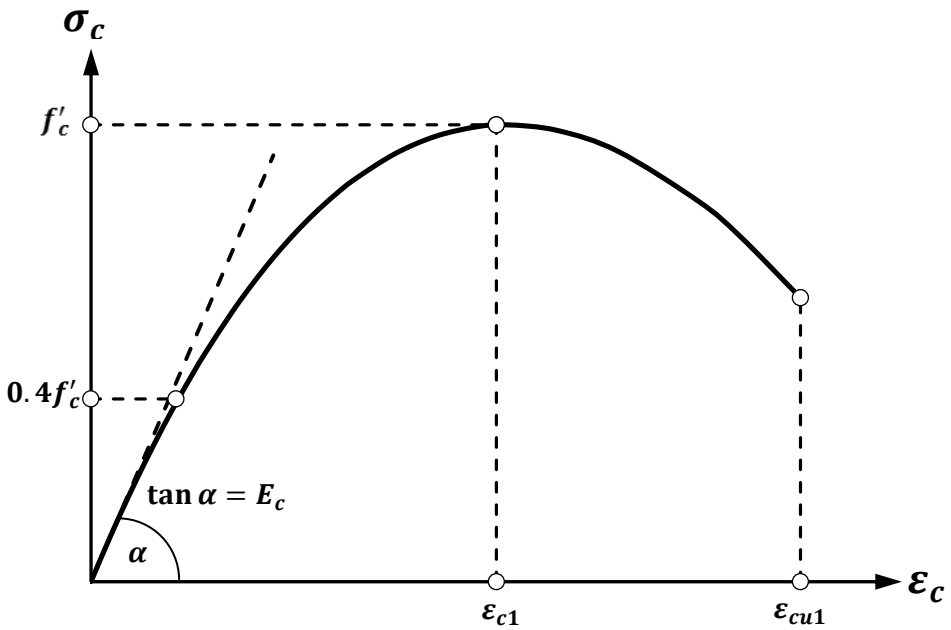

Figure 5.3: Stress-strain relationship of concrete in compression (BS EN 1992-1-1:2004)

5.2.4.4 Tension behaviour

In the literature, there is disagreement among researchers on the behaviour of SCC under tension. A few studies in the literature have focused on this topic. None of these studies have given the stress-strain relationship of SSC in tension. Domone (2007) and ACI 237R (2007) reported that there is no clear difference in the tensile behaviour between SCC and NC. In the current study, these findings were considered and as a result the behaviour of SCC in tension is assumed to be similar to NC.

In the concrete damaged plasticity model, there are three different methods in ABAQUS that can be used to define the behaviour of concrete under uniaxial tension. The first method requires defining the stress-strain softening model of concrete in tension in a tabular form. The second one is to provide the relation between the tensile stress and the crack-opening displacement, also in a tubular form. The third option is to provide a value for the fracture energy as a material property that represents the energy required to open a unit area of stress free crack. Using the first method might lead to mesh sensitivity which in turn results in inaccurate predictions as well as convergence problems due to the narrower crack bands resulted from mesh refinement (ABAQUS Inc, 2012). As a result, it is recommended to use the second method as the value of the fracture energy required in the third method is also required to simulate the stress-displacement relationship.

In the proposed model, the tensile behaviour of concrete was defined by the tensile stress as a function of the crack-opening-displacement as recommended by the CEB-FIP Model Code (1990) as shown in Figure 5.4.

Under uniaxial tension, the behaviour of concrete is linear-elastic up to the ultimate stress (σ_{cr}). Beyond the ultimate stress, the behaviour of concrete becomes nonlinear due to the occurrence of some micro cracks resulted from bond failure between aggregate and cement paste. However, concrete continues to carry tension even after cracking and this phenomenon is known as tension stiffening.

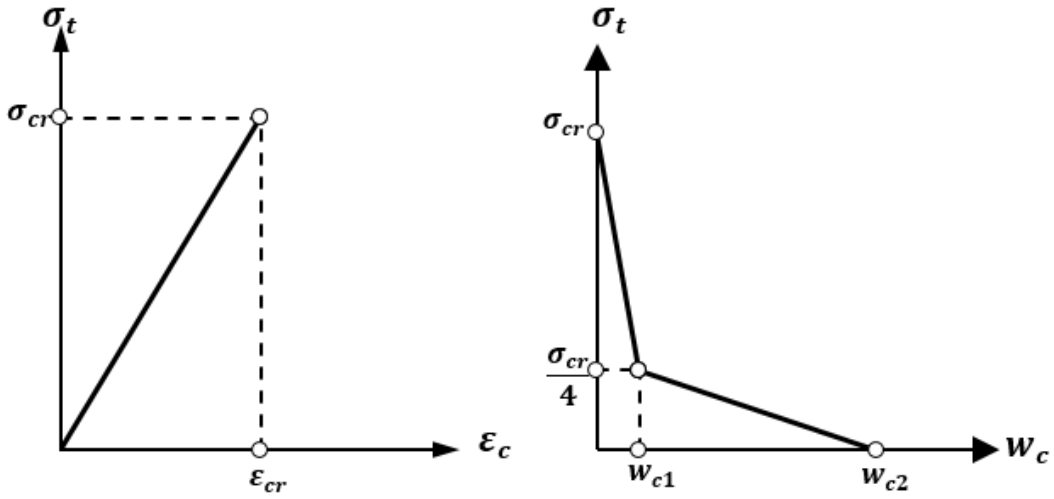

Figure 5.4: Stress-strain and stress-crack opening relationship for uniaxial tension

Equations (5.7) to (5.12) below are used to determine the stress strain and stress-crack opening curves of concrete in tension as shown in Figure 5.4 (CEB-FIP Model Code, 1990). The ascending branch of the curve up to cracking strength of concrete is obtained from equations (5.7) and (5.8), whereas the descending branch which represents the tension softeining is modeled using equations (5.9) to (5.12).

$$\sigma_t = E_c\,\varepsilon_t \qquad \text{For } \sigma_t \le \sigma_{cr} \qquad (5.7)$$

$$E_c = 22000\left[\frac{f_c' + 8}{10}\right]^{0.3} \qquad (5.8)$$

$$w_{c1} = \frac{0.75\,G_f}{\sigma_{cr}} \qquad (5.9)$$

$$\sigma_{cr} = 0.33\sqrt{f_c'} \tag{5.10}$$

$$w_{c2} = \frac{5\,G_f}{\sigma_{cr}} \tag{5.11}$$

$$G_f = 0.03\left[\frac{f_c' + 6.4}{10}\right]^{0.7} \tag{5.12}$$

where σ_t is the tensile stress of concrete in MPa, ε_t is the tensile strain at any stress, E_c is the modulus of elasticity of concrete in MPa, σ_{cr} is the cracking stress of concrete in MPa, ε_{cr} is the cracking strain of concrete, w_c is the crack opening in mm, G_f is the fructure energy in Nmm/mm^2, w_{c1} is the crack opening for $\sigma_t = \frac{\sigma_{cr}}{4}$ and w_{c2} is the crack opening for σ_t=0

5.2.5 Steel reinforcement model

The properties of steel reinforcement are significantly different from those of concrete. The behaviour of steel in tension is similar to that in compression. According to the EC2, the stress-strain relationship of steel starts with a linear elastic ascending branch up to the yield strength followed by a linear strain hardening up to the ultimate strength. In the current study, the reinforcement properties used to idealize the stress-strain relation shown in Figure 5.5 are as the following: the modulus of elasticity (Es) is 210 GPa, the poisson's ratio is 0.3, the yield strength (f_y) is 500 MPa, the ultimate strength (f_u) is 625 MPa, the yield strain ($\varepsilon_y = f_y/E_s$), the ultimate strain (ε_u) is equal to or greater than 0.0075.

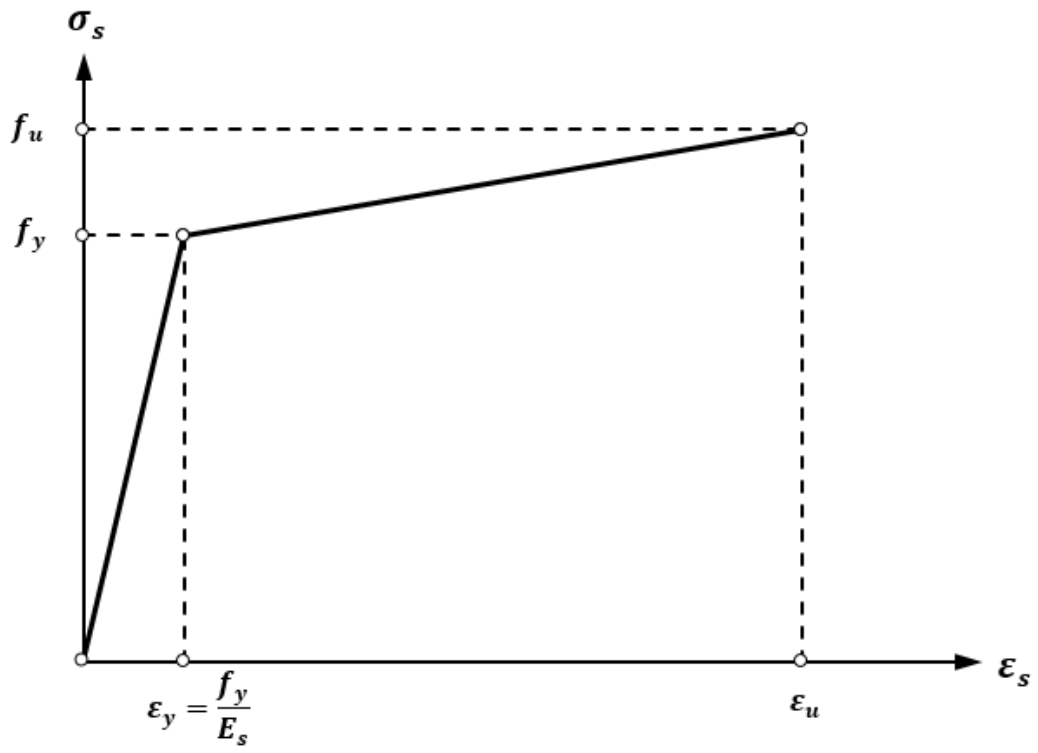

Figure 5.5: Stress-strain relationship of steel reinforcement (BS EN 1992-1-1:2004)

5.2.6 Loading and Boundary Conditions

The load and boundary conditions in ABAQUS can be defined through a sequence of procedures that can be created through a step. There are two types of step in ABAQUS: the first type is a special initial step which is created automatically at the beginning of the model's step and called *Initial*. This step is created in any model and cannot be edited or deleted. The second type of step is called the analysis step which follows the initial step and can be created manually. The model can include one or more analysis step and the analysis procedures can be changed from step to another. The loads, boundary conditions and the output requests can be prescribed by creating one or more analysis step.

On the other hand, two kinds of the analysis step can be found in ABAQUS. The first is the general analysis step which deals with the linear or nonlinear problems whereas the second one is the linear perturbation step which can analyse only linear behaviour. In the current model, the general analysis step was selected to prescribe the load, boundary conditions and output requests. The general analysis step has a variety of methods to deal with different problems such as the static general method, static Riks method, dynamic methods and others. The static general method is used in the current research investigation as it resulted in more accurate predictions with fewer convergence problems when compared to other methods.

In terms of the boundary conditions, the middle support was modelled to allow rotations only but no horizontal or vertical movements whereas the end-support was modelled as a roller to allow rotation and horizontal movements along the length of the beam. The load was defined as a displacement at the middle of the loading plate. The failure load was then calculated by taking the summation of the reactions at the three supports.

5.3 Investigation of the Model Parameters

As mentioned earlier in this chapter, some parameters in ABAQUS require conducting a parametric study in order to choose the most suitable values. The selection of these values depends on the accuracy of the results compared to the experimental ones as well as the time taken to run the model. The parameters investigated in this section are the mesh size, the dilation angle (ψ), the ratio of the second stress invariant in tension to that in compression (K_c) and the viscosity parameters (υ_p). The results were

compared to the experimental results of Beam B2. Figure 5.6 shows the ABAQUS model of beam B2.

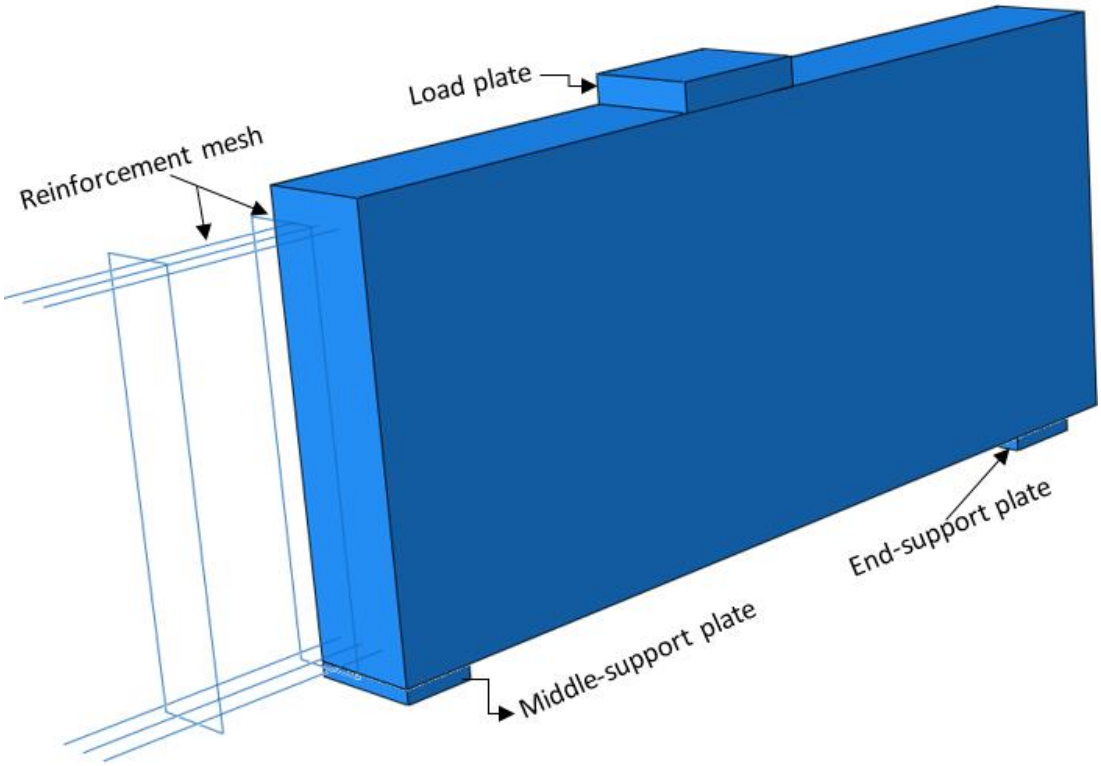

Figure 5.6: ABAQUS model of beam B2

5.3.1 Mesh Size

Despite the fact that the mesh density is not a prominent issue in the FE modelling for RC members with reasonably distributed cracks, a mesh sensitivity investigation was conducted to select the most suitable mesh size for the proposed model. A finer mesh size is recommended to achieve accurate results. However, mesh refinement leads to an increase in the simulation time. In order to select the appropriate element size, the model was run using three different mesh sizes: 15X15X15 mm, 17.5X17.5X17.5 mm and 20X20X20 mm as shown in Figure 5.7.

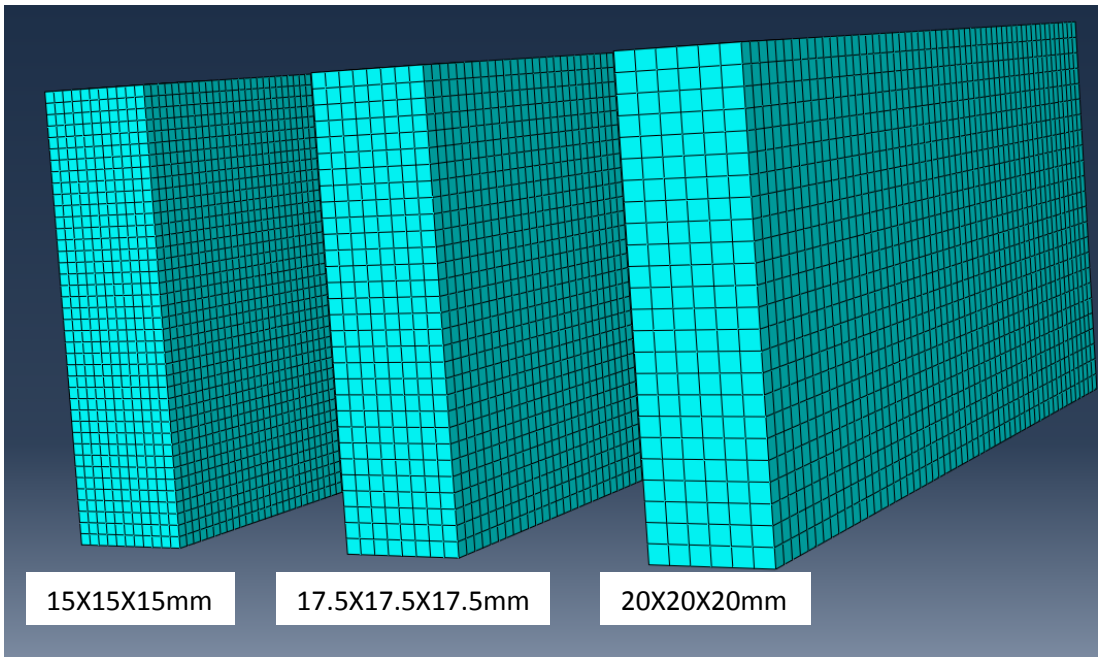

Figure 5.7: Different mesh sizes

The results of the load-deflection relationship obtained from the model were then compared to those of beam B2 as shown in Figure 5.8. The computational time was also investigated and the results are presented in Table 5.2. It can be clearly seen that changing the element size did not have a clear effect on the load-deflection response. However, the mesh refinement resulted in significant increase in the computational time. For example, the time taken to run the model with a mesh size of 15X15X15 mm is approximately three times that taken to run the model with a mesh of 20X20X20 mm. As a result, the element size that was selected for the proposed model is 20X20X20 mm.

Table 5.2: Computational time of the FE model for different mesh sizes

Element size (mm)	Computational time (sec)
15X15X15	3720
17.5X17.5X17.5	2495
20X20X20	1260

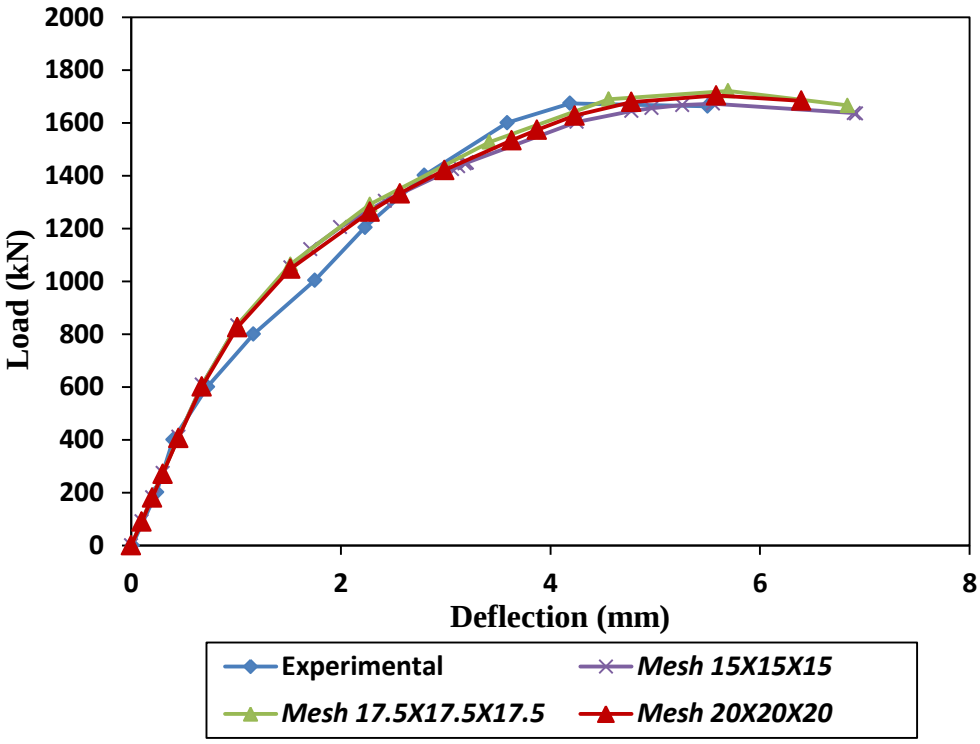

Figure 5.8: Effect of mesh size on the load-deflection response and comparison with experimental results of Beam B2

5.3.2 Dilation Angle

In order to choose a value for the dilation angle (ψ), three different values were adopted in ABAQUS: $\psi=45°$, $\psi=50°$ and $\psi=54°$. The selection of the appropriate dilation angle value was based on the load-deflection response. The results were then compared with the experimental results of Beam B2 as shown in Figure 5.9. It can be clearly seen that changing the value of the dilation angle did not have any effect on the initial stiffness of the beam. However, as the load increased, the load-deflection response starts to be different for each of the dilation angle values. At failure, the difference in the load capacity is significant reaching about 150 kN for a change of 5° in the value of the dilation angle. The value of $\psi=54°$ produced the best results

compared to the experimental results and therefore, it was chosen for the current model.

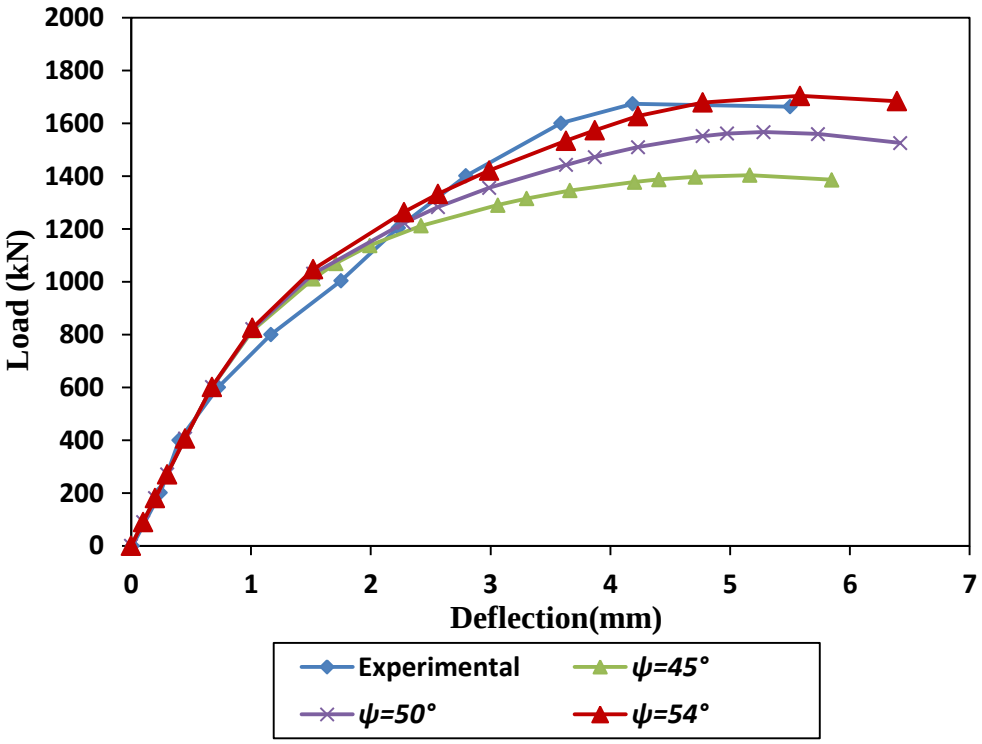

Figure 5.9: The effect of dilation angle on the load-deflection results of Beam B2

5.3.3 Ratio of second stress invariant in tension to that in compression (k_c)

The value of k_c in ABAQUS ranges between 0.5 and 1.0 and the default value is 2/3. Therefore, to choose a suitable value for k_c, a sensitivity study was conducted by running the model using the minimum value, the maximum value and the default value given in ABAQUS. The results were then compared to the experimental ones of Beam B2 as shown in Figure 5.10. The comparison clearly showed that changing the value of k_c did not have any effect on the results. As a result, the value of k_c selected for the proposed model is 2/3 which is the default value suggested by ABAQUS.

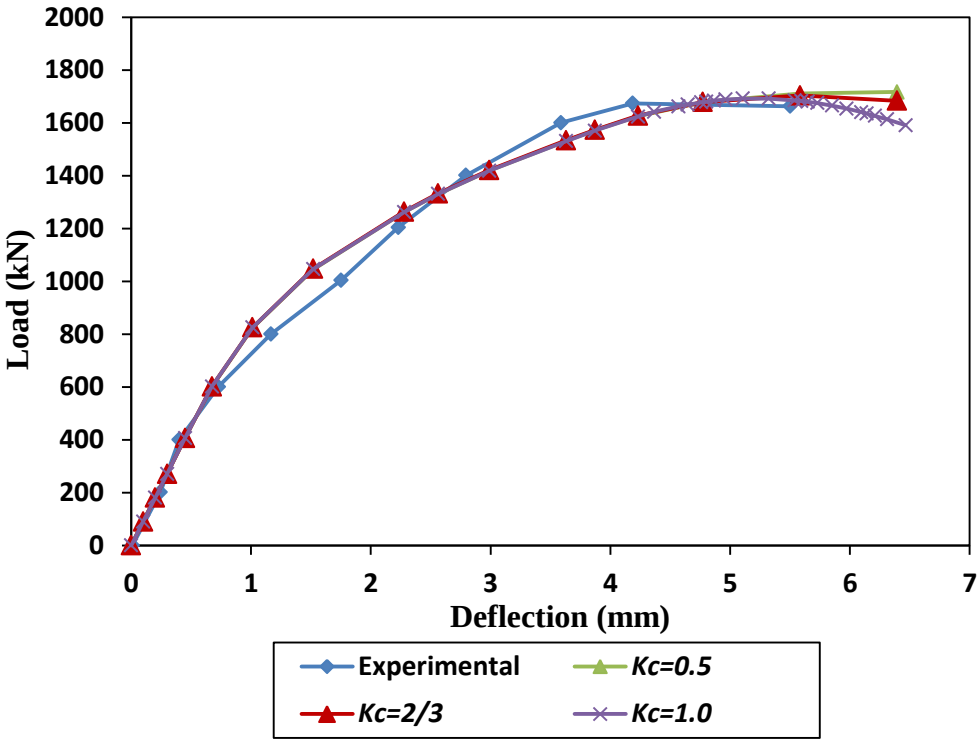

Figure 5.10: The effect of k_c on the load-deflection response of Beam B2

5.3.4 Viscosity Parameters

Similar to the previously mentioned parameters, the value of the viscosity parameter (v_p) was chosen through a sensitivity study. The model was run using three different values: v_p=*0.005*, v_p=*0.01* and v_p=*0.015*. The choice was based on the results of the load-deflection behaviour compared to the experimental results of Beam B2 as shown in Figure 5.11. It can be clearly seen from Figure 5.11 that a small change in the value of v_p can result in a significant change in the load-deflection curve. The difference in the load carrying capacity reached more than 200 kN for a change of 0.005 in the viscosity parameter value. It was also noticed that using v_p=*0* significantly increased the computational time and resulted in some convergence problems. The best results were achieved for a viscosity parameter value of 0.01 and therefore, it was selected for the proposed model.

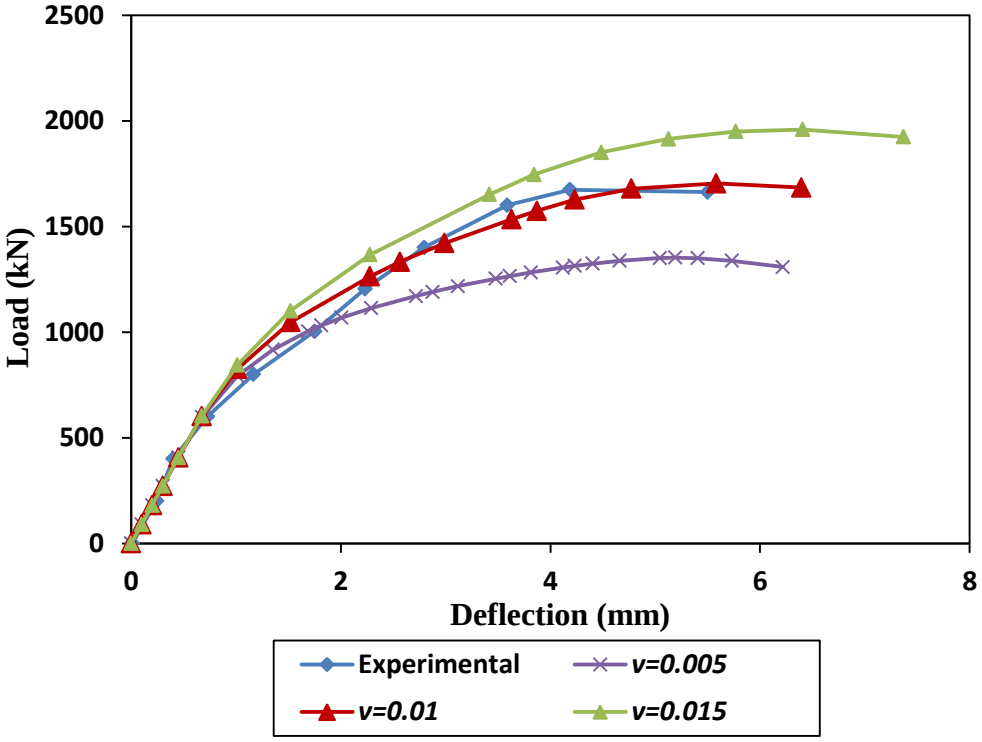

Figure 5.11: Effect of viscosity parameter on the load-deflection behaviour of Beam B2

5.4 Validation of FE Model

In the previous sections, a three dimensional FE model has been proposed using ABAQUS version 6.12. Different parameters required for the model have been investigated to select the most appropriate values and achieve accurate results. In this section, the proposed ABAQUS model is verified against the experimental behaviour of the two-span continuous SCC deep beams as well as some experimental results available in the literature.

5.4.1 Validation of FE Model against Experimental Results

In this section, the proposed model is verified against the experimental results of continuously supported SCC deep beams described in chapter three.

5.4.1.1 Failure Loads and Failure Mode

The failure of all beams predicted from the current model occurs due to major diagonal crack formed between the load and intermediate support plates as shown in Figures 5.12 to 5.15. The figures clearly show the development of a compression strut between the load plate and the middle support. In these figures, generally, the distribution of the component under investigation is represented by different colours. The area that has the highest values is shown in red while the lowest values are presented in blue and the values in between are shown in different other colours. Figure 5.12 shows the stress distribution of the concrete. The highest stress is clearly shown in the area between the load and support plates. These high stresses led to the development of a compression strut and as a result a major diagonal crack connecting the edges of the load and middle support plates and causing the failure of the beam. Similar to the stress distribution, the strain distribution shown in Figure 5.13 indicates that the highest strain was clearly distributed in the area between the load point and the intermediate support leading to the formation of the major diagonal crack which is the main cause of failure for all the beams. In a similar manner, the compression and tension damage are shown in Figures 5.14 and 5.15, respectively. It can be clearly seen that highest compression and tension damage are observed

in the area between the load and middle support plates. Although, there are some more areas showed high tensile damage such as the mid-span and above the intermediate support, the major diagonal crack, which is the main cause of failure, was formed between the load and middle support plates where the highest compression damage coincides with highest tension damage.

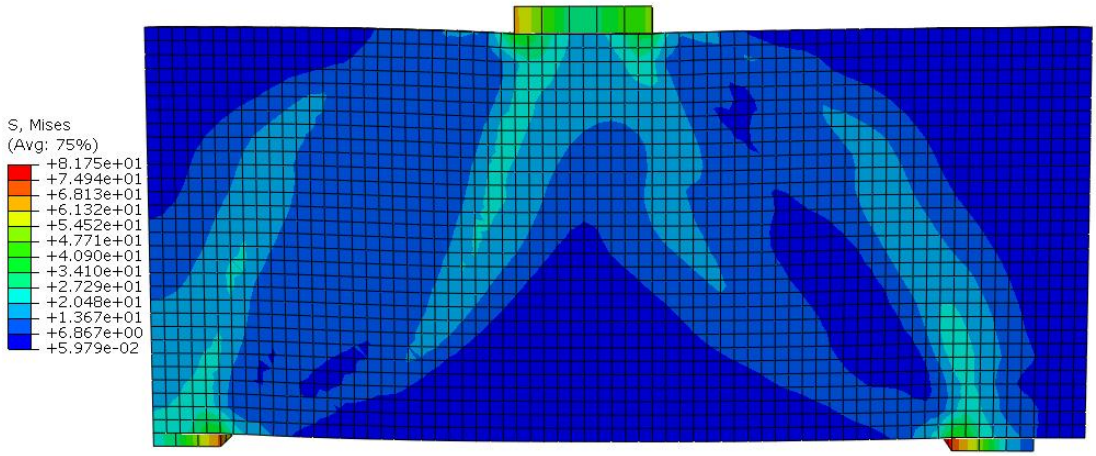

Figure 5.12: Equivalent stress distribution showing the development of a compression strut between load plate and middle support

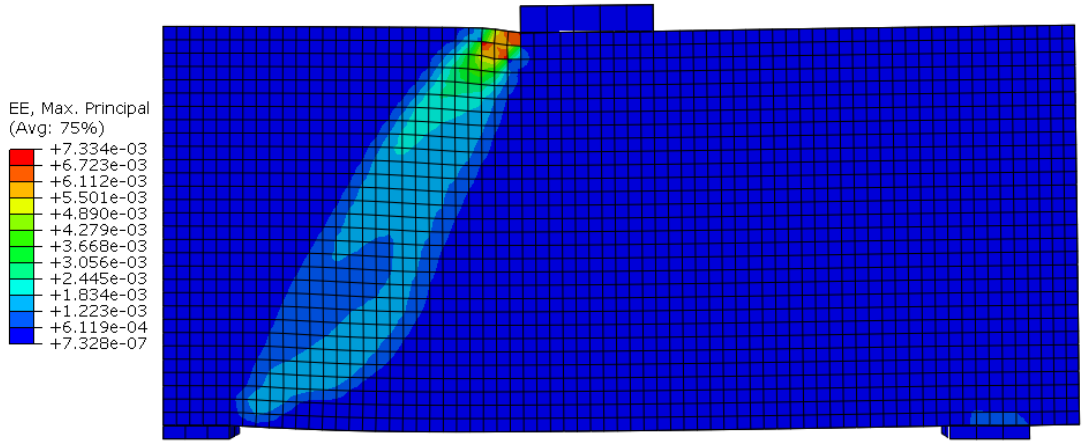

Figure 5.13: Total strain distribution showing the development of a compression strut between load plate and middle support

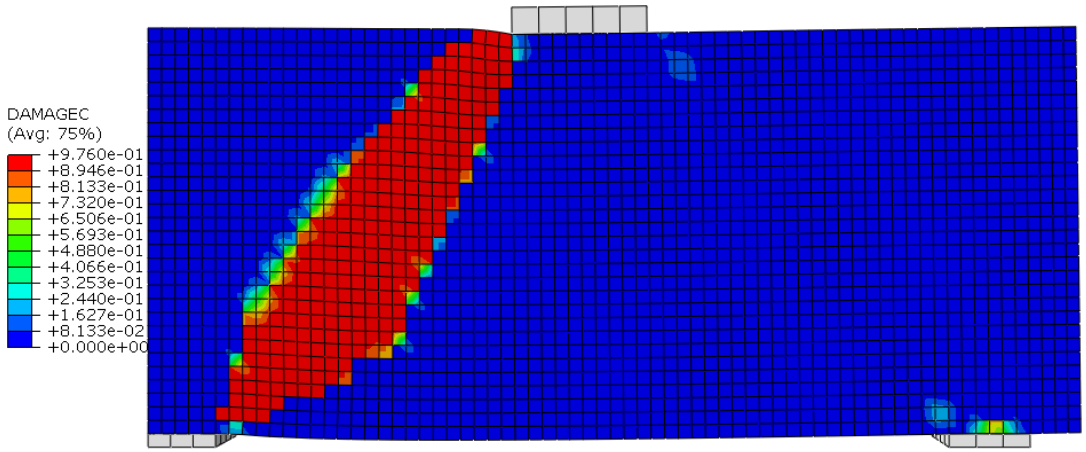

Figure 5.14: Compressive damage of concrete showing a major diagonal crack

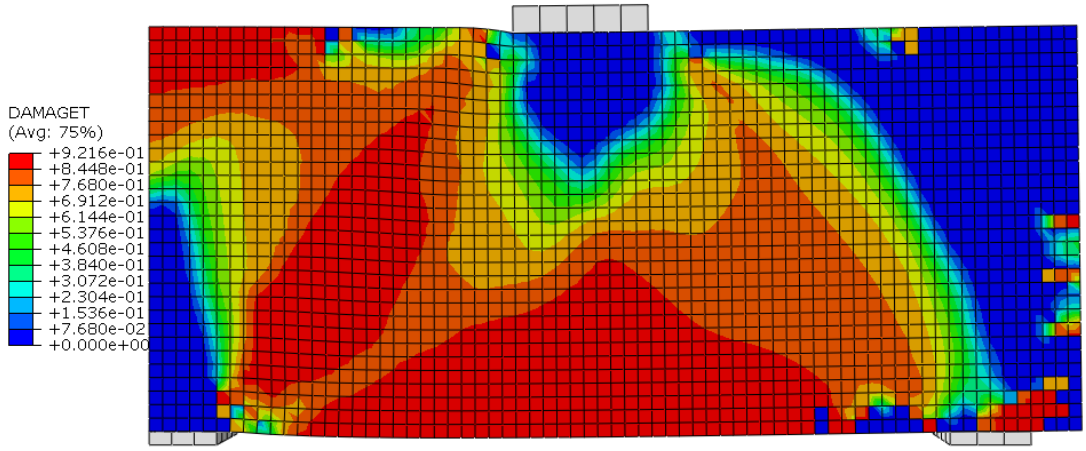

Figure 5.15: Tensile damage of concrete showing the positions of the diagonal and flexural cracks

In terms of the failure loads, comparisons between the failure loads predicted by the proposed FE model and experimental failure loads is presented in Table 5.3. The mean, the standard deviation and the coefficient of variation for the ratio between the predicted load and the experimental load are 1.00, 3.73% and 3.74%, respectively. It can be clearly concluded that the predictions from the present computational analysis of the ultimate load show quite reasonable agreement with the experimental results.

Table 5.3: Comparisons between the predicted failure loads from the current model and experiments

Beam no.	Failure Load kN		P_{EXP} / P_{FE}
	P_{EXP}	P_{FE}	
B1	1295	1247	1.04
B2	1674	1704	0.98
B3	1358	1344	1.01
B4	1861	1932	0.96
B5	1988	1905	1.04
B6	1940	2080	0.93
B7	579	573	1.01
B8	676	678	1.00
Mean			1.00
Standard deviation (%)			3.73
Coefficient of variation (%)			3.74

Note: P_{EXP} is the experimental failure load in kN and P_{FE} is the theoretical failure load predicted by the proposed ABAQUS model in kN.

5.4.1.2 Load-Deflection Behaviour

Comparisons between the load-deflection response predicted by the proposed model and experiments for the eight two-span SCC continuous deep beams is plotted in Figure 5.16. The comparisons clearly show that before the cracking of concrete, the initial stiffness predicted by the present ABAQUS model is almost similar to that observed from the experiments. The comparisons show a reduction in the stiffness after the occurrence of diagonal cracks at approximately the same load as experiments. However, after the occurrence of the first crack, some differences can be noticed between both curves. This can be attributed to assuming a perfect bond between the reinforcing bars and the surrounding concrete which might not be the actual case during the experiments specifically at a high level of

applied load. Overall, it can be concluded that the load-deflection curves predicted from the proposed model reasonably agree with the experiments.

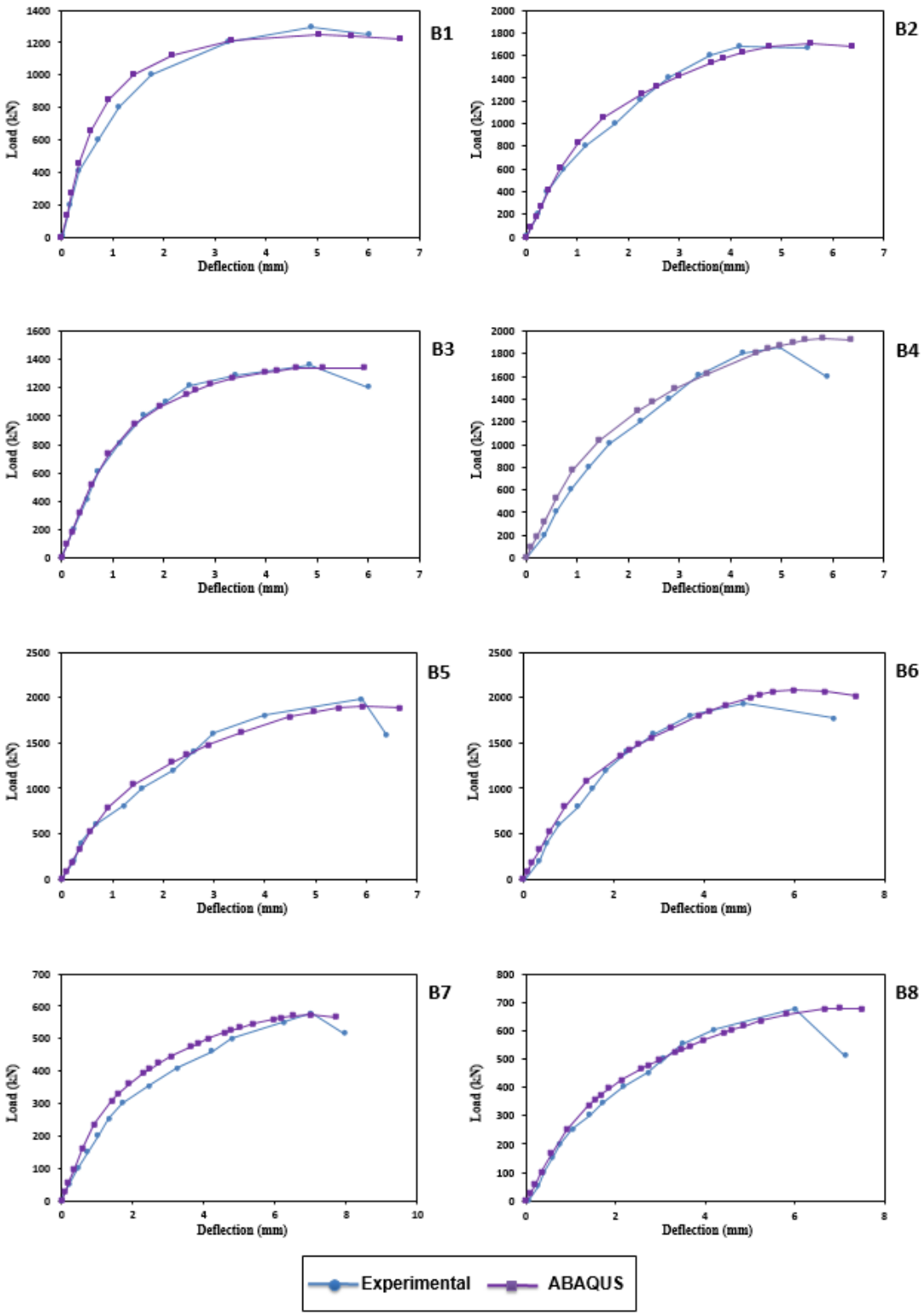

Figure 5.16: Validation of the proposed FE model against the current experimental results

5.4.2 Validation against Tests from the Literature

In this section, the proposed model is validated against some experimental results collected from the literature. The load-deflection behaviour of five continuous reinforced concrete deep beams is predicted using the current model and the results are then compared to the experimental ones. Three of these beams were tested by Yang et al. (2007b) while the other two were tested by Ashour (1997). The details of these beams are given in Table 5.4. All of the selected beams failed in shear due to a major diagonal crack similar to the experimental SCC continuous deep beams tested in the current study.

Comparisons between the load-deflection responses predicted by the proposed model and experimental results of Yang et al. (2007b) and Ashour (1997) are plotted in Figure 5.17. Up to the cracking of concrete, the load-deflection curve predicted by the current model is very similar to that obtained from the selected studies. After that, few differences can be noticed which may be attributed to assuming a perfect bond between the reinforcing bars and the surrounding concrete as mentioned above. In general, the proposed model reasonably predicted the load-deflection behaviour of the selected beams.

Table 5.4: Details of deep beams collected from literature and analysed by the proposed model

Reference	Beam no.	f_c' MPa	h mm	L mm	$\frac{a}{h}$	Longitudinal reinforcement		Web reinforcement	
						Bottom	Top	Vertical	Horizontal
Yang et al. (2007b)	L10NN	31.1	600	1200	1.0	3Ø19 mm	3Ø19 mm	-	-
	L10SN	42.5	600	1200	1.0	3Ø19 mm	3Ø19 mm	-	6Ø6 mm
	L10SS	36.0	600	1200	1.0	3Ø19 mm	3Ø19 mm	22Ø6 mm	6Ø6 mm
Ashour (1997)	CDB3	46.0	625	1340	0.8	4Ø12 mm	4Ø12 mm +2Ø10 mm	-	4Ø8 mm
	CDB4	47.8	625	1340	0.8	4Ø12 mm	4Ø12 mm	15Ø8 mm	-

							+2Ø10 mm		

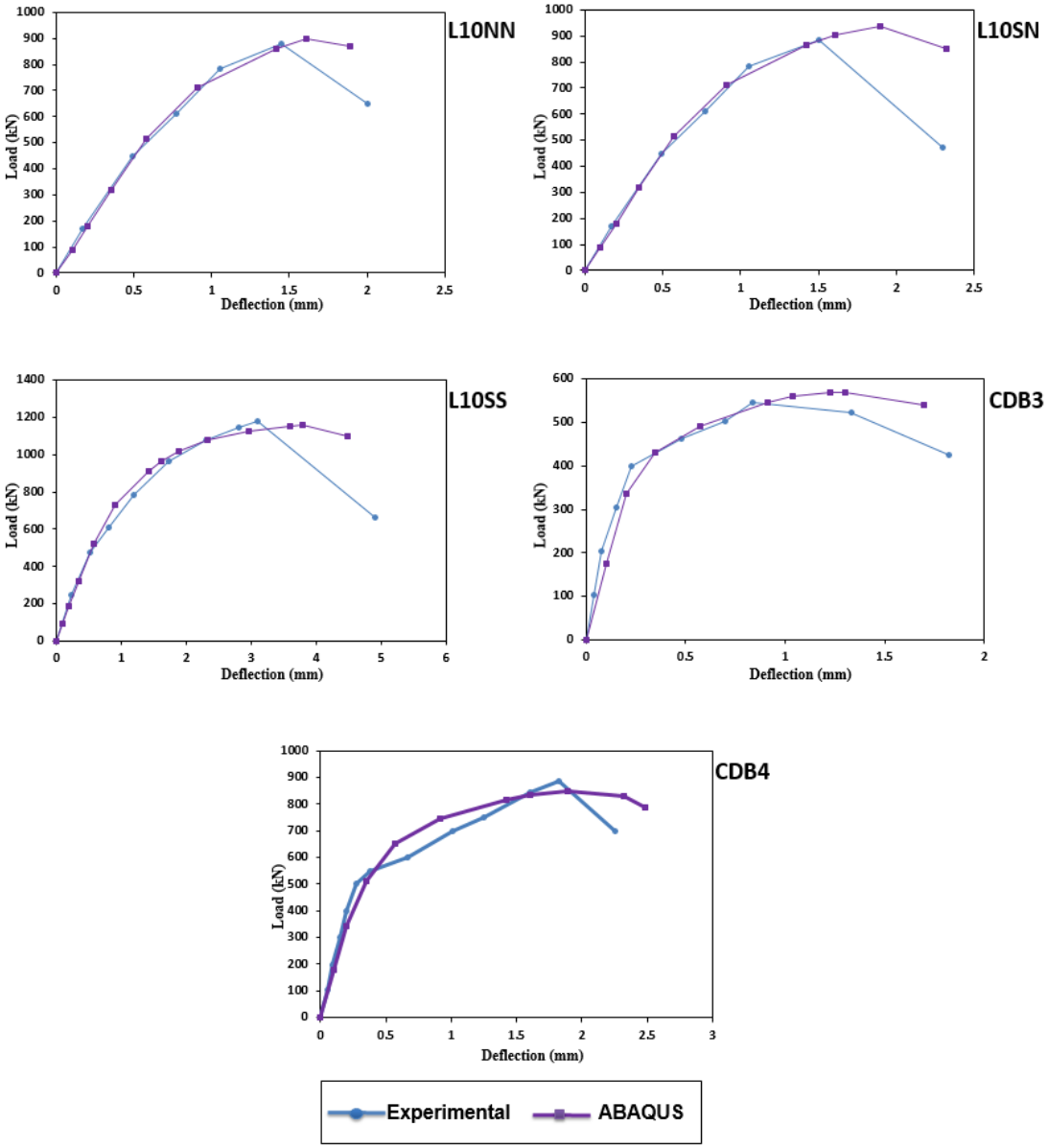

Figure 5.17: Validation of the proposed FE model against previous experimental results (Yang et al., 2007b & Ashour, 1997)

5.5 Concluding Remarks

In this chapter, a three dimensional non-linear finite element model for assessing the behaviour of two-span SCC deep beams has been presented. The proposed model was implemented in ABAQUS version 6.12, a non-linear finite element program. Only one half of the continuous deep beam was modelled taking advantage of the symmetry in the geometry and boundary conditions. The concrete damaged plasticity model was used to model behaviour of concrete. Different parameters related to the material modelling were investigated with the objective of improving the ability of the current model to simulate the behaviour of deep beams. The proposed model was validated against the experimental results of eight two-span SCC deep beams presented in chapter three as well as some case studies selected from the literature.

Overall, the FE method can be adopted for modelling reinforced continuous SCC deep beams. However, there have been some difficulties associated with the use of FE method in this field. Initially, the lack of convergence that may affect the analysis at the early stages and sometimes prevent the completion of the analysis. Moreover, the selection of the material models and the parameters required for the model can have a significant effect on the results. As a result, a comprehensive validation of different FE models with the experimental results is strongly required in order to identify the

appropriate FE model that can be used for further investigations. Based on the work described in this chapter, the following conclusions can be drawn:

- The proposed model seems to be mesh independent and the mesh size was selected depending on the computational time.
- The initial stiffness of the load-deflection curve was well predicted by the proposed model irrespective of the values of different concrete damaged plasticity parameters. However, after cracking of concrete, the effect of some parameters such as viscosity parameter and dilation angle on the trend of the load-deflection curve started to be more clear and affected the maximum load results.
- The failure predicted by ABAQUS for all beams occurred due to major diagonal cracks connecting the load plate and the intermediate support similar to that observed in the experiments.
- The failure loads predicted from the present computational analysis were very close to those obtained experimentally with a mean of 1.00, a standard deviation of 3.73% and a coefficient of variation of 3.74%.
- The load-deflection curves predicted by ABAQUS showed reasonable agreement with that observed during the experiments. The initial stiffness of the predicted curve was similar to experiments. Moreover, the reduction in the stiffness observed in ABAQUS occurs almost in the same time as experiments.

The ABAQUS model presented in this chapter was able to predict with adequate accuracy the behaviour of continuously supported SCC deep beams. Therefore, it can be used to conduct a parametric study to expand the range of the parameters investigated in order to collect more data in

addition to the experimental data and achieve better understanding to the behaviour of SCC continuous deep beams. The results of the parametric study are presented in the next chapter.

CHAPTER SIX

PARAMETRIC STUDY

6.1 Introduction

After verifying the general reliability of the proposed ABAQUS model in predicting the behaviour of continuously supported SSC deep beams, a series of parametric studies was carried out to explore the structural behaviour of continuous SCC deep beams with extended parameter variations, both within and outside the range of experiments. In spite of the fact that experimental investigations are more reliable and very important for any research, they are expensive, time consuming and sometimes difficult to conduct. Comparatively, the numerical analysis is more affordable and allows the investigation to include a wide range of parameters.

In the previous chapter, the efficiency of the proposed FE model was validated through comparisons with experimental results obtained from the current research investigation as well as some examples selected from previous studies. The model was found to be able to accurately predict the load-deflection behaviour and the load capacity and simulate the failure mode as observed in the experiments. In this chapter, a series of extensive parametric studies is conducted to investigate the effect of several geometrical and material parameters on the load carrying capacity of continuous SCC deep beams and generate a comprehensive database in addition to that obtained from the experiments.

6.2 Parameters investigated

The geometrical dimensions of the continuous deep beam used in this parametric study are shown in Figure 6.1. The total length and the shear span of the beams are similar to those used in the experiments and only the total depth of the beam, h, was varied to obtain different shear span-to-depth ratios. Due to the symmetry in geometry, boundary conditions and loading arrangement, only half of the beam was modelled taking the advantage of the symmetric feature available in ABAQUS. The axis of symmetry was taken as the centreline of the middle support as it was explained in chapter five.

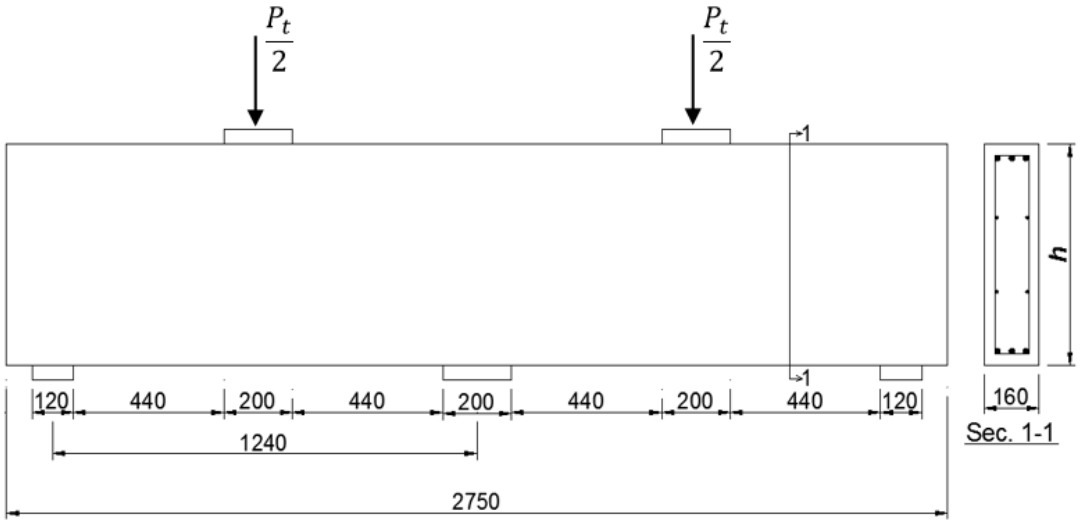

Figure 6.1: Geometrical dimensions of continuous deep beam used in parametric study (dimensions in mm)

As shown in Table 6.1, the key parameters included in the parametric studies are shear span-to-depth ratio, a/d, concrete compressive strength, f_c', amount and configuration of web reinforcement and longitudinal reinforcement ratio. Three a/d ratios were investigated: 0.5, 1.0 and 1.5. The

compressive strength included four different values: 30, 40, 50 and 60 MPa. The horizontal web reinforcement ratio, ρ_h, and the vertical web reinforcement ratio, ρ_v, included four different values each: 0, 0.21, 0.42 and 0.84%. The longitudinal bottom reinforcement ratio, ρ_{Bott}, as well as the top reinforcement ratio, ρ_{Top}, were varied to cover three different ratios: 0.5, 1.0 and 1.5%. For every investigated parameter, the other variables were given a number of values to cover a wide investigation range. The parametric study resulted in some important conclusions related to the effect of the investigated variables on the load carrying capacity of continuously supported SCC deep beams. The results of the parametric study are presented and discussed in this chapter. Due to the similarity in the relationship between the load capacity and the investigated parameters, only sample figures are presented in this chapter to show the effects of these parameters on the load carrying capacity of continuous SCC deep beams. More figures with extended variation in the values of the parameters considered in this study can be found in Appendix C.

Table 6.1: List of the parameters considered in the parametric study

a/d	f_c' MPa	ρ_v %	ρ_h %	ρ_{Bott} %	ρ_{Top} %
0.5	30	0	0	0.5	0.5
1.0	40	0.21	0.21	1.0	1.0
1.5	50	0.42	0.42	1.5	1.5
-	60	0.84	0.84	-	-

where a/d is shear span-to-depth ratio, f_c' is the concrete compressive strength in MPa, ρ_v is the vertical web reinforcement ratio, ρ_h is the horizontal web reinforcement ratio, ρ_{Bott} is the longitudinal bottom reinforcement ratio and ρ_{Top} is the longitudinal top reinforcement ratio.

6.3 Effect of shear span-to-depth ratio

In this study, the shear span-to-depth ratio included three different values: a/d=0.5, a/d=1.0 and a/d=1.5. The effect of a/d ratio was investigated for different concrete compressive strength values, different horizontal and vertical shear reinforcement ratios and different longitudinal top and bottom reinforcement ratios as shown in Figures 6.2 to 6.6. It can be clearly seen that, as expected, the load carrying capacity decreased with the increase in the shear span-to-depth ratio irrespective of the values of the other investigated parameters. Similar results were obtained by many researchers such as Ashour (1997), Yang et al. (2007a) and Yang and Ashour (2008).

In most of the cases, the load carrying capacity of beams having a/d=0.5 was more than twice that of beams having a/d=1.0 and more than four times of that of beams having a/d=1.5. Similar results were obtained by Yang et al. (2007a, 2007b) when comparing the load capacity of beams having a/d=0.5 and that of beams having a/d=1.0. The load carrying capacity of beams having a/d=0.5 increased by about 10% for a 10 MPa increase in the compressive strength of concrete compared to 4% increase rate for beams having a/d=1.5 as shown in Figure 6.2. It can be also noticed that beams having shear reinforcement (vertical, horizontal or orthogonal) showed similar behaviour to those without shear reinforcement with less variation in the results for beams having only vertical shear reinforcement as shown in Figures 6.3 and 6.4. Moreover, increasing the bottom longitudinal reinforcement ratios clearly influenced the increasing rate of the load capacity as shown in Figure 6.5 while changing the top longitudinal

reinforcement ratios had no clear effect on the load capacity for different a/d ratios as shown in Figure 6.6.

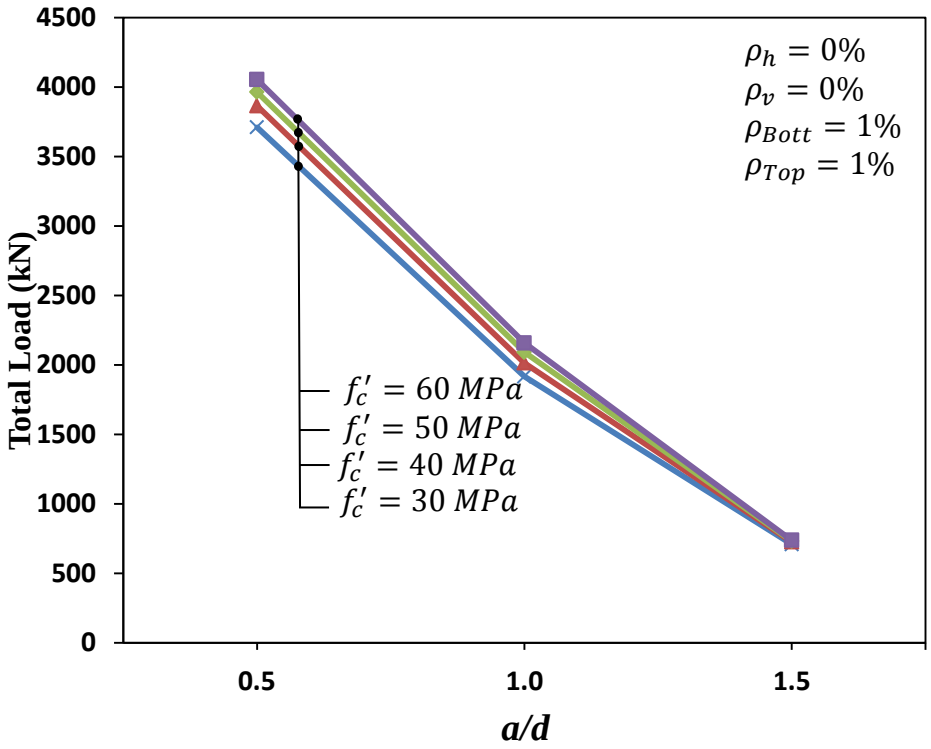

Figure 6.2: Effect of shear span-to-depth ratio on load capacity of continuous SCC deep beams for different values of compressive strength

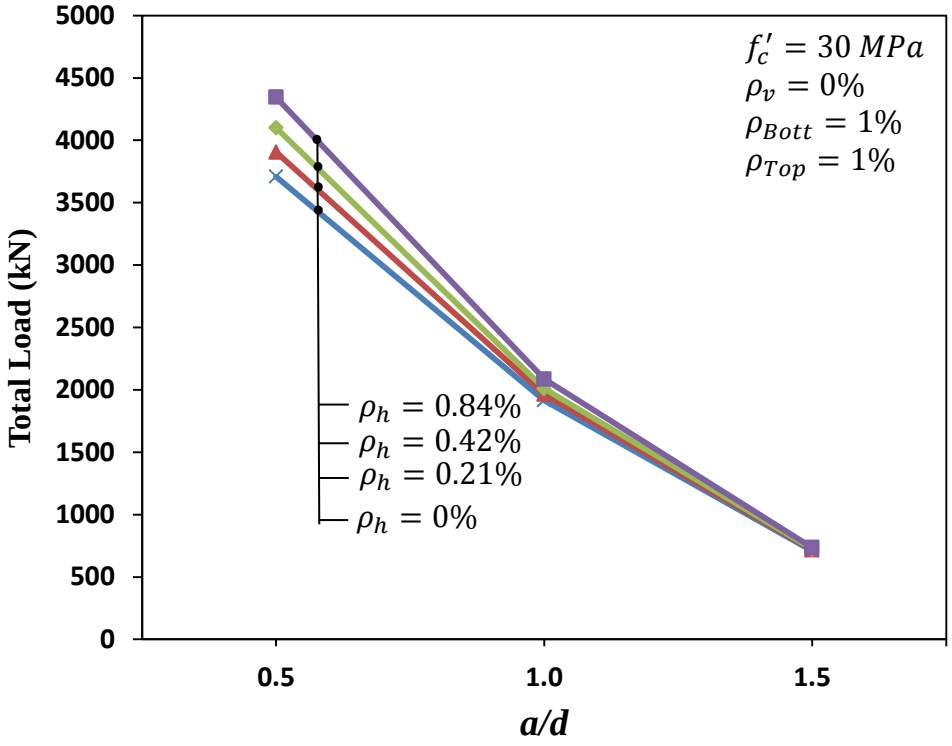

Figure 6.3: Effect of shear span-to-depth ratio on load capacity of continuous SCC deep beams for different amounts of horizontal shear reinforcement

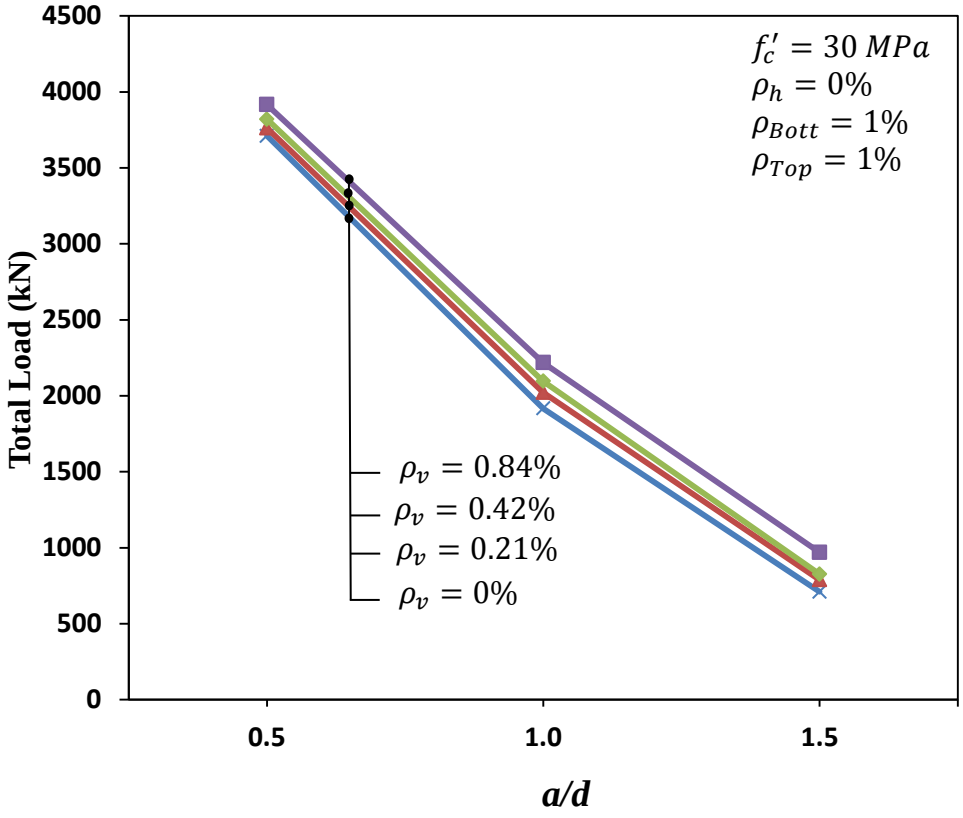

Figure 6.4: Effect of shear span-to-depth ratio on load capacity of continuous SCC deep beams for different amounts of vertical shear reinforcement

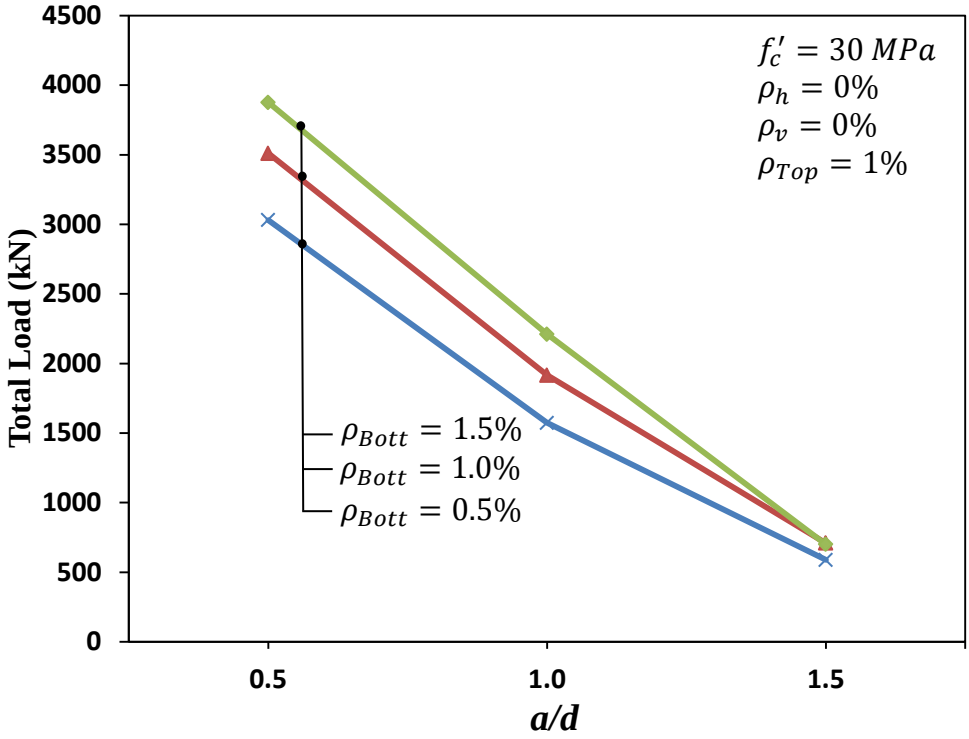

Figure 6.5: Effect of shear span-to-depth ratio on load capacity of continuous SCC deep beams for different longitudinal bottom reinforcement ratios

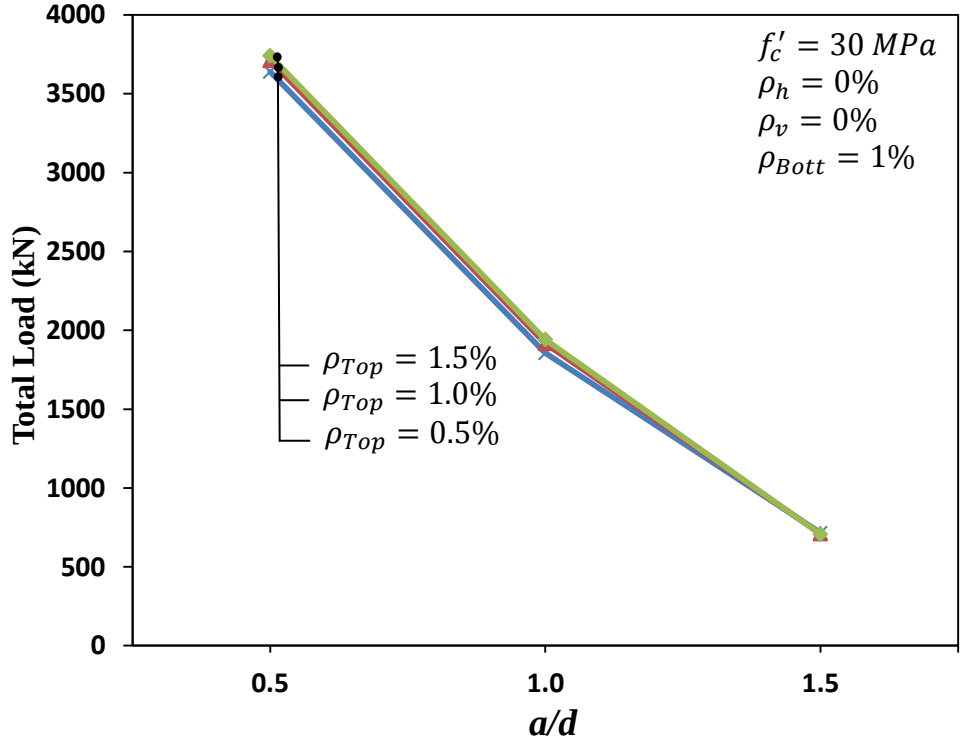

Figure 6.6: Effect of shear span-to-depth ratio on load capacity of continuous SCC deep beams for different longitudinal top reinforcement ratios

6.4 Effect of concrete strength

Concrete compressive strength is considered as one of the most important factors that control the load carrying capacity of deep beams. The load in deep beams is transferred through a compression strut and the failure mainly occurs due to compression strut failure. This means that the capacity of deep beams is significantly influenced by the value of concrete compressive strength. In this study, the concrete compressive strength was chosen to vary between 30 and 60 MPa with an increment of 10 MPa to represent normal and high strength concrete and cover the range of the concrete strengths used in the experimental investigation of the present study. The effect of compressive strength was evaluated for different shear span-to-depth ratios, different amounts and configurations of shear reinforcement and different longitudinal top and bottom reinforcement ratios.

Figures 6.7 to 6.11 show the effects of compressive strength of concrete on the load carrying capacity of continuous SCC deep beams with some variation in the other selected parameters. For all the considered compressive strength values, increasing the compressive strength of concrete led to similar behaviour in all beams irrespective of the values of other parameters. It was observed that irrespective of the values of a/d ratio and the amount and configuration of web and longitudinal reinforcement, increasing the compressive strength leads to a gradual increase in the load carrying capacity as predicted by the proposed ABAQUS model. Similar observations were found by Yang and Ashour (2008).

In all cases, the relationship between concrete strength and load capacity was found to be linear. However, this relation would significantly change with any change in the other investigated parameters. Figure 6.7 shows the effect of concrete compressive strength on the load carrying capacity of two-span continuous deep beams for different a/d ratios. It can be clearly noticed that the effect of increasing the concrete compressive strength is more pronounced in beams having low a/d ratio. Increasing the compressive strength from 30 to 60 MPa increased the load carrying capacity by about 11% for beams having a/d=0.5 compared to less than 4% for beams having a/d=1.5. It can be concluded that as the a/d ratio decreases, the concrete strength becomes more prominent in controlling the load capacity.

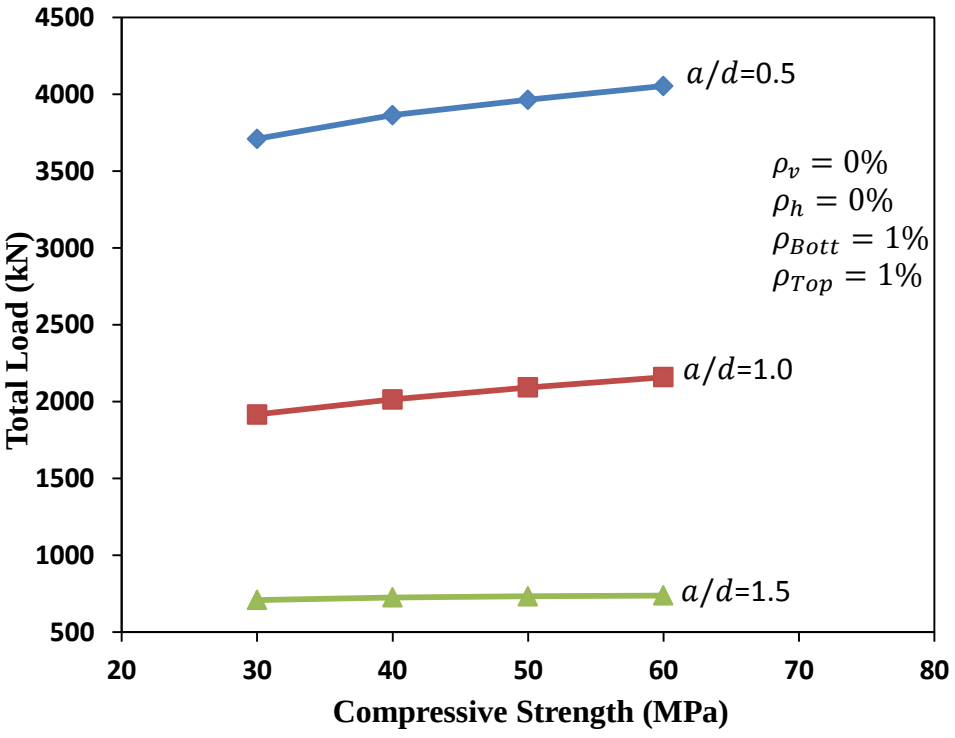

Figure 6.7: Effect of compressive strength on the load capacity for different shear span-to-depth ratios

On the other hand, increasing the compressive strength from 30 to 60 MPa led to approximately 17% increase in the load capacity of beams having high amount of horizontal shear reinforcement ($\rho_h = 0.84\%$) with a low a/d ratio. Comparatively, this percentage decreased to about 8% for beams with no shear reinforcement as shown in Figure 6.8. However, the increasing rates of the load capacity are approximately the same for all beams having only vertical web reinforcement as presented in Figure 6.9.

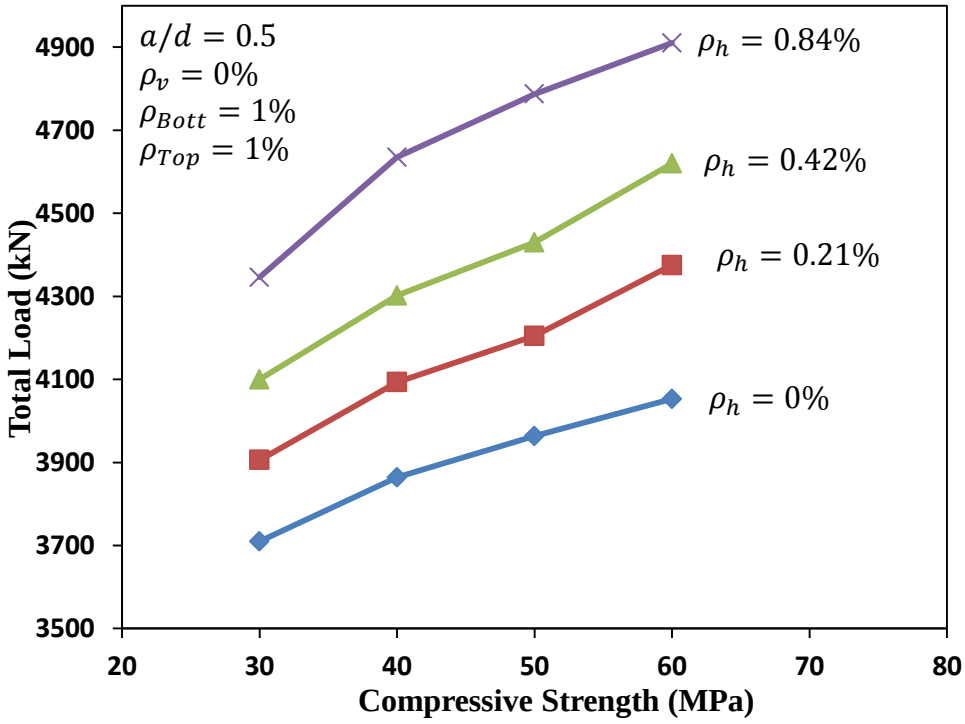

Figure 6.8: Effect of compressive strength on the load capacity for different horizontal reinforcement ratios

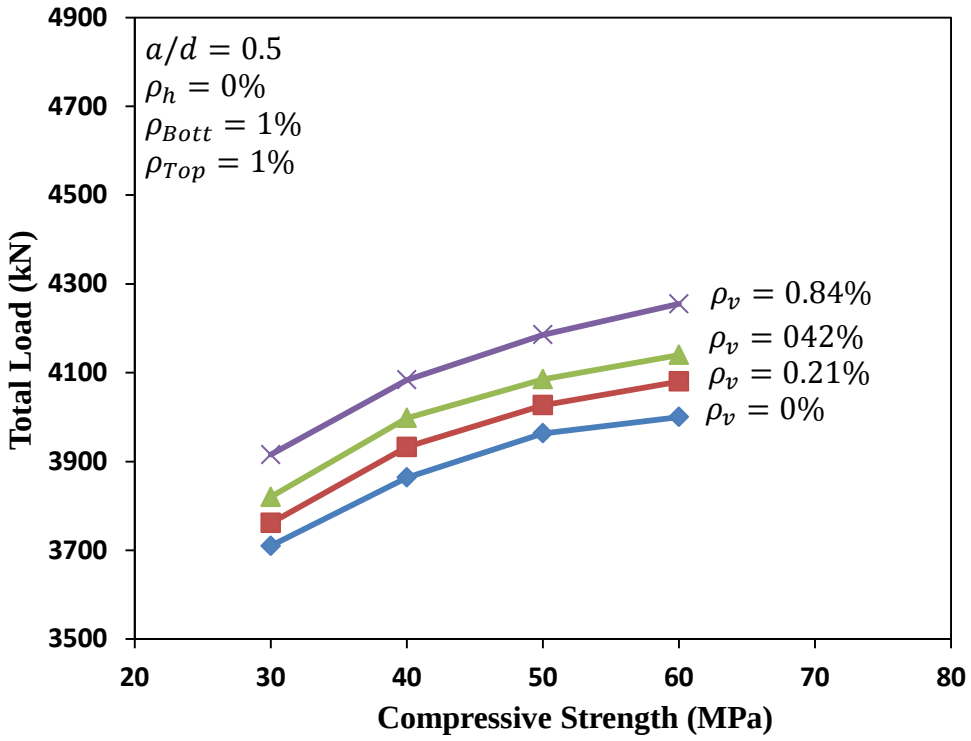

Figure 6.9: Effect of compressive strength on the load capacity for different vertical reinforcement ratios

The effect of concrete compressive strength on the load capacity was also investigated for different longitudinal top and bottom reinforcement ratios as shown in Figures 6.10 and 6.11, respectively. Similar behaviour can be observed for the three different longitudinal reinforcement ratios where the load capacity gradually increased with increasing the compressive strength of concrete. However, the increase in the load capacity was higher in beams with different longitudinal bottom reinforcement ratios than in those with different longitudinal top reinforcement ratios. For example, when increasing the compressive strength from 30 to 60 MPa, the load capacity of beam having a bottom reinforcement ratio of 1.5% reached more than 2500 kN compared to approximately 2200 kN for beam having a top reinforcement ratio of 1.5%.

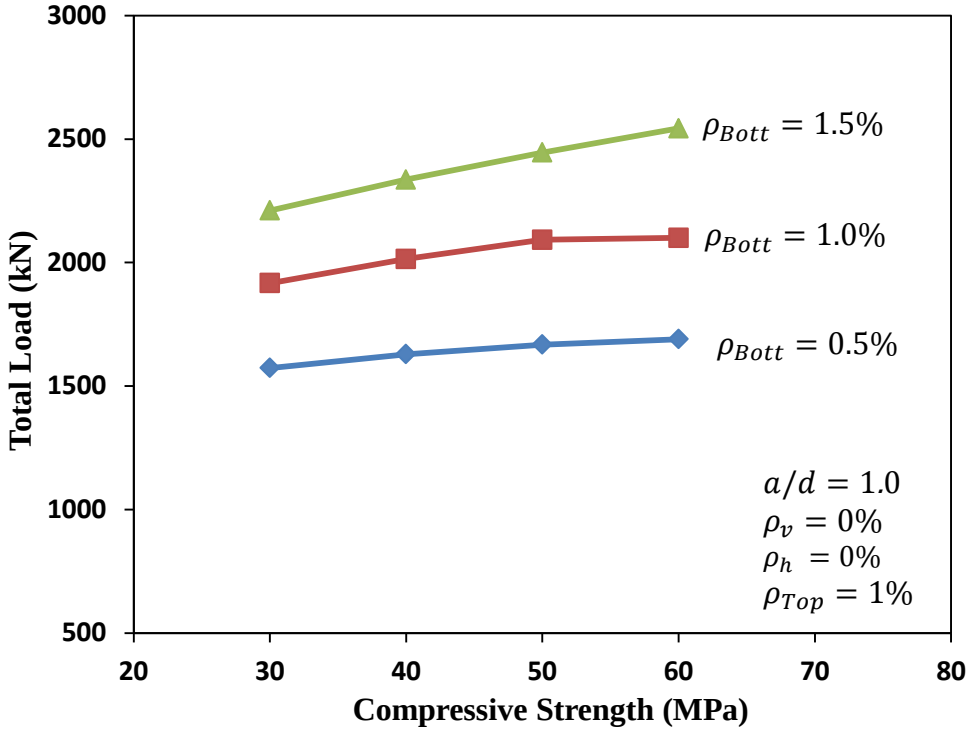

Figure 6.10: Effect of compressive strength on the load capacity for different longitudinal bottom reinforcement ratios

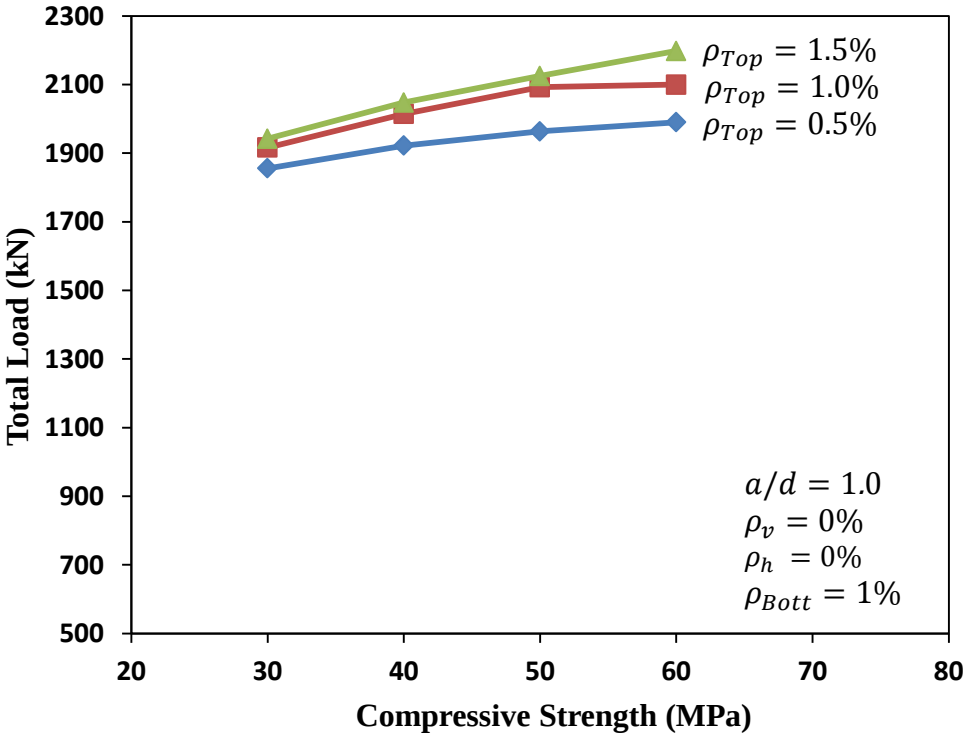

Figure 6.11: Effect of compressive strength on the load capacity for different longitudinal top reinforcement ratios

It can be concluded that the compressive strength of concrete has more influence on the load carrying capacity of beams with a low shear span-to-depth ratio. This influence becomes more significant for beams with a high amount of horizontal web reinforcement. This can be attributed to the fact that the horizontal web reinforcement has a greater effect on beams with a low shear span-to-depth ratio as will be discussed in the following section.

6.5 Effect of amount and configuration of web reinforcement

In deep beams, the shear reinforcement is one of the most important factors that control the load capacity. The presence of web reinforcement improves the shear resistance and provides better confinement for concrete in the compression regions. There is disagreement among researchers about whether the vertical or horizontal web reinforcement is more effective in carrying the loads in deep beams. In this parametric study, the proposed ABAQUS model was used to study the effect of different amounts and configurations of web reinforcement on the load capacity of SCC continuous deep beams. The effect of shear reinforcement was investigated for different shear span-to-depth ratios and different concrete strengths. For vertical and horizontal reinforcement, four different web reinforcement ratios were investigated including the minimum web reinforcement ratio recommended by ACI 318M-11 for deep beams. It should be noticed that the minimum area of web reinforcement (vertical or horizontal) required for deep beams according to ACI 318M-11 shall be equal to or greater than $0.0025\,bs$ where b is the beams web width and s is the spacing between the web reinforcing bars.

6.5.1 Effect of vertical shear reinforcement

The amounts of vertical web reinforcement investigated in this study included four different levels: none, 0.21% (minimum reinforcement ratio), 0.42% and 0.84%. The vertical web reinforcement ratio, ρ_v, was varied by changing the spacing between stirrups. Figures 6.12 and 6.13 show the effect of vertical web reinforcement on the load capacity for beams having concrete strength of 30 and 60 MPa, respectively. It can be observed that irrespective of the value of compressive strength, the effect of vertical shear reinforcement is more pronounced for beams having $a/d = 1.5$ followed by beams having $a/d = 1.0$. Comparatively, the effect of vertical web reinforcement is not clearly shown in beams having $a/d = 0.5$. These results agreed with the results found by Yang and Ashour (2008), Yang et al. (2007a, 2007b), Ashour (1997) and Rogowsky et al. (1986).

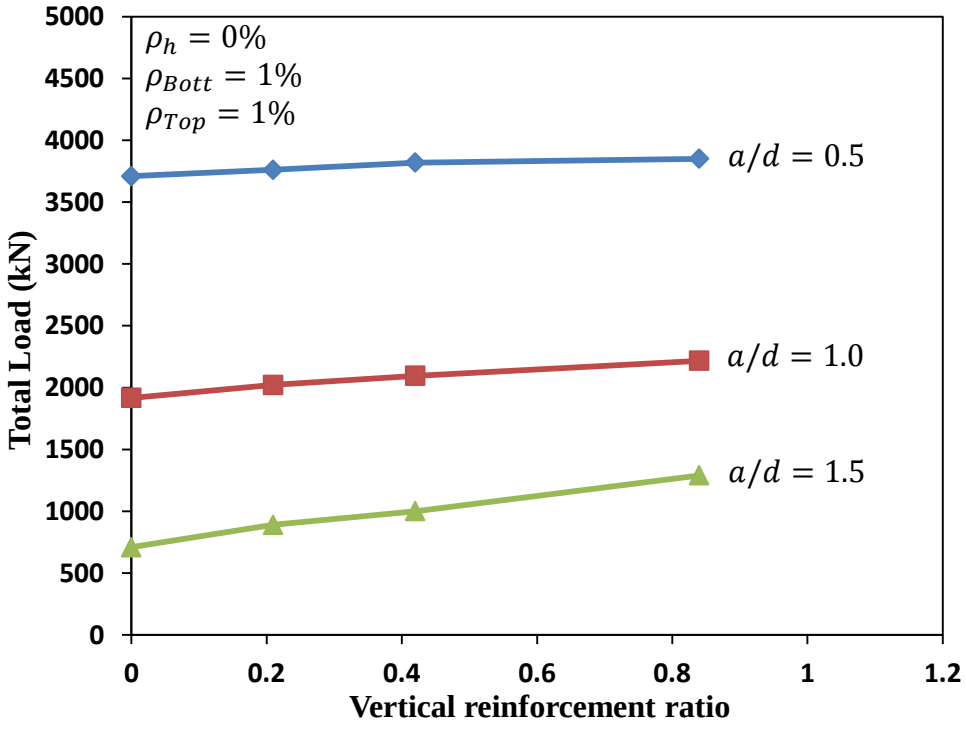

Figure 6.12: Effect of vertical web reinforcement on load capacity of beams having a compressive strength of 30 MPa

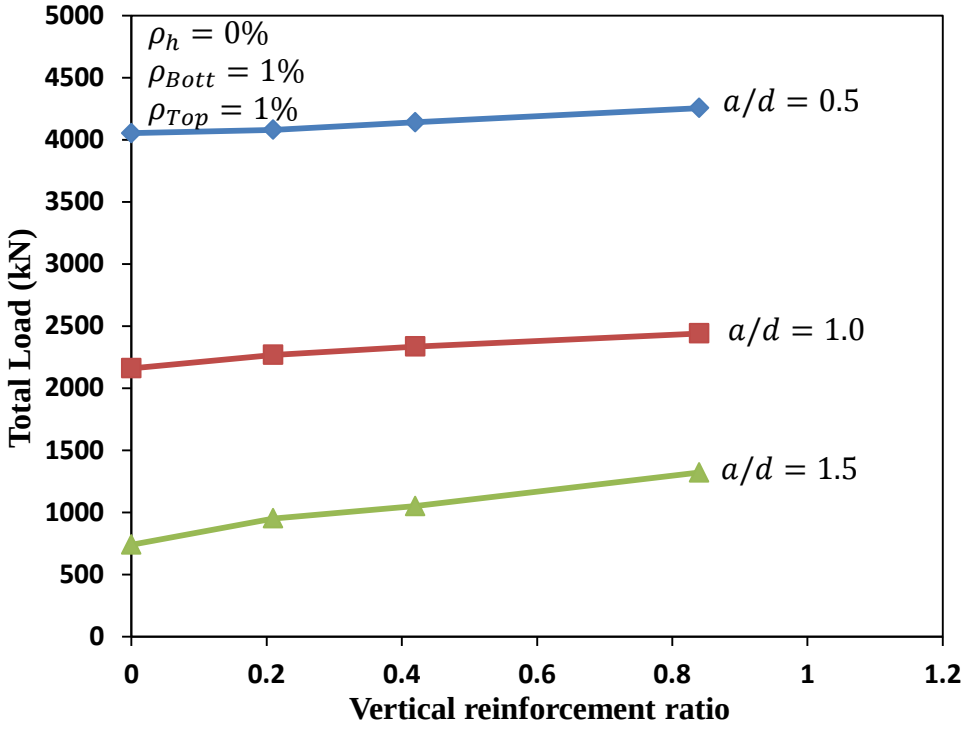

Figure 6.13: Effect of vertical web reinforcement on load capacity of beams having a compressive strength of 60 MPa

6.5.2 Effect of horizontal shear reinforcement

Similar to the vertical shear reinforcement, the horizontal web reinforcement ratios investigated in the parametric study included four different levels: none, 0.21% (minimum reinforcement ratio), 0.42% and 0.84%. The horizontal web reinforcement ratio, ρ_h, was changed by varying the spacing between the horizontal bars on both sides of the beams. Figures 6.14 and 6.15 show the effect of horizontal web reinforcement on the load capacity for beams having concrete strength of 30 and 60 MPa, respectively. It can be clearly seen that increasing the amount of horizontal web reinforcement led to similar behaviour for all beams having the same a/d ratio irrespective of the value of compressive strength. Comparisons between beams having different a/d ratios showed that the horizontal web reinforcement is more

effective in carrying the load in beams having $a/d = 0.5$. For beams having $a/d \geq 1.0$ there was almost no effect on the load capacity when increasing the amount of horizontal reinforcement. For example, beams without shear reinforcement had almost the same load as that with a high amount of horizontal web reinforcement ($\rho_h = 0.84$). Similar results were reported by many other researchers (Yang and Ashour, 2008; Yang et al., 2007a, 2007b; Ashour, 1997; Rogowsky et al., 1986).

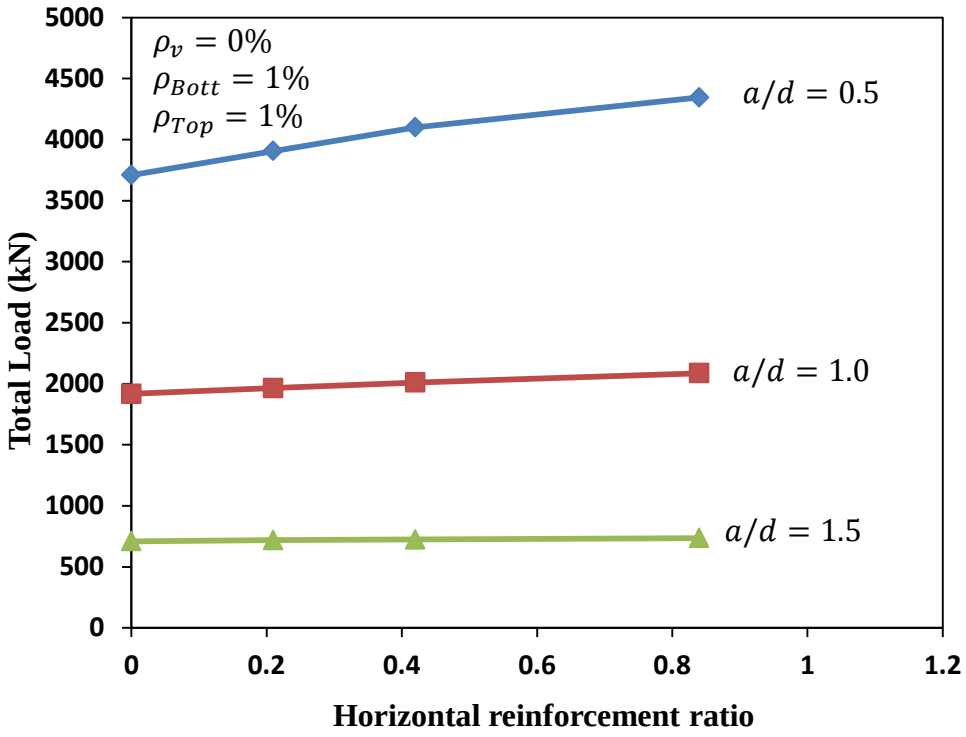

Figure 6.14: Effect of horizontal web reinforcement on load capacity of beams having a compressive strength of 30 MPa

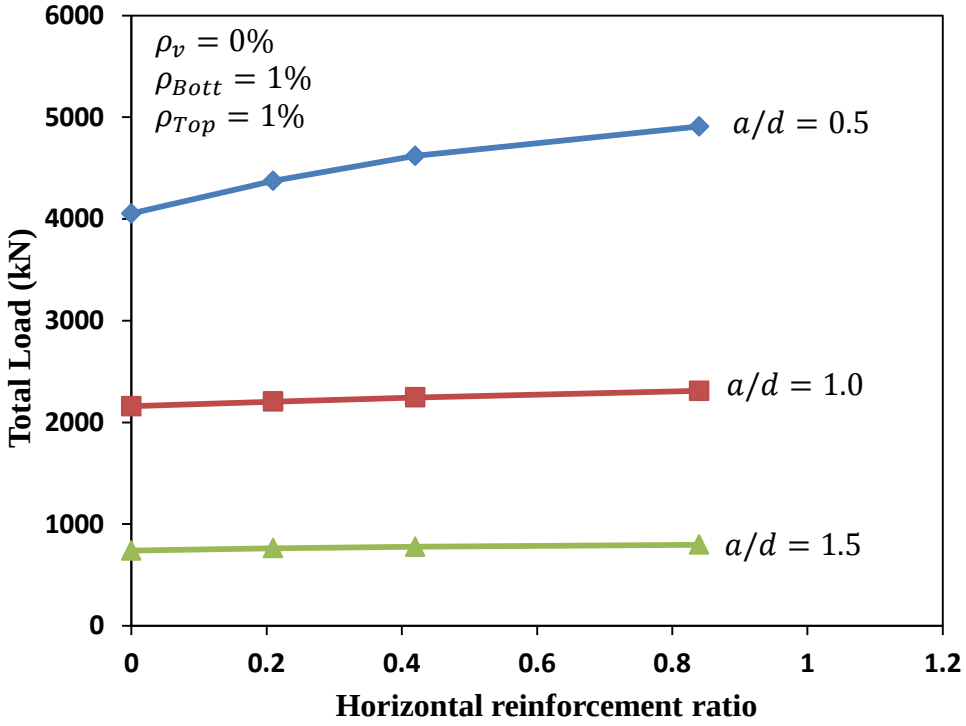

Figure 6.15: Effect of horizontal web reinforcement on load capacity of beams having a compressive strength of 60 MPa

6.6 Effect of longitudinal bottom reinforcement

In this section, the effect of longitudinal bottom reinforcement ratio, ρ_{Bott}, on the load capacity of SCC continuous deep beams is investigated. Three different bottom reinforcement ratios were investigated: 0.5%, 1.0% and 1.5%. The ratio of the top reinforcement was kept constant. The effect of the bottom reinforcement was investigated for different a/d ratios and different concrete compressive strengths as shown in Figures 6.16 and 6.17. It can be clearly seen that beams having the same a/d ratio exhibited similar behaviour irrespective of the value of the compressive strength. For beams having $a/d = 0.5$, increasing the bottom reinforcement ratio from 0.5% to 1.0% significantly improved the load capacity by approximately 30%, whereas percentage decreased to 5% when the reinforcement percentage

increased from 1.0% to 1.5%. On the other hand, the increasing rate is lower for beams with $a/d = 1.0$ while for beams with $a/d = 1.5$ the effect of increasing the bottom reinforcement ratio is less pronounced. The load capacity increasing rate for beams having $a/d \geq 1.0$ was not clearly affected by increasing the reinforcement ratio.

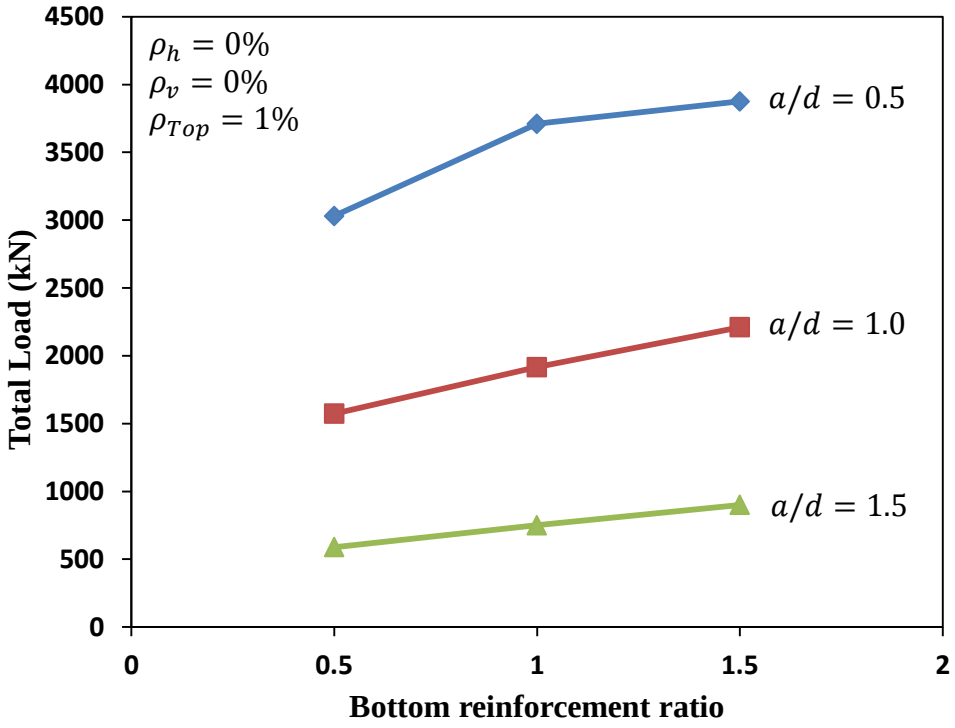

Figure 6.16: Effect of longitudinal bottom reinforcement on load capacity of beams having a compressive strength of 30 MPa

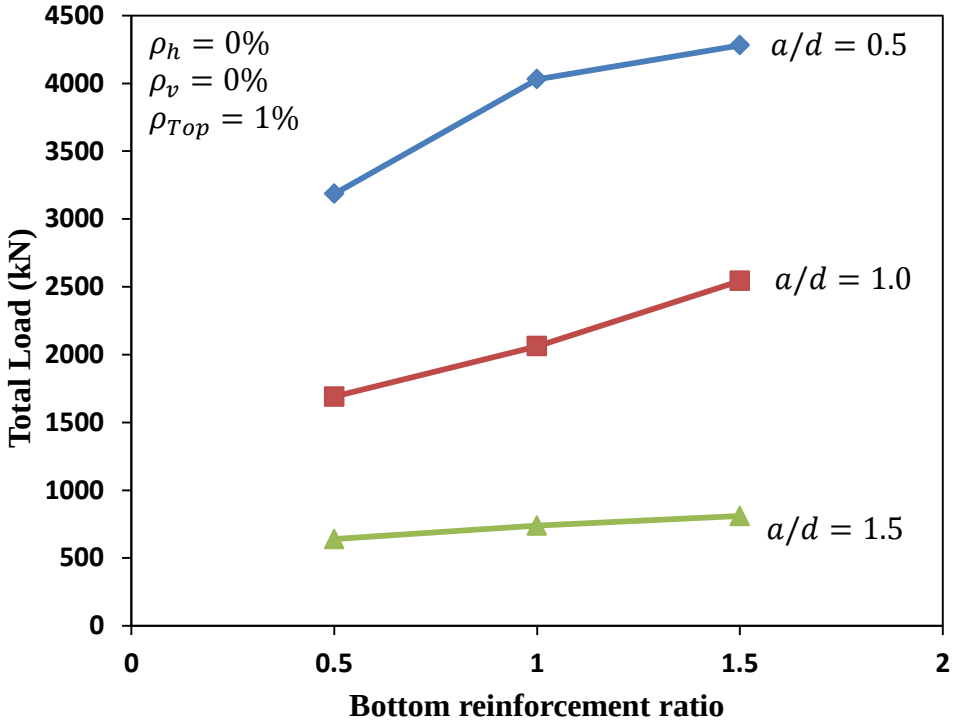

Figure 6.17: Effect of longitudinal bottom reinforcement on load capacity of beams having a compressive strength of 60 MPa

6.7 Effect of longitudinal top reinforcement

Similar to the previously investigated parameters, the proposed model was used to study the effect of the longitudinal top reinforcement ratio, ρ_{Top}, on the load capacity of continuously supported SCC deep beams. The investigated top reinforcement ratios included three different values: 0.5%, 1.0% and 1.5%. Figures 6.18 and 6.19 present the relationship between the load capacity and the top reinforcement ratio for different a/d ratios: Figure 6.18 for beams having a compressive strength of 30 MPa and Figure 6.19 for beams having a compressive strength of 60 MPa. All the investigated beams showed almost similar behaviour irrespective of the values of compressive strength. Increasing the top reinforcement ratio did not show any clear effect on the load capacity. The increase in the load capacity are very low compared to those obtained when increasing the bottom reinforcement ratio.

Beams having $a/d \geq 1.0$ showed a 2% increase in the load capacity for an increase of 0.5% in the top reinforcement ratio while beams having $a/d = 0.5$ did not show any change in the load capacity with the change in the amount of top reinforcement.

It can be concluded that the bottom reinforcement has more influence on the load capacity of continuous deep beams than the top reinforcement. Comparisons with the results of the reinforcement strains obtained experimentally in chapter three showed that all the bottom reinforcing bars reached the yield strain while none of the top ones reached the yield strain, indicating that the bottom reinforcement carry higher load than the top one as shown by the proposed ABAQUS model.

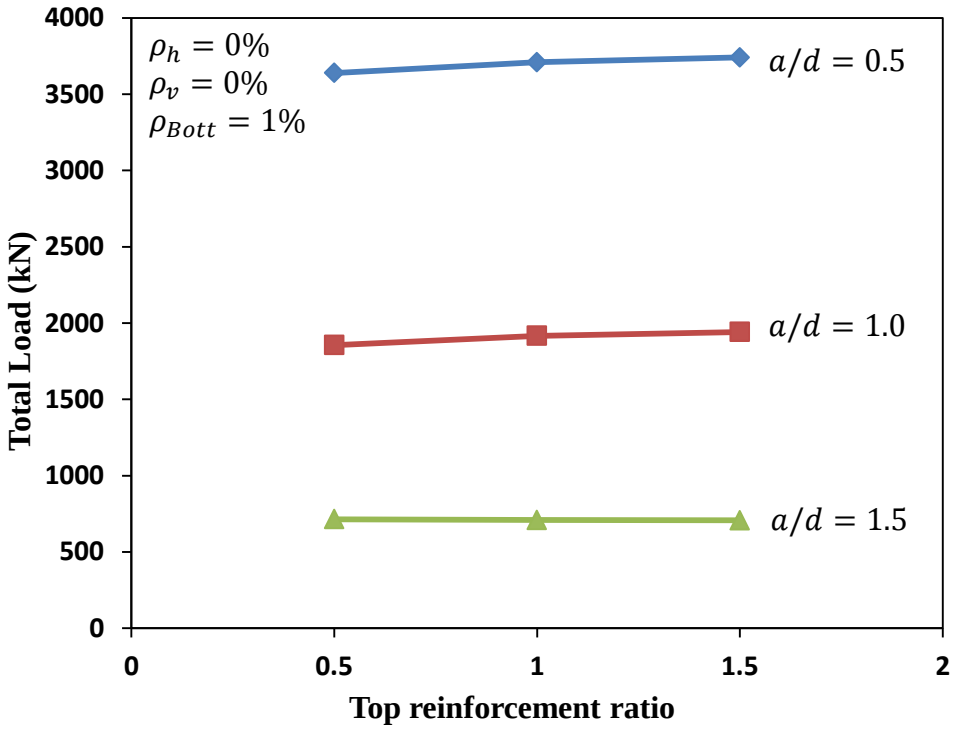

Figure 6.18: Effect of longitudinal top reinforcement on load capacity of beams having a compressive strength of 30 MPa

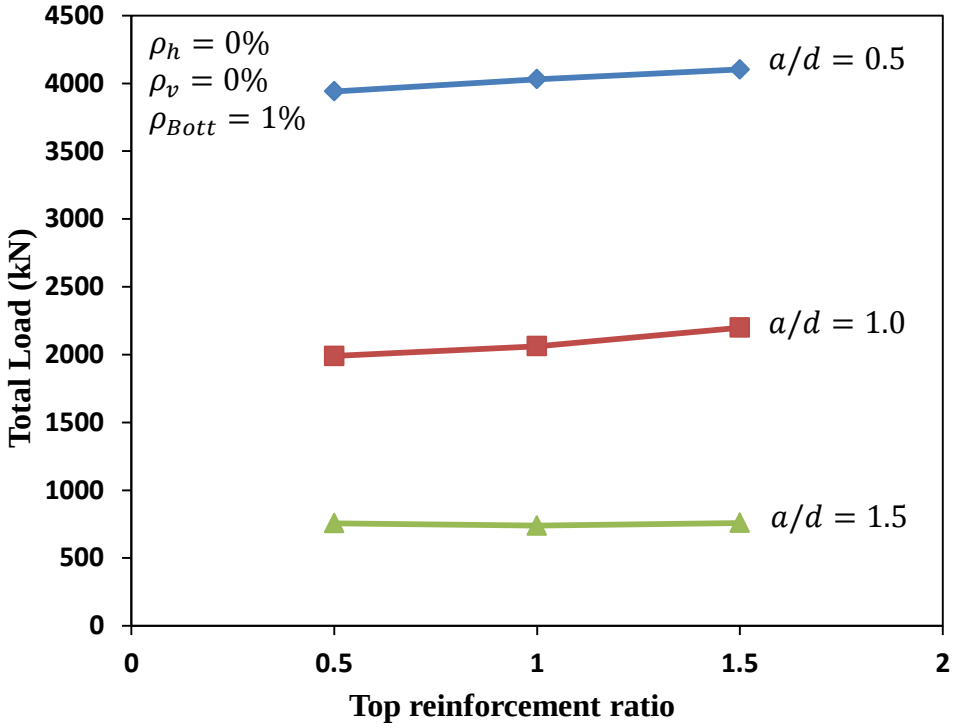

Figure 6.19: Effect of longitudinal top reinforcement on load capacity of beams having a compressive strength of 60 MPa

6.8 Conclusions

In this chapter, the three dimensional FE model proposed and validated in chapter five was used to conduct a parametric study in order to investigate the effect of key parameters on the load capacity of continuously supported SCC deep beams. The parametric study included an extended range of parameters in addition to those investigated experimentally. The parameters investigated included the shear span-to-depth ratio, the concrete compressive strength, amount and configuration of web reinforcement and longitudinal bottom and top reinforcement ratios. The results were compared in terms of the load carrying capacity. The parametric study resulted in some important conclusions regarding the effect of the investigated parameters on

the load capacity of continuously supported SCC deep beams, as summarised below:

- The load carrying capacity of continues SCC deep beams decreased with the increase in the shear span-to-depth ratio irrespective of the values of compressive strength, web reinforcement and longitudinal reinforcement. Beams having a shear span-to-depth ratio of 0.5 showed a load capacity of more than twice that of beams having shear span-to-depth ratio of 1.0 and more than four times of that of beams having shear span-to-depth ratio of 1.5.
- Increasing the concrete compressive strength resulted in a gradual increase in the load capacity. The effect of compressive strength was more pronounced in beams having shear span-to-depth ratio of 0.5 and a high amount of horizontal web reinforcement. Beam having a shear span-to-depth ratio of 0.5 and a horizontal web reinforcement ratio of 84% exhibited a 17% increase in the load capacity when the compressive strength increased from 30 to 60 MPa.
- The effect of vertical web reinforcement on the load capacity was more pronounced in beams having a shear span-to-depth ratio equal to or greater than 1.0. However, beams having a shear span-to-depth ratio of 0.5 showed no change in the load capacity with increasing the vertical web reinforcement ratio.
- The horizontal web reinforcement was more effective in carrying loads in beams having a shear span-to-depth ratio of 0.5. However, changing the horizontal reinforcement ratio had almost no effect on the load capacity of beams having a shear span-to-depth ratio equal to or greater than 1.0.

- The effect of the longitudinal bottom and top reinforcement ratios on the load capacity was more pronounced in deeper beams. However, the bottom reinforcement has more influence on the load capacity of continuous deep beams than the top reinforcement.

CHAPTER SEVEN

CONCLUSIONS AND RECOMMENDATIONS FOR FUTURE WORK

7.1 Summary

The behaviour of continuously supported SCC deep beams was investigated in this thesis. The research consists of three main stages. Firstly, experimental investigation was conducted in chapter three to study the behaviour of full-scale SCC continuous deep beams. Secondly, the predictability of the available theoretical approaches was evaluated against the experimental results of the current research as well as experimental results collected from previous studies as presented in chapter four. Finally, a numerical technique was developed in order to predict the full behaviour of continuously supported SCC deep beams as described in the chapters five and six.

The experimental part includes the construction and testing of eight continuously supported SCC deep beams. All the specimens were tested under a symmetrical two-point loading system. The main parameters investigated were the shear span-to-depth ratio, the amount and arrangement of web reinforcement and the main longitudinal reinforcement ratio. The experimental observation focused on cracking loads, crack pattern, failure modes, strains in reinforcement, deflection, distribution of support reactions and load carrying capacity.

The main focus of the theoretical part of this thesis was to assess the recommendations suggested by the current design codes of practice for the

design of deep beams using a database consisted of 76 continuously supported deep beams made with NC. Moreover, design methods proposed by previous research investigations were also presented. The main aim was to evaluate the applicability of using these recommendations and methods in the prediction of the load capacity of continuous SCC deep beams and propose a new effectiveness factor for SCC.

The final part of the research included the numerical simulation. As the theoretical approaches presented in chapter four can only predict the failure load, a numerical approach is important to predict the full behaviour of continuous deep beams. A three dimensional nonlinear finite element model was proposed using ABAQUS 6.12 package. The proposed model was validated against the experimental results of the beams tested in the present research as well as some examples collected from previous studies.

The main aim of this chapter is to summarize the principal findings of the research carried out in this study and provide a number of recommendations and suggestions for future work.

7.2 Conclusions

As the main conclusions drawn from each section of the work reported in this thesis have been given in full details at the end of each chapter, an overall view of the findings of this research is presented in this section followed by some general recommendations for future work. Based on the research reported in this thesis, the following summarized conclusions can be drawn:

- All the beams tested failed due to a major diagonal crack in the intermediate shear span started at the mid-depth of the beam and

extended along the distance between the edge of the load and intermediate support plates. The significant diagonal crack separated the beam into two concrete blocks: one rotated about the exterior support while the other was fixed over the other two supports similar to the failure mode observed in other investigations for continuous NC deep beams

- Beams with horizontal or orthogonal web reinforcement had less crack width than the beam with only vertical stirrups. Moreover, increasing the amount of main longitudinal reinforcement had a clear effect on both flexural and diagonal crack widths.
- The major redistribution of the strains in the web and longitudinal reinforcement started after the formation of the first diagonal crack. The highest strains were recorded for the web reinforcing bars crossing the main diagonal crack formed between the load plate and the intermediate support.
- The simplified shear provisions of the ACI Building Code (318M-11), which were proposed for the shear strength of NC deep beams, accurately predicted the shear strength of continuously supported SCC deep beams. However, the prediction was unconservative for beams having web reinforcement in one direction only.
- The effectiveness factor formulas proposed in the current study for the lower-bound analysis of continuously supported SCC deep beams resulted in accurate predictions in comparison with the experimental results. However, more validation is required for the proposed equations due to the lack of information on continuous SCC deep beams.

- The mechanism analysis of the upper-bound theory reasonably predicted the load capacity of two-span continuous SCC deep beams. However, the prediction accuracy decreased for beams having shear reinforcement in one direction only and beams having high shear span-to-depth ratio.
- The three dimensional nonlinear finite element model proposed in chapter five accurately predicted the failure modes, the load capacity and the load-deflection response of continuously supported SCC deep beams described in chapter three.
- The parametric study conducted using the proposed ABAQUS model showed that the vertical web reinforcement is more effective than the horizontal one in carrying the load in beams having a shear span-to-depth ratio equal to or greater than 1.0. Moreover, the bottom longitudinal reinforcement has more influence on the load capacity of continuous deep beams than the top reinforcement.

Overall, although the behaviour of SCC continuous deep beams is similar to that of NC continuous deep beams, SCC provides significant quality and improves productivity with more durable structures. The removal of vibration leads to minimize the construction time, reduce the number of worker and eliminate the dangerous arising from the use of vibration equipment.

7.3 Recommendations for future work

For continuously supported deep beams, some important areas still need further investigations. Therefore, the following suggestions are recommended for future work:

- It would be recommended to investigate the applicability of using SCC in the construction of continuously supported deep beams with web opening as it is difficult for NC to properly be placed and vibrated. Deep beams are frequently constructed with opening in the web areas for essential services and accessibility such as doors, heating pipes, electricity cables and air conditioning network.
- Although the effect of different configuration of web reinforcement on the behaviour of continuously supported deep beams was investigated previously, there still disagreement among researchers about the limit at which the vertical or horizontal web reinforcement is more effective. Hence, more experimental investigations are needed with more variations in the shear span-to-depth ratio and the configuration of web reinforcement.
- It is highly recommended to investigate the effect of totally or partially replacing the steel reinforcement by fibre reinforced polymers on the behaviour of continuously supported deep beams especially when deep beams are used in structures exposed to severe environment to minimize the effect of steel reinforcement corrosion.
- More experimental data are needed for continuously supported deep beams made with SCC, through further investigations, to validate the design codes and other theoretical approaches available as well as the proposed numerical model.

REFERENCES

ABAQUS. (2012) A finite Element Computer Program, Version 6.12. *User's and Theory Manuals, Vélizy-Villacoublay, Inc*.

ACI Committee 237 (2007) Building Code Requirements for Self-Compacting Concrete (ACI 237R-07) and Commentary (ACI 237R-07). *American Concrete Institute.*

ACI Committee 318 (2011) Building Code Requirements for Structural Concrete (ACI 318M-11) and Commentary (ACI 318M-11). *American Concrete Institute.*

ACI Committee 318 (2014) Building Code Requirements for Structural Concrete (ACI 318R-14) and Commentary (ACI 318R-14). American Concrete Institute.

Aggarwal, P., Siddique, R., Aggarwal, Y. and Gupta, S. M. (2008) Self compacting concrete–Procedure for mix design. *Leonardo electronic journal of practices and technologies* 12, 15-24.

Alih, S. and Khelil, A. (2012) Behavior of inoxydable steel and their performance as reinforcement bars in concrete beam: Experimental and nonlinear finite element analysis. *Construction and Building Materials* 37, 481-492.

Almeida Filho, F. M., Barragán, B. E., Casas, J. R. and El Debs, A. L. H. C. (2010) Hardened properties of self-compacting concrete — A statistical approach. *Construction and Building Materials* 24 (9), 1608-1615.

Alrifai, A., Aggoun, S., Kadri, A., Kenai, S. and Kadri, E.-h. (2013) Paste and mortar studies on the influence of mix design parameters on autogenous shrinkage of self-compacting concrete. *Construction and Building Materials* 47, 969-976.

Ashour, A. F. (1997) Tests of reinforced concrete continuous deep beams. *ACI Structural Journal* 94 (1), 3-11.

Ashour, A. F. and Morley, C. T. (1996) Effectiveness factor of concrete in continuous deep beams. *Journal of structural engineering New York, N.Y.* 122 (2), 169-178.

Ashour, A. F. and Rishi, G. (2000) Tests of reinforced concrete continuous deep beams with web openings. *Structural Journal* 97 (3), 418-426.

Asin, M. (2000) *The behaviour of reinforced concrete continuous deep beams.* Amsterdam: TU Delft, Delft University of Technology.

Barzegar, J., Fariborz and Schnobrich, W. C. (1986) *Nonlinear finite element analysis of reinforced concrete under short term monotonic loading.* University of Illinois Engineering Experiment Station. College of Engineering. University of Illinois at Urbana-Champaign.

Bashur, F. K. and Darwin, D. (1978) Nonlinear model for reinforced concrete slabs. *Journal of the Structural Division* 104 (1), 157-170.

Bazant, Z. P. and Kim, J.-K. (1984) Size effect in shear failure of longitudinally reinforced beams. *Journal Proceedings.* Vol. 81.

BIBM, CEMBUREAU, ERMCO, EFCA and FEFNARC (2005) *The European guidelines for self-compacting concrete. Specification, Production and Use*.

Binh, C. T., Gernay, T., Dotreppe, J.-C. and Franssen, J.-M. (2016) Steel hollow columns with an internal profile filled with self-compacting concrete under fire conditions. *Proceedings of the Romanian Academy Series, A-Mathematics Physics Technical Sciences, Information Science* 17 (2), 152-159.

British Standards Institution (BSI) (2004) Design of concrete structures-Part 1-1: General rules and rules for buildings, BS EN 1992-1-1: 2004. *British Standards (BSi).*

British Standards Institution (BSI) (2012) Testing of hardened concrete shapes, dimensions and other requirements for specimens and moulds, BS EN 12390-1:2012. *British Standards (BSi).*

Canadian Standards Association (CSA) (2004) CSA A23.4-04 R2010: Design of Concrete Structures.

CEB-FIP Model Code. (1990) Model code for concrete structures. *Euro-International Committee for Concrete (CEB)* (117-E).

Chai, H.-W. (1998) *Design and testing of self-compacting concrete*. University of London.

Choi, Y., Lee, H., Chu, S., Cheong, S. and Jung, W. (2012) Shear behavior and performance of deep beams made with self-compacting concrete. *International Journal of Concrete Structures and Materials* 6 (2), 65-78.

Daczko, J. A. (2012) *Self-consolidating concrete: applying what we know*. CRC Press.

Dinakar, P., Babu, K. and Santhanam, M. (2008) Mechanical properties of high-volume fly ash self-compacting concrete mixtures. *Structural Concrete* 9 (2), 109-116.

Domone, P. L. (2006) Self-compacting concrete: An analysis of 11 years of case studies. *Cement and Concrete Composites* 28 (2), 197-208.

Domone, P. L. (2007) A review of the hardened mechanical properties of self-compacting concrete. *Cement and Concrete Composites* 29 (1), 1-12.

Druta, C., Wang, L. and Stephen Lane, D. (2014) Tensile strength and paste–aggregate bonding characteristics of self-consolidating concrete. *Construction and Building Materials* 55, 89-96.

Du, L. and Folliard, K. J. (2005) Mechanisms of air entrainment in concrete. *Cement and Concrete Research* 35 (8), 1463-1471.

Fava, C., Bergol, L., Fornasier, G., Giangrasso, F., Rocco, C., Wallevik, O. and Nielsson, I. (2003) Fracture behaviour of self-compacting concrete. *Proceedings of the 3rd international RILEM symposium on self-compacting concrete. Reykjavik: RILEM Publications SARL.*

Felekoğlu, B., Türkel, S. and Baradan, B. (2007) Effect of water/cement ratio on the fresh and hardened properties of self-compacting concrete. *Building and Environment* 42 (4), 1795-1802.

Gibbs, J. and Zhu, W. (1999) Strength of hardened self-compacting concrete. *Proceedings of First international RILEM Symposium on Self-Compacting Concrete (PRO 7), Stockholm, Suede.*

Han, L.-H., Yao, G.-H. and Zhao, X.-L. (2005) Tests and calculations for hollow structural steel (HSS) stub columns filled with self-consolidating concrete (SCC). *Journal of Constructional Steel Research* 61 (9), 1241-1269.

Hassan, A. A. A., Hossain, K. M. A. and Lachemi, M. (2008) Behavior of full-scale self-consolidating concrete beams in shear. *Cement and Concrete Composites* 30 (7), 588-596.

Hassan, A. A. A., Hossain, K. M. A. and Lachemi, M. (2010a) Strength, cracking and deflection performance of large-scale self-consolidating concrete beams subjected to shear failure. *Engineering Structures* 32 (5), 1262-1271.

Hassan, A. A. A., Hossain, K. M. A. and Lachemi, M. (2010b) Structural assessment of corroded self-consolidating concrete beams. *Engineering Structures* 32 (3), 874-885.

Heirman, G. and Vandewalle, L. (2003) The influence of fillers on the properties of self-compacting concrete in fresh and hardened state. *Proc. of the 3rd Int. Symp. on Self-Compacting Concrete (SCC2003).*

Hu, H.-T., Lin, F.-M. and Jan, Y.-Y. (2004) Nonlinear finite element analysis of reinforced concrete beams strengthened by fiber-reinforced plastics. *Composite Structures* 63 (3–4), 271-281.

Hwang, C.-L. and Hung, M.-F. (2005) Durability design and performance of self-consolidating lightweight concrete. *Construction and Building Materials* 19 (8), 619-626.

Hwang, S.-D. and Khayat, K. H. (2008) Effect of mixture composition on restrained shrinkage cracking of self-consolidating concrete used in repair. *ACI Materials Journal* 105 (5), 499-509.

Jensen, J. (1979) Plastic solutions for reinforced concrete beams in shear. *IABSE-Colloquium" Plasticity in Reinforced Concrete", Copenhagen.*

Jin, J. (2002) *Properties of mortar for self-compacting concrete*. University of London.

Kemp, K. O. and Al-Safi, M. T. (1981) An upper-bound rigid–plastic solution for the shear failure of concrete beams without shear reinforcement. *Magazine of Concrete Research* 33 (115), 96-102.

Keuser, M. and Mehlhorn, G. (1987) Finite element models for bond problems. *Journal of Structural Engineering* 113 (10), 2160-2173.

Khaleel, O. R., Al-Mishhadani, S. A. and Abdul Razak, H. (2011) The Effect of Coarse Aggregate on Fresh and Hardened Properties of Self-Compacting Concrete (SCC). *Procedia Engineering* 14, 805-813.

Khayat, K., Hu, C. and Monty, H. (1999) Stability of self-consolidating concrete, advantages, and potential applications. *1st International RILEM Symposium on Self-Compacting Concrete.*

Kheder, G. F. and Al Jadiri, R. S. (2010) New method for proportioning self-consolidating concrete based on compressive strength requirements. *ACI Materials Journal* 107 (5), 490-497.

Kim, J.-K., Han, S. H., Park, Y. D. and Noh, J. H. (1998) Material properties of self-flowing concrete. *Journal of Materials in Civil Engineering* 10 (4), 244-249.

Kim, Y., Trejo, D. and Hueste, M. (2007) Shear characteristics of self-consolidating concrete for precast prestressed concrete members. *ACI Special Publication* 247.

Klug, Y., Holschemacher, K., Wallevik, O. and Nielsson, I. (2003) Comparison of the hardened properties of self-compacting and normal vibrated concrete. *3rd RILEM Symposium on Self Compacting Concrete, Reykjavik.*

Kumar, R., Singh, B. and Bhargava, P. (2011) Flexural capacity predictions of self-compacting concrete beams using stress-strain relationship in axial compression. *Magazine of Concrete Research* 63, 49-59.

Lachemi, M., Hossain, K. M. and Lambros, V. (2005) Shear resistance of self-consolidating concrete beams-experimental investigations. *Canadian journal of civil engineering* 32 (6), 1103-1113.

Lapczyk, I. and Hurtado, J. A. (2007) Progressive damage modeling in fiber-reinforced materials. *Composites Part A: Applied Science and Manufacturing* 38 (11), 2333-2341.

Leemann, A. and Hoffmann, C. (2005) Properties of self-compacting and conventional concrete–differences and similarities. *Magazine of Concrete Research* 57 (6), 315-319.

Lin, C.-H. and Chen, J.-H. (2012) Shear behavior of self-consolidating concrete beams. *ACI Structural Journal* 109 (3), 307-315.

Lu, H., Han, L.-H. and Zhao, X.-L. (2010) Fire performance of self-consolidating concrete filled double skin steel tubular columns: Experiments. *Fire safety journal* 45 (2), 106-115.

Malm, R. (2009) *Predicting shear type crack initiation and growth in concrete with non-linear finite element method*. Royal Institute of Technology (KTH), Stockholm.

Maslehuddin, M., Saricimen, H. and Al-Mani, A. (1987) Effect of Fly Ash Addition on the Corrosion Resisting Characteristics of Concrete. *Materials Journal* 84 (1), 42-50.

Mata, L. A. (2004) Implementation of Self-Consolidating Concrete (SCC) for Prestressed Concrete Girders.

Meyer, C. and Okamura, H. (1986) Finite element analysis of reinforced concrete structures. ASCE.

Mohammadhassani, M., Jumaat, M. Z., Ashour, A. and Jameel, M. (2011) Failure modes and serviceability of high strength self-compacting concrete deep beams. *Engineering Failure Analysis* 18 (8), 2272-2281.

Mohammadhassani, M., Jumaat, M. Z. and Jameel, M. (2012a) Experimental investigation to compare the modulus of rupture in high strength self-compacting concrete deep beams and high strength concrete normal beams. *Construction and Building Materials* 30, 265-273.

Mohammadhassani, M., Jumaat, M. Z., Jameel, M., Badiee, H. and Arumugam, A. M. S. (2012b) Ductility and performance assessment of high strength self-compacting concrete (HSSCC) deep beams: An experimental investigation. *Nuclear Engineering and Design* 250, 116-124.

Mörtsell, E. and Rodum, E. (2001) Mechanical and durability aspects of SCC for road structures. *Proceedings of the 2nd International Symposium on Self-Compacting Concrete, eds. Ozawa K, Ouchi M, Tokyo, Japan.*

Nepomuceno, M., Oliveira, L. and Lopes, S. M. R. (2012) Methodology for mix design of the mortar phase of self-compacting concrete using different mineral additions in binary blends of powders. *Construction and Building Materials* 26 (1), 317-326.

Ngo, D. and Scordelis, A. (1967) Finite element analysis of reinforced concrete beams. *ACI Journal Proceedings.* Vol. 64. ACI.

Nielsen, M. P. (1975) Plastic Shear Strength of Reinforced Concrete Beams. *Bygningsstatiske Meddelelser* 46 (3), 61-99.

Nielsen, M. P. (1984) *Limit analysis and concrete plasticity.* Englewood Cliffs.

Nielsen, M. P. and Braestrup, M. (1978) Shear strength of prestressed concrete beams without web reinforcement. *Magazine of Concrete Research* 30 (104), 119-128.

Nielsen, M. P. and Hoang, L. C. (2010) *Limit analysis and concrete plasticity.* CRC press.

Nilson, A. H. (1972) Internal measurement of bond slip. *ACI Journal Proceedings.* Vol. 69. ACI.

Noguchi, T., Oh, S. and Tomosawa, F. (1999) Rheological approach to passing ability between reinforcing bars of self-compacting concrete. *Self-Compacting Concrete: Proceedings of the First International RILEM Symposium.*

Okamura, H. and Ouchi, M. (2003) Self-compacting concrete. *Journal of Advanced Concrete Technology* 1 (1), 5-15.

Okamura, H., Ozawa, K. and Ouchi, M. (2000) Self-compacting concrete. *Structural Concrete* 1 (1), 3-17.

Ozawa, K., Maekawa, K. and Okamura, H. (1990) High performance concrete with high filling capacity. *Admixtures for Concrete-Improvement of Properties: Proceedings of the International RILEM Symposium.* Vol. 5. CRC Press.

Parra, C., Valcuende, M. and Gómez, F. (2011) Splitting tensile strength and modulus of elasticity of self-compacting concrete. *Construction and Building Materials* 25 (1), 201-207.

Pentti, G. H.-E. P. (1999) Properties of SCC-especially early age and long term shrinkage and salt frost resistance. *Proceedings of the 1 st International Rilem Symposium on Self-compacting Concrete, Stockholm, Sweden. Rilem, Bagneux, France.*

Persson, B. (1999) Creep, shrinkage and elastic modulus of self-compacting concrete. *First International RILEM Symposium on Self-Compacting Concrete.* RILEM Publications SARL.

Persson, B. (2001) A comparison between mechanical properties of self-compacting concrete and the corresponding properties of normal concrete. *Cement and Concrete Research* 31 (2), 193-198.

Petersson, O., Billberg, P. and Van, B. (1996) A model for self-compacting concrete. *RILEM PROCEEDINGS.* London. Paisley, E&FN Spon.

Rasheed, M. M. and Alobaidi, I. H. K. (2012) Experimental Study of Self Compacting Reinforced Concrete Deep Beams under Four Point Loads. *Eng &Tech. Journal* 30 (12), 2197-2208.

Rogowsky, D. M., MacGregor, J. G. and Ong, S. Y. (1986) Tests of reinforced concrete deep beams. *Journal Proceedings.* Vol. 83.

Rots, J. G., Nauta, P., Kuster, G. M. A. and Blaauwendraad, J. (1985) Smeared Crack Approach and Fracture Localization in Concrete.

Rui, X., Lu, Z., Ren, Z. and Changwu, X. (2013) Experimental Study of Self-stressing of Self-compacting Concrete Filled Steel Tubular Short Columns. *Advances in Information Sciences and Service Sciences* 5 (2), 623.

Sahmaran, M., Yaman, O. and Tokyay, M. (2007) Development of high-volume low-lime and high-lime fly-ash-incorporated self-consolidating concrete. *Magazine of Concrete Research* 59 (2), 97-106.

Salman, M. M., Jarallah, H. K. and Delef, E. A. N. (2013) Experimental Study for Shear Behavior of Hybrid Self-Compacting Concrete Beams. *Journal of Engineering and Development* 17, 97-118.

Schindler, A. K., Barnes, R. W., Roberts, J. B. and Rodriguez, S. (2007) Properties of self-consolidating concrete for prestressed members. *ACI Materials Journal* 104 (1), 53-61.

Schneider, S. P. (1998) Axially loaded concrete-filled steel tubes. *Journal of structural Engineering* 124 (10), 1125-1138.

Scordelis, A., Ngo, D. and Franklin, H. (1974) Finite element study of reinforced concrete beams with diagonal tension cracks. *ACI Special Publication* 42.

Sedran, T., De Larrard, F., Hourst, F. and Contamines, C. (1996) Mix design of self-compacting concrete (SCC). *In Proc. of the Mt. RILEM conf on production methods and workability of concrete.* London.

Shah, D. and Modhera, C. (2010) Evaluation of shear strength of self-compacting concrete deep beam. *International Journal of Advanced Engineering Technology* 1 (2), 292-305.

Shah, D. L. and Modhera, C. D. (2012) Evaluation of shear strength in self-compacting fibre-reinforced concrete and conventional concrete deep beams. *Magazine of Concrete Research* 64, 527-537.

Shen, J., Yurtdas, I., Diagana, C. and Li, A. (2015) Experimental investigation on the shear performance of prestressed self-compacting concrete beams without stirrups. *Materials and Structures* 48 (5), 1291-1302.

Sinaei, H., Mahdi Shariati, A. H. A., Aghaei, M. and Shariati, A. (2012) Evaluation of reinforced concrete beam behaviour using finite element analysis by ABAQUS. *Scientific Research and Essays* 7 (21), 2002-2009.

Skarendahl, Å. and Petersson, Ö. (2000) *Report 23: Self-Compacting Concrete–State-of-the-Art report of RILEM Technical Committee 174-SCC.* Vol. 23. RILEM publications.

Sonebi, M. (2004) Applications of statistical models in proportioning medium-strength self-consolidating concrete. *ACI Materials Journal* 101 (5), 339-346.

Sonebi, M. and Bartos, P. (2002) Filling ability and plastic settlement of self-compacting concrete. *Materials and Structures* 35 (8), 462-469.

Spacone, E., Ciampi, V. and Filippou, F. (1996) Mixed formulation of nonlinear beam finite element. *Computers & Structures* 58 (1), 71-83.

Su, N., Hsu, K.-C. and Chai, H.-W. (2001) A simple mix design method for self-compacting concrete. *Cement and Concrete Research* 31 (12), 1799-1807.

Su, N. and Miao, B. (2003) A new method for the mix design of medium strength flowing concrete with low cement content. *Cement and Concrete Composites* 25 (2), 215-222.

Subedi, N. (1998) Reinforced concrete two-span continuous deep beams. *Proceedings of the Institution of Civil Engineers. Structures and buildings* 128 (1), 12-25.

Sukumar, B., Nagamani, K. and Srinivasa Raghavan, R. (2008) Evaluation of strength at early ages of self-compacting concrete with high volume fly ash. *Construction and Building Materials* 22 (7), 1394-1401.

Tan, K. and Lu, H. (1999) Shear behavior of large reinforced concrete deep beams and code comparisons. *ACI Structural Journal* 96 (5), 836-845.

Taylor, H. (1974) The fundamental behavior of reinforced concrete beams in bending and shear. *ACI Special Publication* 42.

Topçu, İ. B. and Uygunoğlu, T. (2010) Effect of aggregate type on properties of hardened self-consolidating lightweight concrete (SCLC). *Construction and Building Materials* 24 (7), 1286-1295.

Turcry, P., Loukili, A. and Haidar, K. (2002) Mechanical properties, plastic shrinkage, and free deformations of self-consolidating concrete. *First North American Conference on the Design and Use of Self-Consolidating Concrete.*

Vecchio, F. J. (1989) Nonlinear finite element analysis of reinforced concrete membranes. *ACI Structural Journal* 86 (1), 26-35.

Vecchio, F. J. and Collins, M. P. (1993) Compression response of cracked reinforced concrete. *Journal of Structural Engineering* 119 (12), 3590-3610.

Wang, W., Jiang, D.-H. and Hsu, C.-T. T. (1993) Shear strength of reinforced concrete deep beams. *Journal of Structural Engineering* 119 (8), 2294-2312.

Warwick, W. and Foster, S. J. (1993) *Investigation into the efficiency factor used in non-flexural reinforced concrete member design.* University of New South Wales.

Wolanski, A. J. (2004) *Flexural behavior of reinforced and prestressed concrete beams using finite element analysis*. Citeseer.

Yang, K.-H. and Ashour, A. F. (2011) Aggregate interlock in lightweight concrete continuous deep beams. *Engineering Structures* 33 (1), 136-145.

Yang, K.-H., Chung, H.-S. and Ashour, A. F. (2007a) Influence of shear reinforcement on reinforced concrete continuous deep beams. *ACI Structural Journal* 104 (4), 420-429.

Yang, K.-H., Chung, H.-S., Lee, E.-T. and Eun, H.-C. (2003) Shear characteristics of high-strength concrete deep beams without shear reinforcements. *Engineering structures* 25 (10), 1343-1352.

Yang, K. H. and Ashour, A. F. (2008) Load capacity of reinforced concrete continuous deep beams. *Journal of Structural Engineering* 134 (6), 919-929.

Yang, K. H., Chung, H. S. and Ashour, A. F. (2007b) Influence of section depth on the structural behaviour of reinforced concrete continuous deep beams. *Magazine of Concrete Research* 59 (8), 575-586.

Zainai, B. (1987) *Shear strength of reinforced concrete wall-beam structures: upper-bound analysis and experiments*. University of Cambridge.

Zainai, B. and Morley, C. (1991) Shear strength of reinforced concrete wall-beam structures: an improved solution. *International Conference on solid Mechanics and Structures, Singapore.*

Zhu, W., Sonebi, M. and Bartos, P. (2004) Bond and interfacial properties of reinforcement in self-compacting concrete. *Materials and structures* 37 (7), 442-448.

APPENDIX A. DATABASE OF CONTINUOUSLY SUPPORTED DEEP BEAMS

Table A-1 shows the details of the database of continuous NC deep beams. The database was used in chapter two to identify the most important parameters the affect behaviour of continuously supported NC deep beams and draw some relationships between the load capacity and these parameters. The database was also used in chapter two and chapter four to validate different design approaches of deep beams including the design methods suggested by different design codes as well as those proposed by different researchers.

Table A-1: Database of continuously supported NC deep beams

Reference	Notation	h mm	a mm	a/h	b mm	L mm	f_c' Mpa	A_{s_2} mm^2	A'_{s_2} mm^2	ρ_v	ρ_h	V_{EXP} kN
Yang et al., (2007b)	L5NN	600	300	0.5	160	600	32.4	851	851	0	0	456
	L5NS	600	300	0.5	160	600	32.4	851	851	0.003	0	486
	L5NT	600	300	0.5	160	600	32.4	851	851	0.006	0	512
	L5SN	600	300	0.5	160	600	32.4	851	851	0	0.003	546
	L5SS	600	300	0.5	160	600	32.4	851	851	0.003	0.003	607
	L5TN	600	300	0.5	160	600	32.4	851	851	0	0.006	655

	L10NN	600	600	1.0	160	1200	32.1	851	851	0	0	264
	L10NS	600	600	1.0	160	1200	32.1	851	851	0.003	0	349
	L10NT	600	600	1.0	160	1200	32.1	851	851	0.006	0	446
	L10SN	600	600	1.0	160	1200	32.1	851	851	0	0.003	266
	L10SS	600	600	1.0	160	1200	32.1	851	851	0.003	0.003	357
	L10TN	600	600	1.0	160	1200	32.1	851	851	0	0.006	288
	H6NN	600	360	0.6	160	720	65.1	851	851	0	0	634
	H6NS	600	360	0.6	160	720	65.1	851	851	0.003	0	683
	H6NT	600	360	0.6	160	720	65.1	851	851	0.006	0	757

Reference	Notation	h mm	a mm	a/h	b mm	L mm	f_c' Mpa	A_s mm^2	A_s' mm^2	ρ_v	ρ_h	V_{EXP} kN
	H6SN	600	360	0.6	160	720	65.1	851	851	0	0.003	708
	H6SS	600	360	0.6	160	720	65.1	851	851	0.003	0.003	799
	H6TN	600	360	0.6	160	720	65.1	851	851	0	0.006	854
	H10NN	600	600	1.0	160	1200	68.2	851	851	0	0	373
	H10NS	600	600	1.0	160	1200	68.2	851	851	0.003	0	414
	H10NT	600	600	1.0	160	1200	68.2	851	851	0.006	0	638
	H10SN	600	600	1.0	160	1200	68.2	851	851	0	0.003	387
	H10SS	600	600	1.0	160	1200	68.2	851	851	0.003	0.003	492
	H10TN	600	600	1.0	160	1200	68.2	851	851	0	0.006	393
Yang et al., (2007a)	L5-40	400	200	0.5	160	400	32.4	574	574	0	0	411
	L5-60	600	300	0.5	160	600	32.4	861	861	0	0	473
	L5-72	720	360	0.5	160	720	32.4	1148	1148	0	0	502
	L10-40	400	400	1.0	160	800	32.1	574	574	0	0	202
	L10-60	600	600	1.0	160	1200	32.1	861	861	0	0	264
	L10-72	720	720	1.0	160	1440	32.1	1148	1148	0	0	302
	H6-40	400	240	0.6	160	480	65.1	574	574	0	0	592
	H6-60	600	360	0.6	160	720	65.1	861	861	0	0	634
	H6-72	720	432	0.6	160	864	65.1	1148	1148	0	0	698

	H10-40	400	400	1.0	160	800	76.5	574	574	0	0	335
	H10-60	600	600	1.0	160	1200	68.2	861	861	0	0	373
	H10-72	720	720	1.0	160	1440	67.5	1148	1148	0	0	393
Ashour, (1997)	CDB1	625	660	1.1	120	1340	30.0	452	610	0.0084	0.0084	351
	CDB2	625	660	1.1	120	1340	33.1	452	610	0.0042	0.0042	306
	CDB3	625	660	1.1	120	1340	22.0	452	610	0	0.0042	180
	CDB4	625	660	1.1	120	1340	28.0	452	610	0.0042	0	284
	CDB5	625	660	1.1	120	1340	28.7	226	226	0.0042	0.0042	258
	CDB6	425	660	1.6	120	1340	22.5	383	383	0.0047	0.0047	156
	CDB7	425	660	1.6	120	1340	26.7	383	383	0.0024	0.0024	140
Reference	Notation	h mm	a mm	a/h	b mm	L mm	f_c' Mpa	A_s mm^2	A_s' mm^2	ρ_v	ρ_h	V_{EXP} kN
	CDB8	425	660	1.6	120	1340	23.6	226	226	0.0024	0.0024	124
Rogowsky et al., (1986)	3/1.0	1000	1000	1	200	2100	28.9	943	1257	0.0015	0	689
	4/1.0	1000	1000	1	200	2100	28.5	943	1257	0	0.0015	667
	5/1.0	1000	1000	1	200	2100	36.9	943	1257	0.006	0	875
	6/1.0	1000	1000	1	200	2100	35.8	943	1257	0	0.0045	646
	7/1.0	1000	1000	1	200	2100	34.5	943	1257	0	0	424
	3/1.5	600	1000	1.67	200	2100	14.5	864	1060	0.002	0	243
	4/1.5	600	1000	1.67	200	2100	32.5	864	1060	0	0.0015	206
	5/1.5	600	1000	1.67	200	2100	39.6	864	1060	0.006	0	565
	6/1.5	600	1000	1.67	200	2100	45	864	1060	0	0.0045	260
	7/1.5	600	1000	1.67	200	2100	30.4	864	1060	0	0	223
	8/1.5	600	1000	1.67	200	2100	37.2	864	1060	0.002	0.0015	342
	3/2.0	500	1000	2	200	2100	42.5	864	864	0.0015	0	261
	4/2.0	500	1000	2	200	2100	38.3	864	864	0	0.0015	195
	5/2.0	500	1000	2	200	2100	41.1	864	864	0.006	0	453
	6/2.0	500	1000	2	200	2100	37.4	864	864	0	0.0045	260
	7/2.0	500	1000	2	200	2100	46.8	864	864	0	0	188
Subedi, (1998)	1CB1	400	250	0.63	50	500	56.5	201	201	0.0057	0.0057	215

	2CB2	400	500	1.25	50	1000	56.5	201	201	0.0057	0.0057	117
	1CB3	600	840	1.4	75	1680	44.7	628	628	0.0075	0.0075	276
	1CB4	600	840	1.4	75	1680	44.7	628	226	0.0075	0.0075	273
Asin, (2000)	1.0/1/1	1000	1100	1.1	150	2300	37.1	452	628	0.005	0	527
	1.0/1/2	1000	1100	1.1	150	2300	30.2	452	628	0.0038	0	495
	1.0/1/3	1000	1100	1.1	150	2300	30.4	452	628	0.0022	0	388
	1.0/2/1	1000	1100	1.1	150	2300	28.2	628	452	0.005	0	586
	1.0/2/2	1000	1100	1.1	150	2300	34.3	628	452	0.0038	0	469
	1.0/2/3	1000	1100	1.1	150	2300	36.8	628	452	0.0022	0	423
	1.5/1/1	600	1100	1.8	150	2300	34.9	628	785	0.005	0	399
Reference	Notation	h mm	a mm	a/h	b mm	L mm	f_c' Mpa	A_s mm^2	A_s' mm^2	ρ_v	ρ_h	V_{EXP} kN
	1.5/1/2	600	1100	1.8	150	2300	33.3	628	785	0.0038	0	346
	1.5/1/3	600	1100	1.8	150	2300	32.6	628	785	0.0022	0	262
	1.5/2/1	600	1100	1.8	150	2300	33.2	785	628	0.005	0	373
	1.5/2/2	600	1100	1.8	150	2300	33.2	785	628	0.0038	0	338
	1.5/2/3	600	1100	1.8	150	2300	34.4	785	628	0.0022	0	250

where a/h is the shear span-to-overall depth ratio, h is the beam total depth, a is the shear span, b is the beam width, L is the span length, f_c' is the concrete compressive strength, A_s is the area of longitudinal bottom reinforcement, A_s' is the area of longitudinal top reinforcement, ρ_v is the ratio of vertical web reinforcement, ρ_h is the ratio of horizontal web reinforcement and V_{EXP} is the experimental shear capacity.

APPENDIX B. MIX DESIGN METHODS FOR SELF-COMPACTING CONCRETE

B.1 Introduction

The fresh and hardened properties of concrete, whether it is self-compacting (SCC) or normally vibrated concrete (NC), are significantly affected by the characteristics and content of its raw materials. The proportioning of the raw materials requires careful consideration in order to maintain a proper balance between the requirements of fresh and hardened properties of concrete. The well-known mix design methods proposed to produce NC cannot be used for SCC because of the difference of SCC constituents which require more fine materials, less coarse aggregate content and extra quantities of HRWRA and VMA.

In spite of the fact that SCC was firstly introduced in 1987 and since then a great amount of research has been carried out with the aim of finding an appropriate mix design method (Su et al., 2001; Su and Miao, 2003; Hwang and Hung, 2005; Aggarwal et al., 2008; Kheder and Al Jadiri, 2010; Sonebi, 2004), there has been no standard method for proportioning the raw

materials and predict the resultant properties of SCC. Moreover, all the research and experiments on SCC required a high number of trial mixes in order to obtain the required results and this has led to waste raw materials, time and money.

Underneath is a description of some popular mix design methods for SCC including the simple method proposed by Su et al. (2001) used in this research.

B.2 Japanese Method

Skarendahl and Petersson (2000) described the earliest mix design method for SCC which was proposed by Japanese researchers followed by Ozawa's Method. This method was then modified in 1995 by Okamura and Ozawa. Generally, it was focused on reducing the quantity of coarse aggregate to about 50% of the solid volume, 40% by volume of the mortar is fine aggregate and lower water to powder (w/p) ratio of about 30% depending on the results of fresh properties (Aggarwal et al., 2008; Chai, 1998). However, this approach is available only for low w/p ratio and it results in high mortar content which increases the cost of SCC (Su et al., 2001; Chai, 1998; Su and Miao, 2003). This method was then modified by Edamatsu et al. (2003). The coarse aggregate content was kept constant at 50% of the solid volume whereas the fine aggregate content, the w/p ratio and the HRWRA were calculated using the V-funnel and flow tests.

B.2 Chinese Method

On the other hand, in 1996, researchers in China suggested that the fine aggregate content of SCC should be approximately 50% of the total aggregate volume. Moreover, to control the passing ability and shrinkage, the paste volume should be kept at around 0.4 m^3/m^3. It was also suggested that the cement can be replaced by fly ash by 30% to 45% without significantly affecting the compressive strength (Chai, 1998). In contrast, this method did not clearly describe how to proportion the raw materials. Also, the low binder content with no vibration leads to a remarkable reduction in the strength properties of SCC.

B.3 LCPC Method

Sedran et al. (1996) proposed LCPC's method for proportioning SCC. In this method a discrete model is used to optimize the granular skeleton of concrete. It depends on specifying the content of binders and uses the results from the rheological tests of fresh concrete, L-box test and segregation resistance test. These results were correlated with the packing density of the concrete skeleton to find the relationship between the packing density with the plastic viscosity and yield stress. These relationships were then run using special software to obtain and optimise the components of SCC. The quantity of mixing water can be selected by carrying out trial mixes and test the slump flow. However, this method cannot be applied unless the software is available. It also results in a decrease in the paste content which negatively affects the flowability of SCC. Moreover, to carry out this approach, there are some limitations such as a slump flow of 600 to 700 mm and plastic viscosity of 100 to 200 Pa must be considered (Su et al., 2001; Chai, 1998).

B.4 Swedish Method

The Swedish Cement and Concrete Research suggested different approach for SCC mix design. It applies the relationship between the paste volume and coarse aggregate content to calculate the paste volume depending on the gaps between reinforcement. Nevertheless, this relationship is based on trial mixes that were made by coarse aggregate and paste only neglecting the effect of fine aggregate which plays an important part in improving the segregation resistance (Su et al., 2001; Petersson et al., 1996).

B.5 Hwang's Method

Another mix design method is Hwang's method which has been widely used in Taiwan. It depends on a densified mixture design algorithm which divides the mixture into two parts. The first part includes aggregate, fly ash and GGBS whereas the other includes water, cement and superplasticizer (Su et al., 2001; Chai, 1998; Hwang and Hung, 2005). However, this method was proposed by using coarse aggregate of 20 mm maximum size and no results was mentioned for aggregate size of 10mm which is the most preferred size for SCC. Furthermore, fly ash and GGBS were added as a ratio of aggregate instead of cement which is different from the conventional methods (Chai, 1998).

B.6 A Simple Mix Design Method

Su et al. (2001) and Su and Miao (2003) proposed a new method for proportioning medium strength SCC based on lowering the amount of cement. Firstly, the amount of coarse and fine aggregate is calculated from

equations (B.1) and (B.2), respectively, depending on the unit volume mass and packing factor of aggregate. The packing factor of aggregate was suggested by the researchers to be between 1.12 and 1.16. Secondly, the cement content is based on the required compressive strength as it was mentioned that 1 kg of cement provides a compressive strength of 0.14 MPa. Thirdly, the w/c ratio is obtained according to previous studies and the amount of water can be determined based on the results. Finally, the amount of fly ash, slag and superplasticizer can be calculated depending on the weight and volume of concrete (Su et al., 2001; Su and Miao, 2003).

$$W_g = PF * W_{gL} \, (1 - \frac{s}{a}) \quad \text{(B.1)}$$

$$W_s = PF * W_{sL} \, \frac{s}{a} \quad \text{(B.2)}$$

where W_g is the amount of coarse aggregate, W_s is the amount of fine aggregate, W_{gL} is the unit volume mass of coarse aggregate, W_{sL} is the unit volume mass of fine aggregate, PF is the packing factor and s/a is the ratio of fine aggregate to total aggregate (50-57%).

B.7 European Guidelines for SCC

The European Guidelines for SCC (BIBM et al., 2005) produced some limitations and specifications for SCC based on the mix design methods that have been proposed and the results obtained by other researchers. It was reported that in order to produce SCC of acceptable properties, the w/p ratio should be between 0.8 and 1.1 by volume, the mixing water should be from 150 kg/m^3 to 210 kg/m^3 and total binder content is [400- 600] kg/m^3. Moreover, the volume of coarse aggregate is in the range of 28% to 35% of

the total volume of concrete and the fine aggregate content should be from 48% to 55% of the total weight of aggregate (BIBM et al., 2005).

Overall, the described methods have many disadvantages and therefore they cannot be used as standards for SCC mix design. These methods have their own requirements and results and were proposed depending upon a specific set of materials and relationships which cannot be applied to other materials unless new relationships are created (Nepomuceno et al., 2012).

APPENDIX C. PARAMETRIC STUDY

Based on the parametric study conducted in chapter six to investigate the effect of some important parameters on the load currying capacity of continuously supported SCC deep beams, this appendix presents more figures, in addition to those presented in chapter six, for the relationship between the load capacity and the parameters under investigation. The prameters included in the parametric study were the shear span-to-depth ratio (a/d), the compressive strength of concrete (f_c'), the longitudinal bottom reinforcement ratio (ρ_{Bott}), the longitudinal top reinforcement ratio (ρ_{Top}), the vertical web reinforcement ratio (ρ_v) and the horizontal web reinforcement ratio (ρ_h).

C-1 Effect of shear span-to-depth ratio on load capacity

The effect of a/d ratio was investigated for different concrete compressive strength values, different horizontal and vertical shear reinforcement ratios

and different longitudinal top and bottom reinforcement ratios as shown in Figures C-1 to C-5 below.

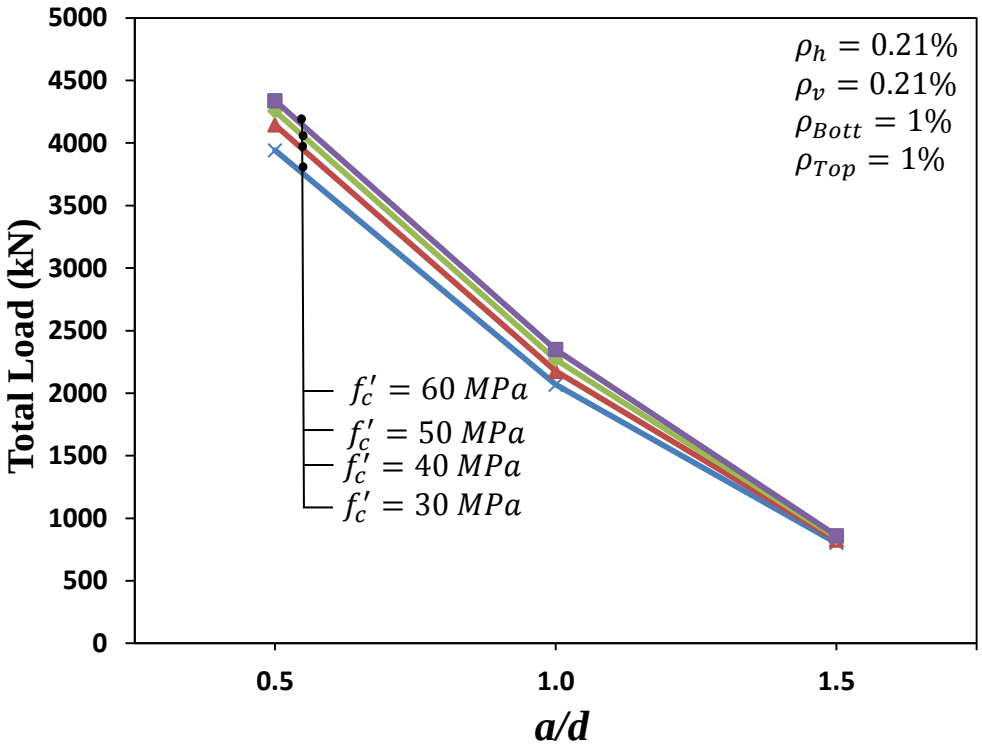

Figure C-1: Effect of shear span-to-depth ratio on load capacity of continuous SCC deep beams for different values of compressive strength

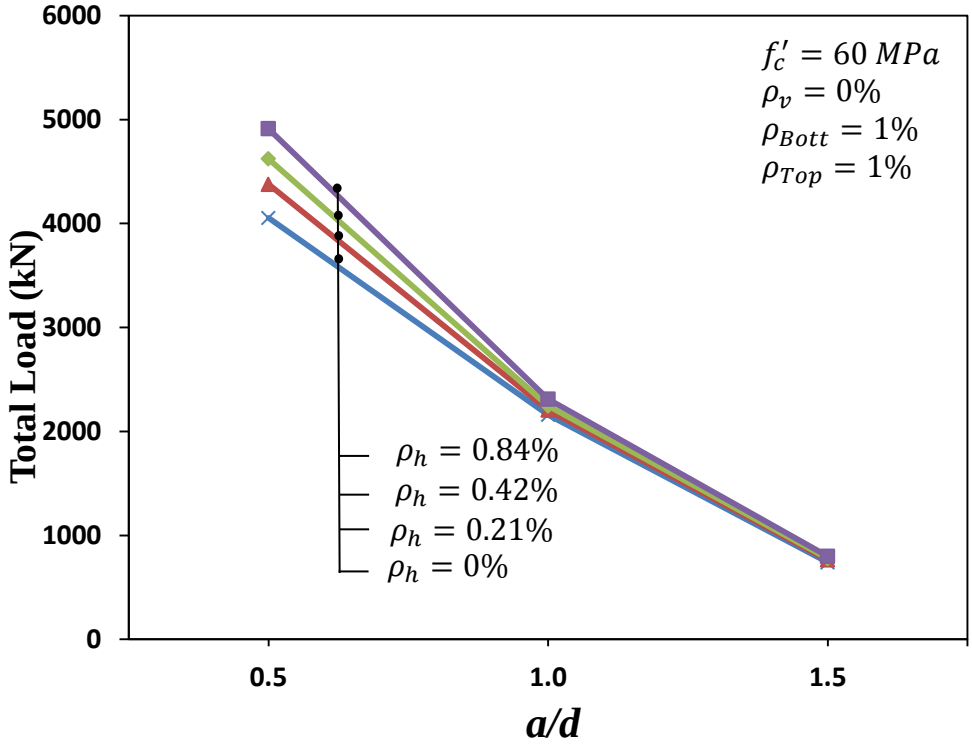

Figure C-2: Effect of shear span-to-depth ratio on load capacity of continuous SCC deep beams for different amounts of horizontal shear reinforcement

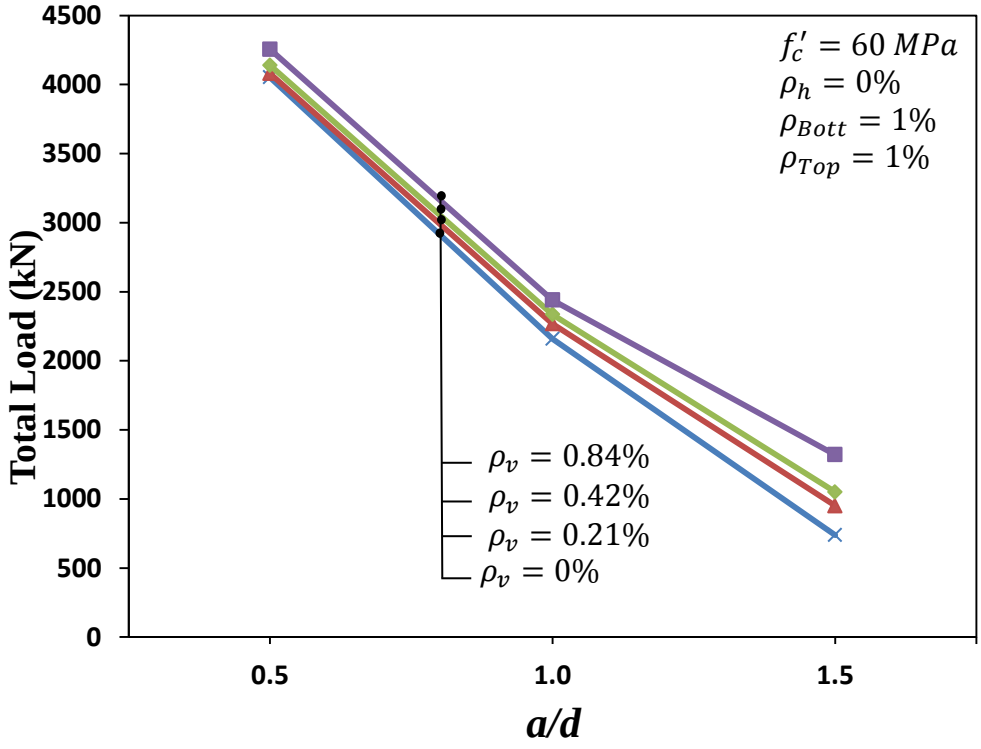

Figure C-3: Effect of shear span-to-depth ratio on load capacity of continuous SCC deep beams for different amounts of vertical shear reinforcement

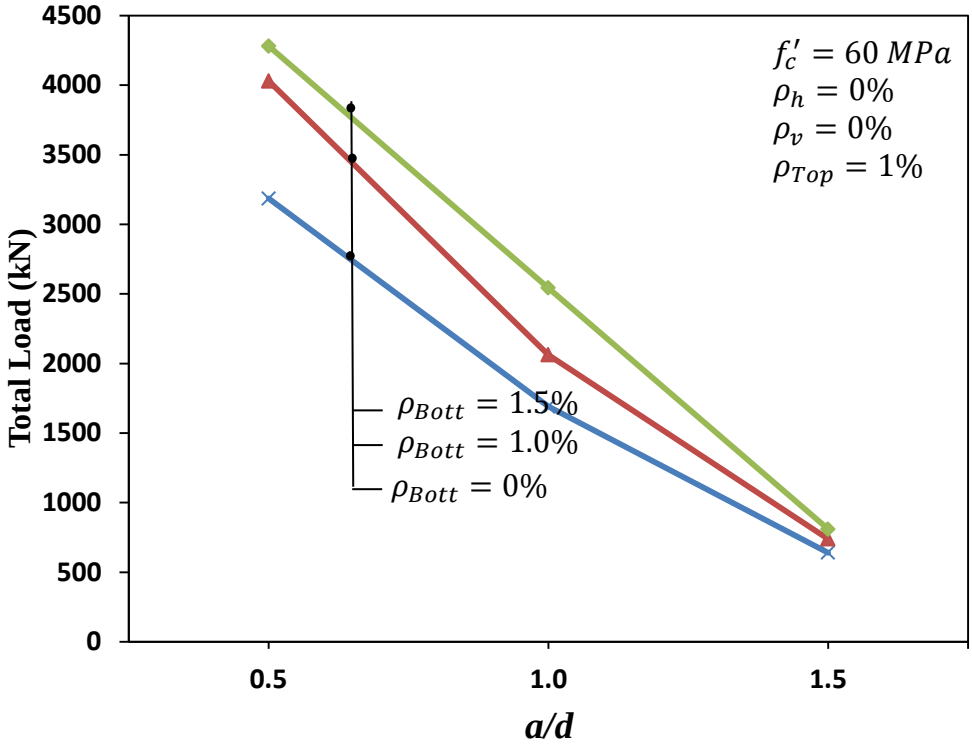

Figure C-4: Effect of shear span-to-depth ratio on load capacity of continuous SCC deep beams for different longitudinal bottom reinforcement ratios

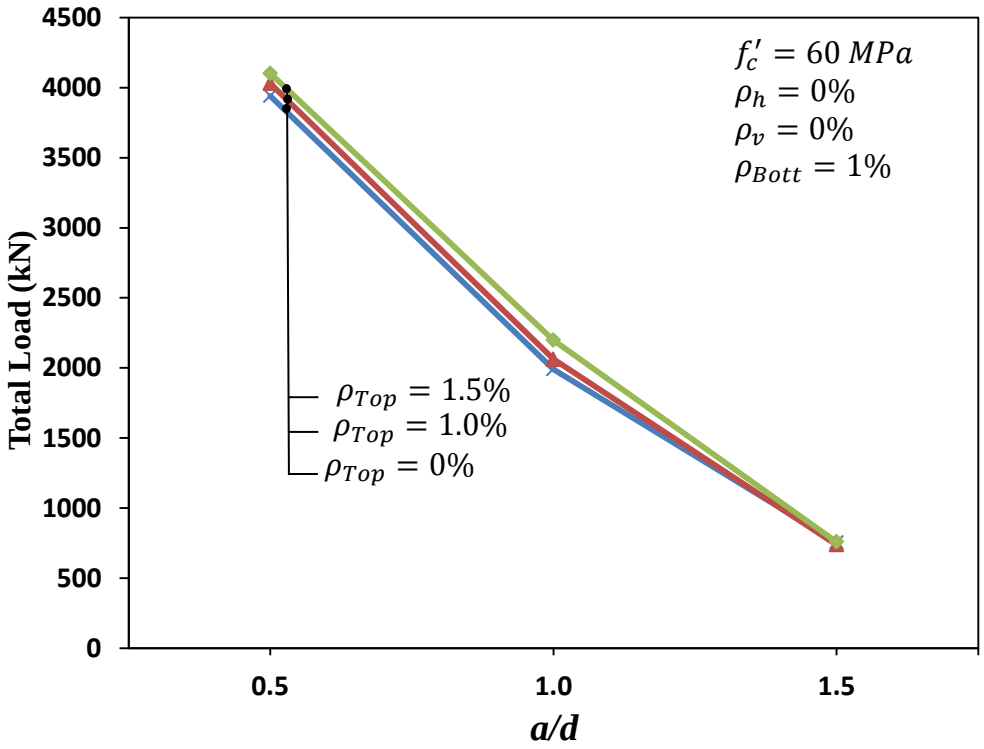

Figure C-5: Effect of shear span-to-depth ratio on load capacity of continuous SCC deep beams for different longitudinal top reinforcement ratios

C-2 Effect of compressive strength on load capacity

The effect of compressive strength of concrete was investigated for different shear span-to-depth-ratios, different horizontal and vertical shear reinforcement ratios and different longitudinal top and bottom reinforcement ratios as shown in Figures C-6 to C-10.

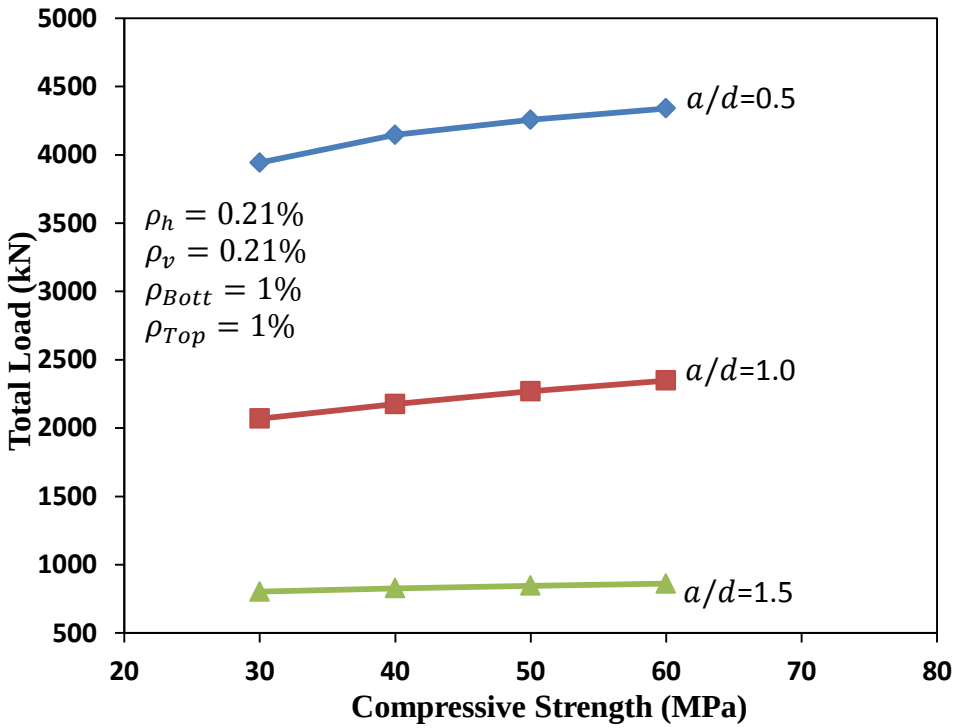

Figure C-6: Effect of compressive strength on the load capacity for different shear span-to-depth ratios

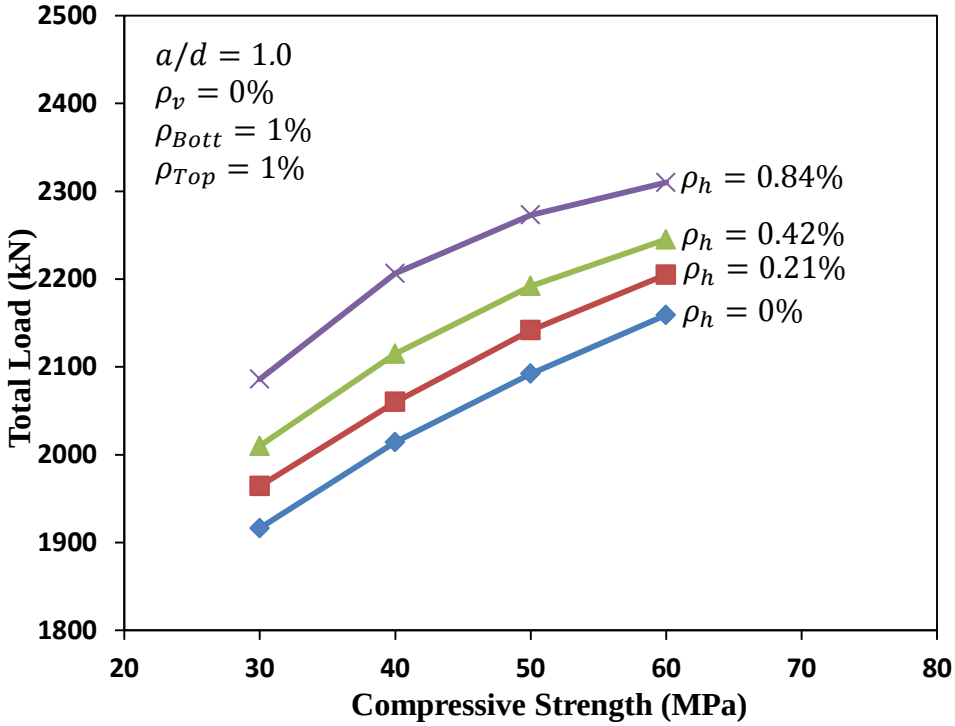

Figure C-7: Effect of compressive strength on the load capacity for different horizontal reinforcement ratios

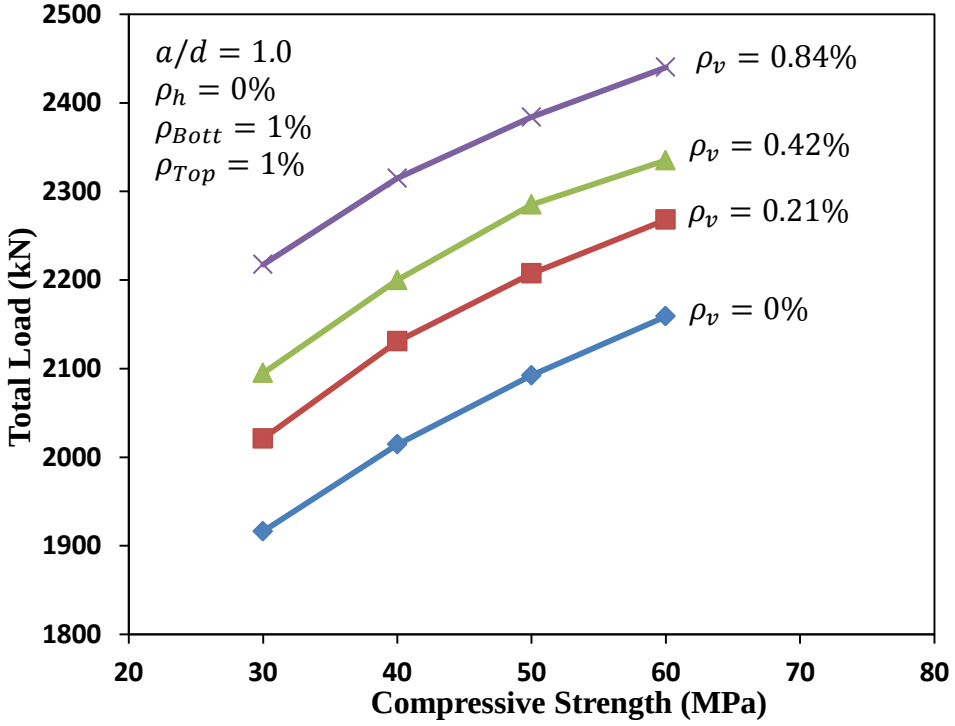

Figure C-8: Effect of compressive strength on the load capacity for different vertical reinforcement ratios

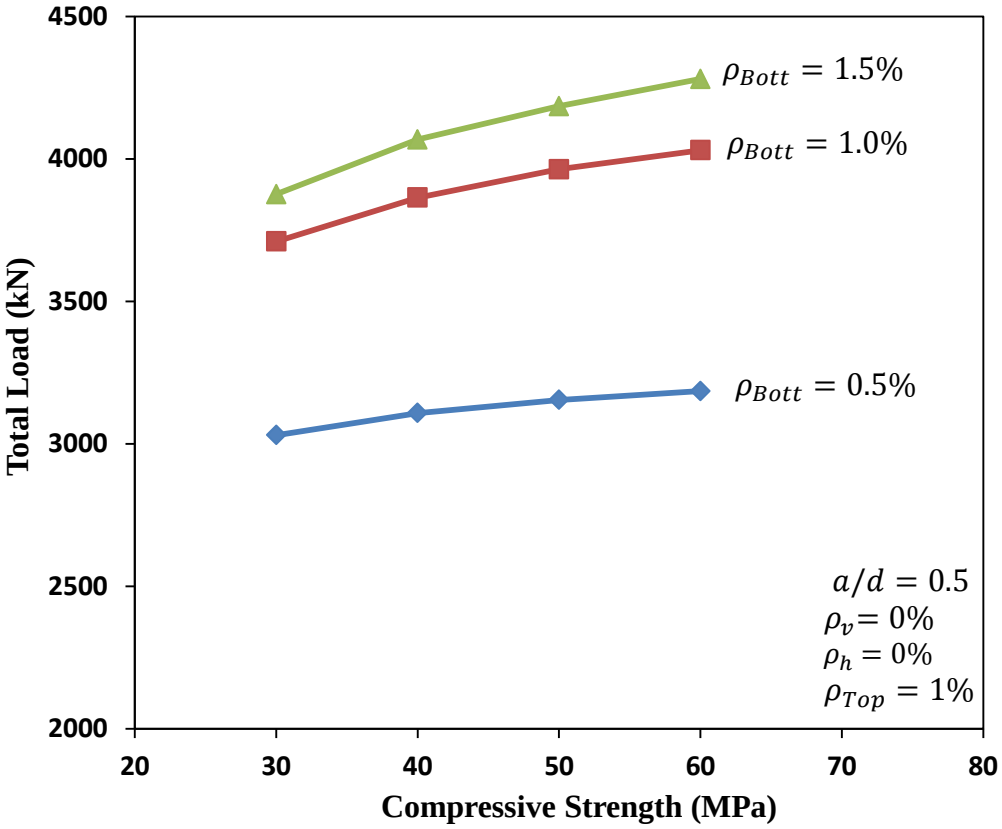

Figure C-9: Effect of compressive strength on the load capacity for different longitudinal bottom reinforcement ratios

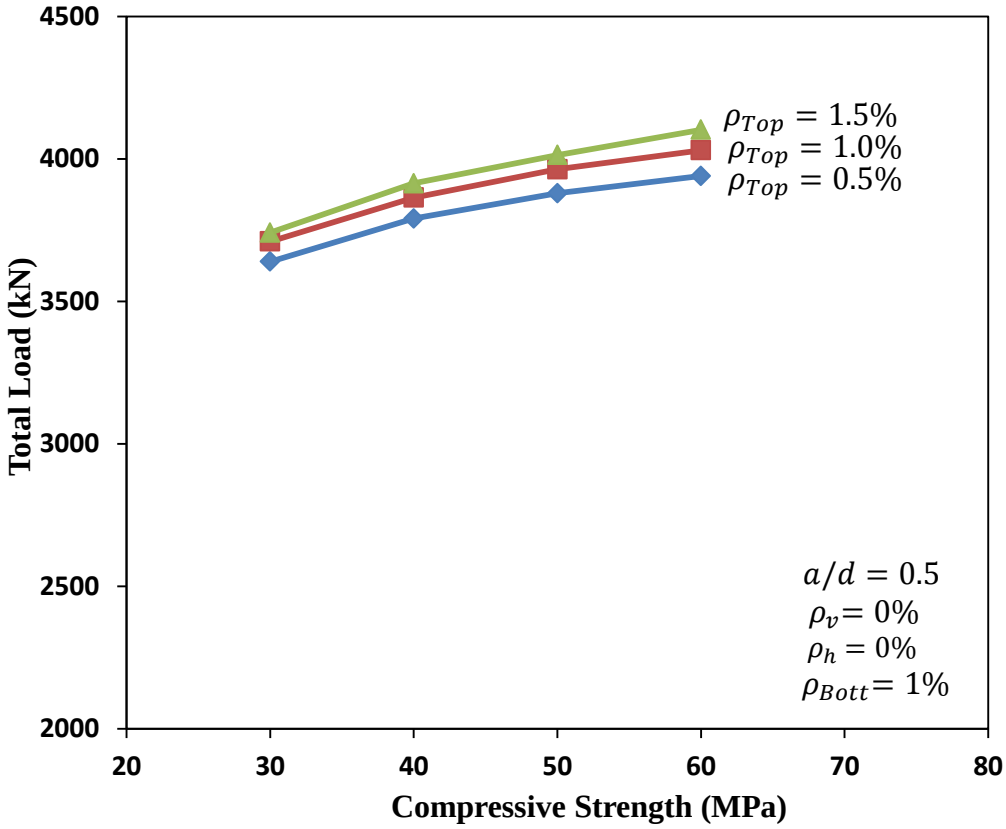

Figure C-10: Effect of compressive strength on the load capacity for different longitudinal top reinforcement ratios

C-3 Effect of vertical web reinforcement on load capacity

The effect of vertical web reinforcement ratio was investigated for different shear span-to-depth ratios, different concrete compressive strength values, different horizontal web reinforcement ratios and different longitudinal top and bottom reinforcement ratios as shown in Figures C-11 to C-12.

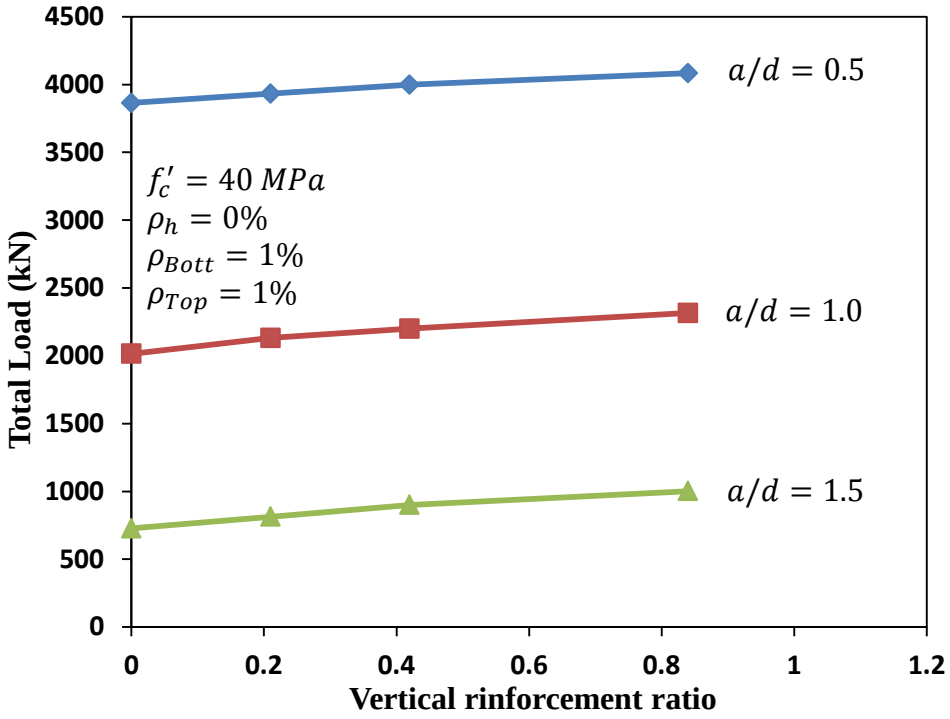

Figure C-11: Effect of vertical web reinforcement on load capacity of beams having a compressive strength of 40 MPa

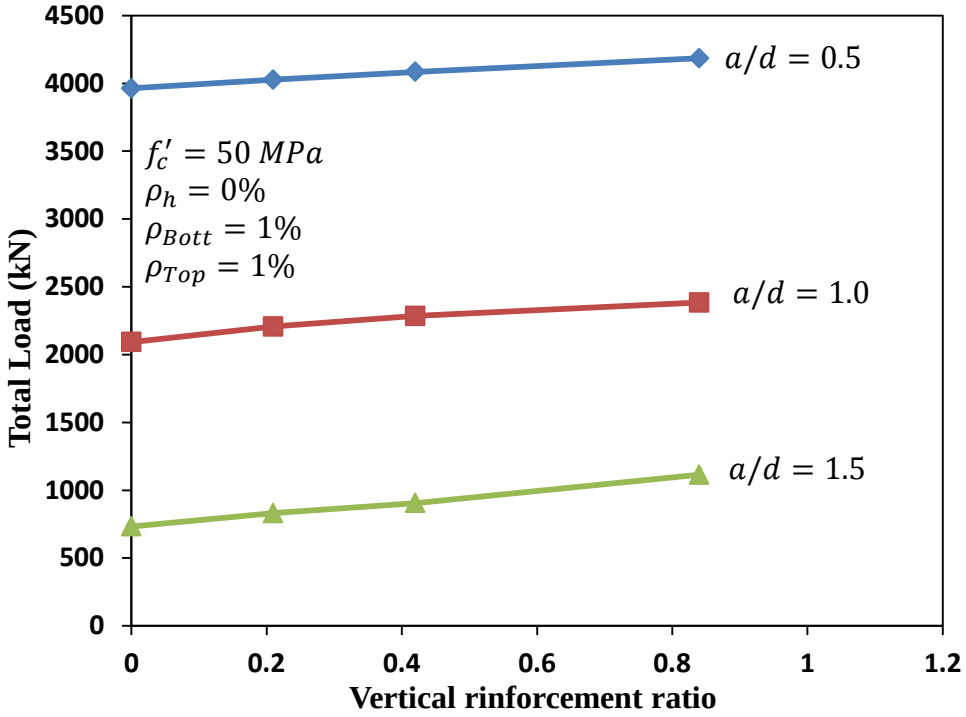

Figure C-12: Effect of vertical web reinforcement on load capacity of beams having a compressive strength of 50 MPa

C-4 Effect of horizontal web reinforcement on load capacity

The effect of horizontal web reinforcement ratio was investigated for different shear span-to-depth ratios, different concrete compressive strength values, different vertical web reinforcement ratios and different longitudinal top and bottom reinforcement ratios as shown in Figures C-13 to C-14.

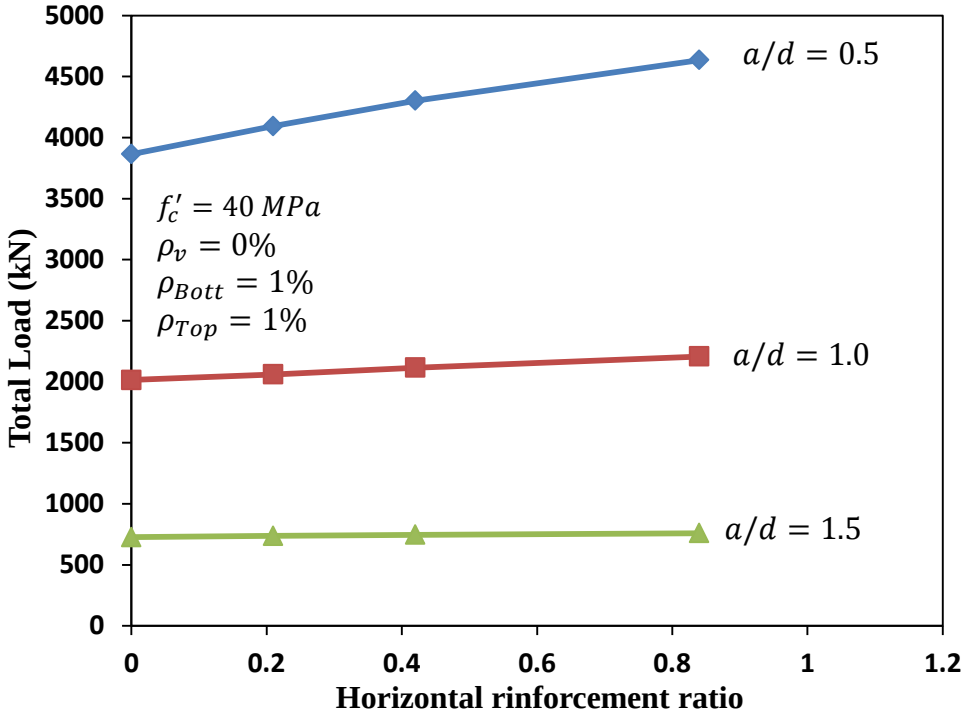

Figure C-13: Effect of horizontal web reinforcement on load capacity of beams having a compressive strength of 40 MPa

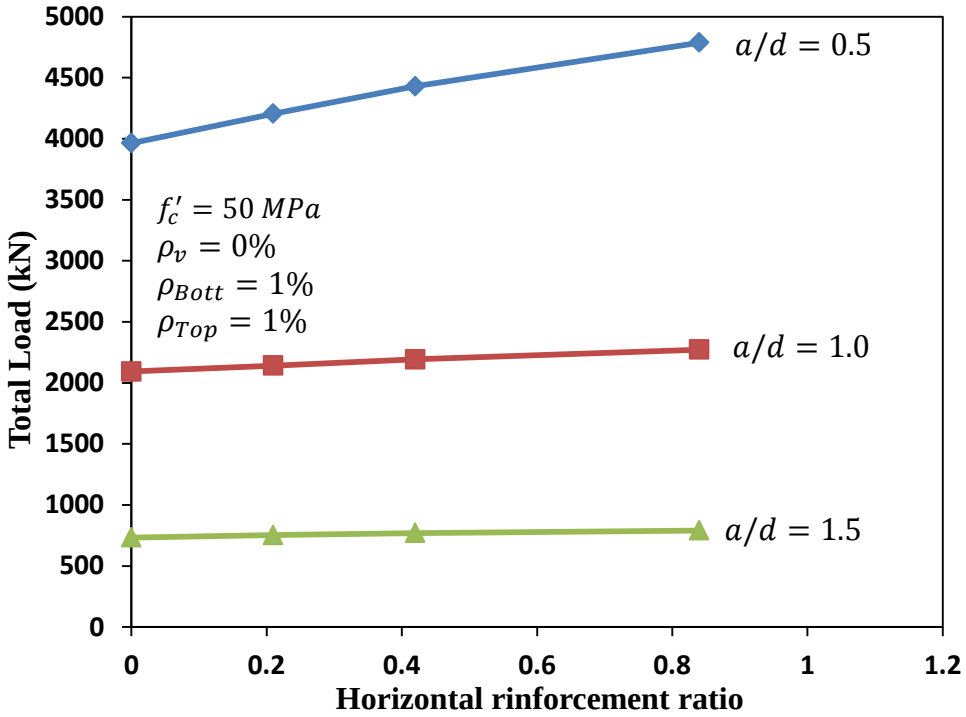

Figure C-14: Effect of horizontal web reinforcement on load capacity of beams having a compressive strength of 50 MPa

C-5 Effect of longitudinal bottom reinforcement on load capacity

The effect of longitudinal bottom reinforcement ratio was investigated for different shear span-to-depth ratios, different concrete compressive strength values, different vertical and horizontal web reinforcement ratios and different longitudinal top reinforcement ratios as shown in Figures C-15 to C-16.

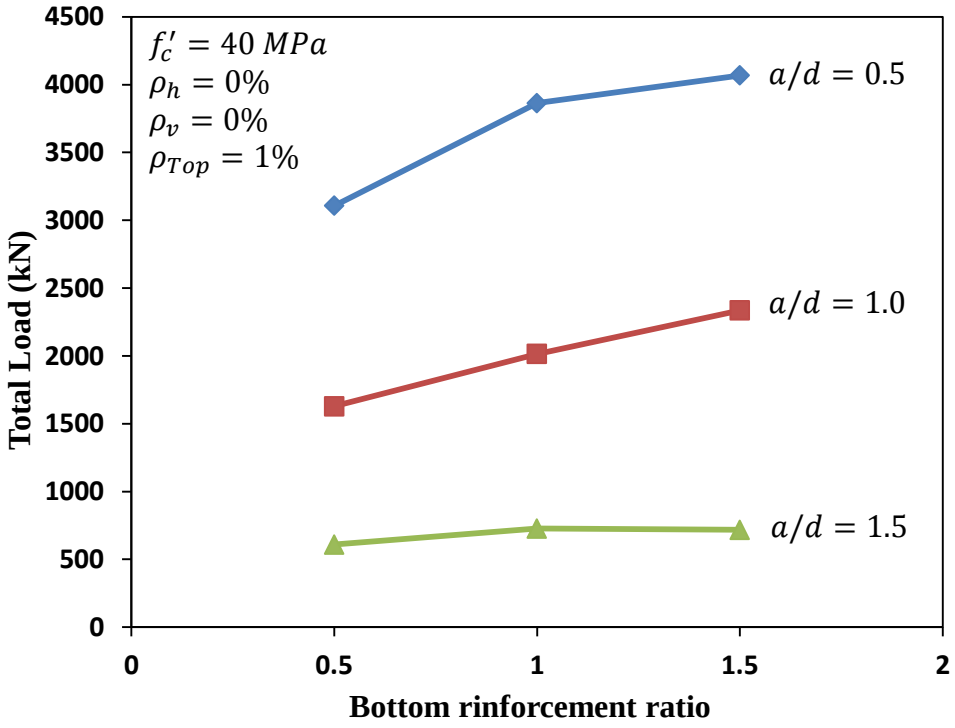

Figure C-15: Effect of longitudinal bottom reinforcement on load capacity of beams having a compressive strength of 40 MPa

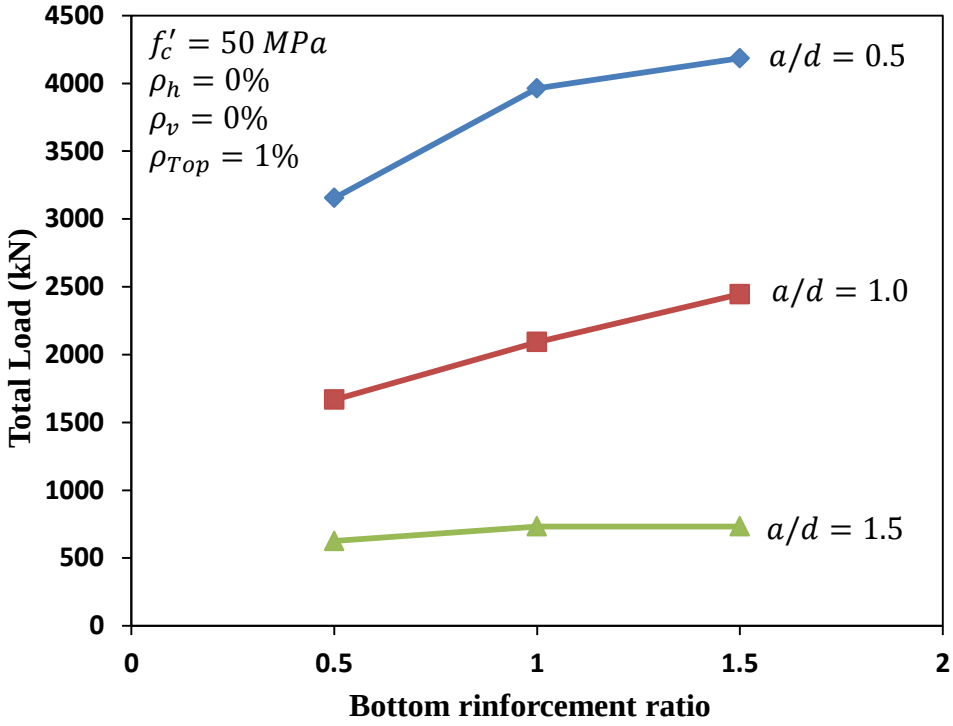

Figure C-16: Effect of longitudinal bottom reinforcement on load capacity of beams having a compressive strength of 40 MPa

C-6 Effect of longitudinal top reinforcement on load capacity

The effect of longitudinal top reinforcement ratio was investigated for different shear span-to-depth ratios, different concrete compressive strength values, different vertical and horizontal web reinforcement ratios and different longitudinal bottom reinforcement ratios as shown in Figures C-15 to C-16.

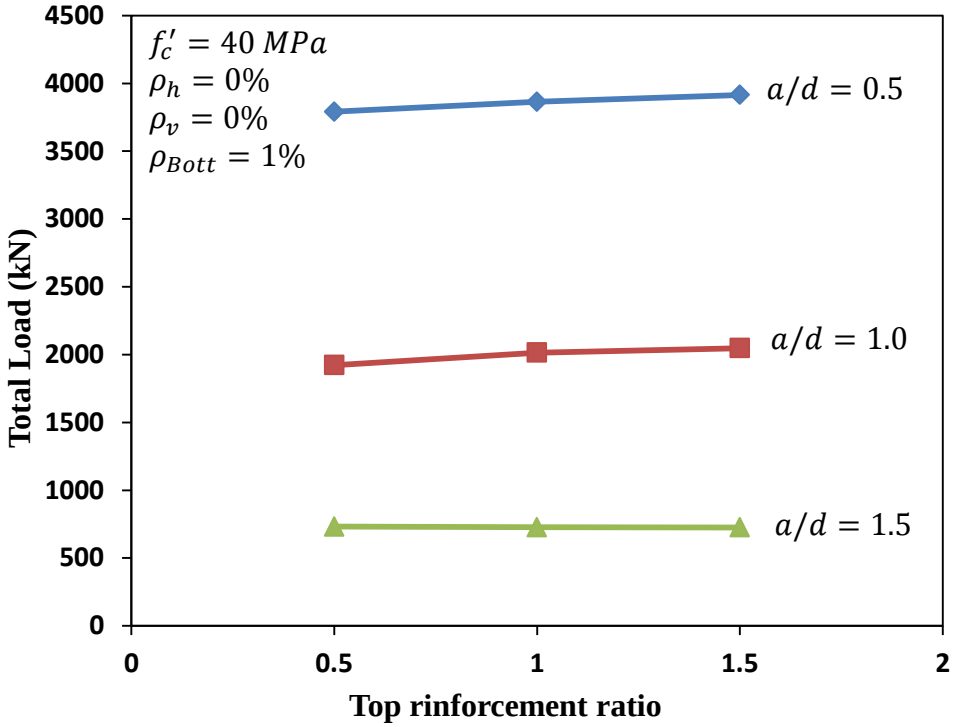

Figure C-17: Effect of longitudinal top reinforcement on load capacity of beams having a compressive strength of 40 MPa

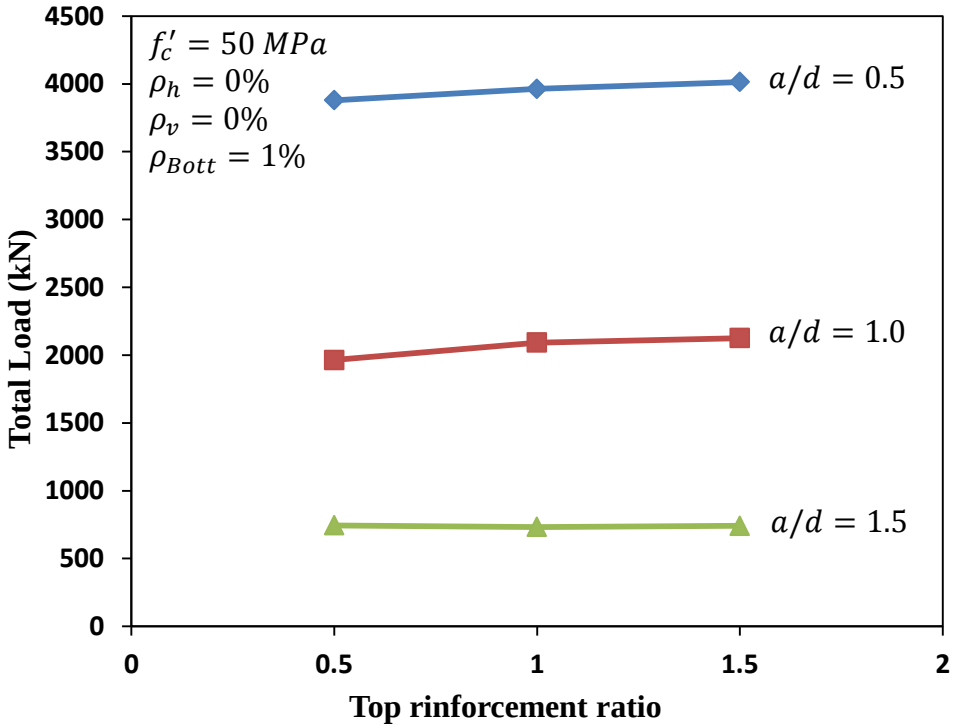

Figure C-18: Effect of longitudinal top reinforcement on load capacity of beams having a compressive strength of 50 MPa